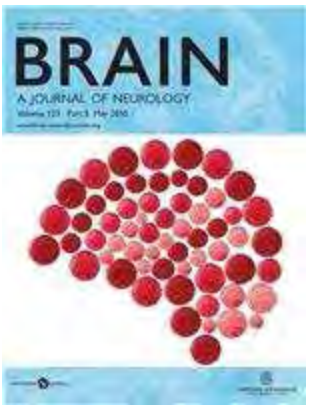

Molecular reorganization of endocannabinoid signalling in Alzheimer's disease

Journal:	*Brain*
Manuscript ID:	BRAIN-2010-01821.R1
Manuscript Type:	Original Paper
Date Submitted by the Author:	n/a
Complete List of Authors:	Mulder, Jan; University of Aberdeen, ENI-Aberdeen Zilberter, Misha; Karolinska Institutet, Medical Biochemistry & Biophysics Pasquare, Susana; Cajal Institute, Department of Cellular, Molecular and Developmental Neuroscience Alpar, Alan; University of Aberdeen, ENI-Aberdeen Schulte, Gunnar; Karolinska Institutet, Pharmacology & Physiology Ferreira, Samira; University of Coimbra Köfalvi, Attila; University of Coimbra Martin Moreno, Ana; Cajal Institute, Department of Cellular, Molecular and Developmental Neuroscience Keimpema, Erik; University of Aberdeen, ENI-Aberdeen Tanila, Heikki; University of Eastern Finland, A.I. Virtanen Institute Watanabe, Masahiko; Hokkaido University School of Medicine, Department of Anatomy Mackie, Ken; Indiana University, Gill Center for Neuroscience Hortobagyi, Tibor; King's College London, Institute of Psychiatry de Ceballos, María; Cajal Institute, Department of Cellular, Molecular and Developmental Neuroscience Harkany, Tibor; Karolinska Institutet, Medical Biochemistry & Biophysics; University of Aberdeen, ENI-Aberdeen
Key Words:	
Please choose up to 5 keywords from the list:	cannabinoids, Alzheimers disease, synapse function, cerebral cortex, Neuronal Plasticity

ScholarOne, 375 Greenbrier Drive, Charlottesville, VA, 22901 Support (434) 964 4100

SCHOLARONE™
Manuscripts

For Peer Review

Specific responses to Referee 1:

Thank you for your supportive comments, useful criticism and balanced view on our manuscript. We were glad to learn that you find our manuscript significant. We have dealt with each of your queries in detail. Please find our specific responses to your criticism below.

Q1: *'1. Fig. 1A: The data appear to show a profound reduction in SNAP25 and PSD95, common synaptic proteins, in AD preparations compared to control. Does this reflect a decrease in synaptic numbers? If so, this might contribute to synaptic transmission deficiency irrespective of 2-AG signalling. Other conclusions which the authors base on a difference in immunostaining might also be affected by this general trend.'*

Synaptic dysfunction is a key pathogenic component of Alzheimer's disease. It is generally accepted that excitatory synapses may be preferentially targeted by beta-amyloid (Aβ). Therefore, it is relevant to assess synaptic protein concentrations (Fig. 1A, Supporting Fig. 1). Endocannabinoids can affect both excitatory and inhibitory neurotransmission through CB_1 cannabinoid receptors (CB_1Rs). Indeed, disease-related deficiency of synaptic neurotransmission may impact endocannabinoid signalling that is, in our view, one key neuromodulatory homeostatic system to define the dynamics of presynaptic neurotransmitter release.

- To address the mechanistic scenario you have outlined we have introduced an additional paragraph in our discussion (page 17, text in blue).
- Is the loss of CB_1R-mediated 2-AG signalling a simple reflection of synapse elimination? We think not given the lack of a relationship between CB_1R and presynaptic protein (SNAP25) concentrations in Alzheimer's brains. Similarly, a lack of PSD95/DAGL relationship (in the postsynapse) suggests that modifications to 2-AG synthesis in AD are, at least in part, independent from synapse loss.
- Our manuscript aims to describe changes to the molecular control of 2-AG availability and signal competence. We, in the present report, did not address the synapse specificity of 2-AG dysfunction. Is this question of overall importance? We stand firm in our view that, in a primary research report, it is not. We nevertheless believe that follow-up studies may uncover interesting contributions of e.g., specific basket cell subtypes or pyramidal cell subsets to regulating particular aspects of endocannabinoid signalling in AD.
- During studying DSI, we have considered endocannabinoid signalling as a subsystem which may play a modulatory role in synaptic processing. We used acute Aβ superfusion (60 min). This brief synaptotoxic insult is unlikely to (physically) eliminate synapses from the hippocampal networks we have studied. Therefore, our conclusions that Aβ instead disrupts the timing of DSI are warranted. Since perisomatic DSI is largely induced at a homogenous population of GABAergic terminals (originating from cholecystokinin-positive basket cells), we believe that the apparent change in DSI decay will reflect the response of this specific terminal subset. We have stated this on page 17 of the revised manuscript.

Q2: '*2. Fig. 1E: The text mentions "strong inverse relationship between DAGalpha and DAGbeta levels". This is however not what the data scatter suggests.*'

Fig. 1E (revised Fig. 1D) examines the expressional relationship between DAGLalpha and DAGLbeta.

- There is no correlation between the levels of these two enzymes when sampling the overall subject cohort.

For Peer Review

- However, a negative correlation is evident when specifically sampling the Braak 6 cohort.
- We have clarified the expressional relationship existing in severe Alzheimer's by specifically retaining the regression line for the Braak 6 group (in red).

Q3: *'Colocalisation studies based on fluorescence imaging are notoriously prone to spurious correlation. Because conclusions of the present manuscript rely heavily on such data it would be important to understand the error involved. The authors should attempt to assess spatial resolution of the methods involved, which is unlikely to be better than 0.5-0.7 micron in the z-direction. Further detail should be provided with respect to the 3-D reconstruction and surface rending approaches used. Ideally, control samples with non-specific staining obtained in similar conditions should be used to gauge the spurious correlations involved. Seeing a difference between healthy and AD preparations deals with this issue only to some extent.'*

We agree with your view that assessment of the reliability of the imaging techniques we used requires detailed description of the methods involved and presenting control data. In the original submission, we have only provided a succinct passage on the imaging tools used given that we have provided a relatively detailed description of these recently, including spectral image controls (Halleskog *et al*., Glia (2011) 59;119-131).

- Since we rely on laser-scanning microscopy analysis, the spatial resolution (in *z* direction) will not be better than 500-700 nm (considering Abbe's diffraction limit and the NA of our objectives). But, we have imaged structures in the micrometer range throughout and therefore do not think that these obvious physical limits will affect the quality of our data. We have specified the *x/y/z* resolution scale used during three-dimensional on page 4 of the Supplementary Information.

We also have:

- provided spectral analysis of the specificity of each fluorochrome (Supplementary Fig. 3),
- compared the various background quenching, antigen retrieval and staining protocols (Supplementary Fig. 3) to control for non-specific background,
- described in detail the imaging and reconstruction protocols we have used (pages 3-4 (text in blue) of the Supplementary Methods),
- homogenized fluorescence excitation of fluorochromes from different specimens (Supplementary Fig. 6) to minimize bias in our quantitative profiling. Please note that the extensive revisions have, in some instances, affected the total (%) values of e.g., area coverage. However, none of the modifications we introduced affected the *ratio* of co-localization of select marker combinations. Our conclusions are warranted since we use this latter parameter throughout the study as decisive read-out.
- edited the manuscript text accordingly.

Q4: *'Fig. 8B: Because this is the only physiological experiment lending support to the main hypothesis it would be important to understand its details. The AM281 control data need to be shown, either here or in the Supplementary. Because TTX is not mentioned, one assumes that the recorded spontaneous activity is action potential dependent. If so the observed changes may reflect network activity rather than changes in synaptic transmission per se. In general, extending physiological tests would greatly improve the manuscript.'*

Thank you for raising these important points. We have:

For Peer Review

- included data on AM251 effects: AM251-induced inhibition of DSI under control conditions has previously been shown in many publications. Therefore, we present only the summary diagram in Fig. 8C. In turn, we show an example experiment in Supplementary Fig. 10.
- We have performed another series of important control experiments to exclude that the Aβ-induced enhancement of DSI is due to the release of a non-endocannabinoid retrograde messenger. We show (Fig. 8D,D_1) that AM251 eliminates DSI even upon Aβ exposure.
- TTX was not present in ACSF during the DSI recordings, and accordingly, the recorded activity is referred to as "spontaneous IPSCs (sIPSC)", rather than "miniature IPSCs (mIPSC)", which would be the case in action potential-independent, quantal neurotransmission. However, our DSI recordings were done under a blockade of both AMPA and NMDA channels (by applying CNQX and APV throughout the duration of the experiment), and thus in the absence of excitatory neurotransmission. As the recorded postsynaptic cell, a CA1 pyramidal neuron is itself glutamatergic, it is reasonable to conclude that the observed Aβ-induced changes in DSI kinetics are not network-related.

Q5: *'Because CB1 receptors are thought to affect predominantly inhibitory transmission the enhancement in cannabinoid signalling attributed to AD may actually result in enhanced excitatory activity in the brain. This general issue has to be dealt with.'*

This is a very important point, which we did not specifically address in the original manuscript: mainly, what, if any, changes does Aβ induce in 2AG-mediated modulation of excitatory neurotransmission? It has been reported that glutamatergic neurons in hippocampus also exhibit depolarization-induced suppression of excitation (DSE), which is mediated by endocannabinoids (reviewed by Kano *et al*. Physiol Rev (2009) 89: 308-380). It is possible that the release of endocannabinoids from the postsynaptic cell has a double effect, in suppressing both its inhibitory and excitatory inputs. In relation to neuronal excitability, then, what is the total effect of such endocannabinoid release, and what are the changes brought about by Aβ?

- **We have performed additional experiments in an attempt to address these questions.**

- Previous studies on DSE have recorded both spontaneous and evoked excitatory currents (EPSCs) under the blockade of $GABA_A$ receptors. We feel, however, that such an approach introduces a variable that, while influencing the outcome, is impossible to compensate for. Namely, it is accepted that under a total $GABA_A$ receptor blockade (whether by picrotoxin or bicuculline), the neuronal network becomes highly hyperactive, even epileptic. The hyperactivity is not constant, but dynamic, with periods of high activity followed by quiescent periods. Thus, recording any long-term changes of EPSC amplitudes under an unpredictable factor of an epileptic network activity is – in our opinion – highly unreliable.

  We have attempted, therefore, to elucidate the possible effect of Aβ on endocannabinoid modulation of excitatory neurotransmission using alternative means. Namely, Hajos & Freund have reported that the application of WIN55,212-2, a CB_1R/CB_2R agonist, significantly reduces the observed magnitude of excitatory synaptic inputs (Neuropharmacology (2002) 43: 503-510). We have attempted to replicate these experiments (see Fig. 2A in the above paper) but without the use of $GABA_A$ receptor blockade. Instead, we have used an intracellular pipette solution containing 10mM [Cl^-] and clamped the neuronal membrane potential to that of calculated E_{GABA} (-70mV). Thus, with dF_{GABA} (driving force, the difference between V_m and E_{GABA}) being 0mV, there should be no I_{GABA} and the only recorded activity should be glutamate-mediated (E_{AMPA} and E_{NMDA} are around 15 mV). Unfortunately, *our experiments failed to confirm the findings of Hajos and Freund (Fig. 1 below)*

For Peer Review

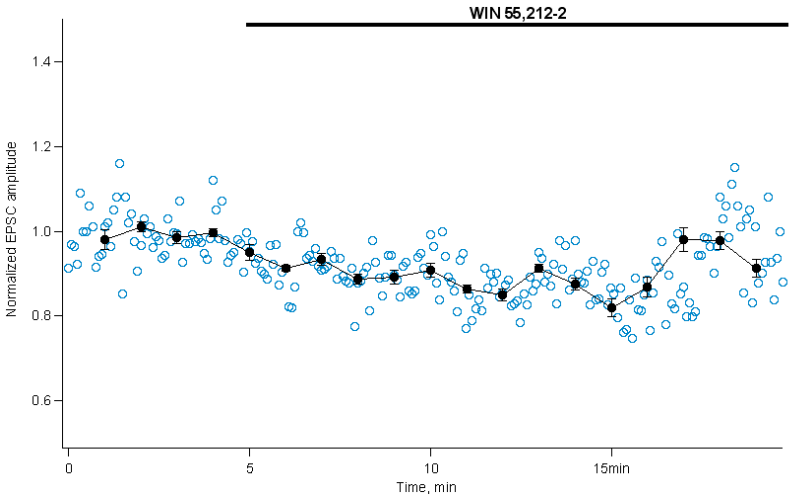

Fig. 1 - *Summary mean data figure of 8 experiments, where after recording a 5-minute control period, 2μM WIN 55-212,2-containing solution was washed in. EPSCs were evoked by a 1 ms stimulation pulse delivered via a theta-glass pipette in stratum radiatum of CA1 region.*

- We have therefore attempted to elucidate the net effect of endocannabinoid signalling on postsynaptic excitability using yet another experimental protocol:

  Clamping the postsynaptic membrane to the Cl^- reversal potential and eliminating inhibitory currents still leaves another function of inhibitory neurotransmission unaffected. Even if $GABA_A$ receptor activation does not result in a Cl^- current and subsequent membrane potential change, the opening of the Cl^- ion channel still results in the decrease in the membrane's input resistance (R_{in}). Such a decrease serves to change the filtering properties of the membrane, affecting other synaptic currents travelling along the dendrite, in the effect known as shunting. Shunting has been suggested to be a major effect of inhibitory neurotransmission (Borg-Graham et al. Nature (1998) 393: 369–373; Mitchell SJ & Silver RA, Neuron (2003) 38: 433–445; Prescott SA & de Koninck Y, Proc Natl Acad Sci USA (2003) 100: 2076–2081).

  Assuming that shunting is unaffected by our experimental protocol, it Is theoretically possible to record any net effect of postsynaptic endocannabinoid release on the total excitatory input. One might expect that by inducing DSI and reducing the inhibition's shunting effect, the observed excitatory currents might become enhanced during the duration of DSI. We have, therefore, recorded spontaneous excitatory currents (sEPSCs) in a postsynaptic cell prior to and after inducing a standard DSI protocol (1s, 0mV). Unfortunately, such a protocol failed to uncover any changes in excitatory neurotransmission. Aβ also failed to induce a significant change in such a protocol (Fig. 2):

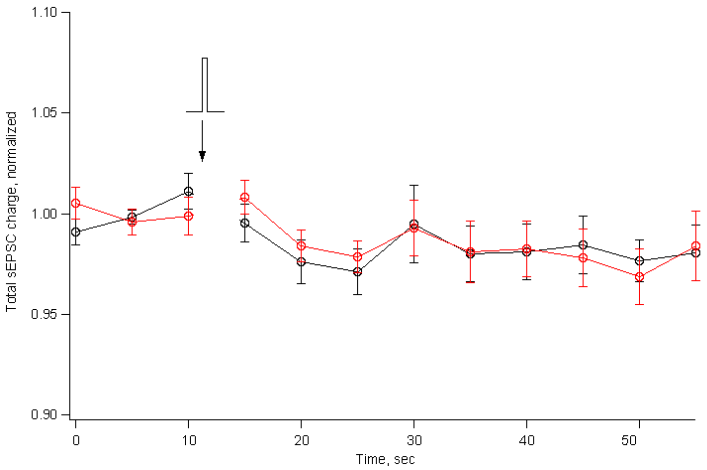

Fig. 2 - *Mean summary graph of such experiments. Standard DSI protocol fails to induce any observed changes in excitatory spontaneous activity (black trace, n = 10). Pre-incubation in 1uM Aβ does not result in additional change (red trace, n = 12).*

While our preliminary results failed to elucidate the net effect of cannabinoid signalling on excitability, these do not mean that the effect is in itself absent – only that given the experimental constraints it is difficult to manipulate the network environment without introducing unpredictable

For Peer Review

variables. As our present manuscript focuses on Alzheimer's effects on the brain's endocannabinoid signalling system, we feel that a full examination of the net effect on wider network activity requires a larger, detailed and separate study.

Q6: *'"Mean age of death" is abbreviated as mad, but the same abbreviation is used for "mild AD", which is a bit confusing. In addition, "severe AD" is abbreviated as sAD. I find it somewhat disconcerting that the carriers of AD might appear in the text as "mad" and "sad".'*

Thank you for drawing our attention to these inevitably disturbing details.

- We have spelled out 'mean age of death ' throughout the manuscript,
- We have replaced 'mAD' by 'B2-4' (referring to Braak stages 2-4). 'B6' (Braak stage 6) is used instead of 'sAD' throughout.

For Peer Review

Specific responses to Referee 2:

Thank you for your positive and supportive comments on our manuscript. We appreciate your balanced review, constructive criticism and suggestions. Please find our detailed responses to your specific queries as follows:

Q1A: *'some important quotations are missing, whilst others have been made but seem to have been underestimated. In the conception of this study, the authors must have been at least minimally inspired by the previous findings that: a) CB1 receptor blockade reduces memory retention loss in a mouse model of Aβ(1-42)-induced neurotoxicity (Mazzola et al., Eur J Pharmacol 2003; Micale et al, Pharmacol Res 2010); b) sterotaxic injection of Aβ(1-42) in rats induces a transient elevation of DAGLa expression and 2-AG levels (van der Stelt et al., Cel Mol Life Sci 2010, already quoted by the authors). This latter study demonstrated that elevation of endocannabinoid levels is not always beneficial towards memory retention loss in mice, and needs to be carried about early, in order to reduce this symptom, whereas, if occurring too late after the insult, it contributes to memory retention loss. This concept is very important, and should have been mentioned, together with all the above papers, already in the Introduction.'*

Thank you for bringing these points to our attention. Indeed, we have discussed these concepts only in the 'Discussion' of our original submission. Our reason was to minimize the length of the 'Introduction'. In the revised manuscript we have:

- inserted an additional introductory paragraph to introduce the above concepts (text in blue on page 4),
- referenced the above work (including Mazzola *et al*, 2003; Micale *et al.,* 2010)
- logically linked existing evidence on endocannabinoid functions in Alzheimer's and its experimental models with our specific aims.

Q1B: '*Instead, the authors, whose findings strongly support this concept, and provide the underlying mechanisms, do not even mention that the idea that endocannabinoids are not only beneficial (as suggested by Ramirez et al and Palazuelos et al) via CB2 receptors in animal models of AD, but can also contribute to symptoms in advanced AD via CB1, was already put forward in these previous papers; this concept is also highlighted in a review article by Bisogno and Di Marzo, Curr Pharm Des. 2008, that again the authors should quote.'*

- We discuss the role of CB_1 and CB_2 cannabinoid receptors and the possible contribution of endocannabinoid signalling to worsen AD symptoms on page 4.
- We have referenced the above review when formulating our introductory statement.

Q2: *'the authors have used URB602 at a very high concentration to gain evidence that the 2-AG hydrolysing activity that augments in cytosolic fractions and is reduced in the plasmalemma is at least in part due to MAGL. Indeed, much better tools (more potent and more selective), such as JZL184 and OMDM166 (Long et al., Nat Chem Biol. 2009; Bisogno et al., Biochim Biophys Acta 2009) have been developed. If the authors cannot perform experiments with these tools, or with a selective FAAH inhibitor too, they should reconsider entirely their conclusion that the 2-AG hydrolysing activity they are measuring is partly due to MAGL, also because evidence exists for a strong upregulation of FAAH in AD plaques from post-mortem brain (Benito et al). Furthermore, there is really no evidence in the literature that cytosolic 2-AG hydrolysing activities do not contribute to 2-AG inactivation in neurons and microglia.'*

For Peer Review

We have performed all experiments and added corresponding data to the revised manuscript, including:

- MGL inhibition by JZL184. We used JZL184 at a final concentration of 5 μM to selectively inhibit MGL. Data from these experiments corroborate our previous findings with URB602.
- replacing Fig. 7C,C_1 by corresponding data upon JZL184-induced MGL inhibition.
- moving experimental data with URB602 to Supplementary Fig. 8B,B_1.
- providing Western blot data on FAAH levels in Alzheimer's (Braak II-IV and Braak VI) and age-match control tissues (Supplementary Fig. 5A-B_1),
- performing experiments with URB597 and showing that *i*) FAAH does not contribute to degrading 2-AG in Alzheimer's brain (Fig. 7D), 2) FAAH enzymatic activity decreases in Alzheimer's disease (Supplementary Fig. 8C).
- modifying our statement on the importance of the subcellular segregation of MGL activities to particularly focus on 2-AG inactivation that targets transmembrane receptors during retrograde signalling.

Q3: *'van der Stelt et al., 2006, also showed that a late decrease of anandamide levels in the ipislateral hippocampus occurs in rats injected with Aβ(1-42). Did the authors measure metabolic enzymes for anandamide at all? Likewise, did the authors measure CB2 expression or that of TRPV1 (another endocannabinoid target recently suggested to participate in memory control, see Micale et al., Pharmacol Res 2010). Even negative results should be provided if obtained by the authors. At any rate this previous finding of the changes of the other endocannabinoid (going in an opposite direction to 2-AG) should be quoted'*

During the revision process, we have performed extensive experimentation to extend existing knowledge on modifications to anandamide metabolism and signalling in Alzheimer's disease. Our results include:

- Western analysis of FAAH levels (AEA degradation) in Alzheimer's (Supplementary Fig. 5A-B_1),
- Western analysis of NAPE-PLD levels (one of the putative enzymes involved in AEA synthesis) in Alzheimer's subjects and age-matched controls (Supplementary Fig. 5A,C,C_1),
- histochemical localization of TRPV1-like immunoreactivity in human brain and identification of a postsynaptic (dendritic) expression locus (Supplementary Fig. 5D-E_2). We have been advised on the choice of anti-TRPV1 antibody, including knock-out verification of signal specificity by Drs. Vincenzo Di Marzo and Istvan Katona, leading experts in the study of endovanilloid/endocannabinoid signalling networks,
- TRPV1 ligand binding experiments, showing the lack of a progressive change in TRPV1 binding in Alzheimer's,
- reference to Micale *et al*., 2010,
- an introductory statement at the 'Results' section to justify why these data are only showed in Supplementary Information,
- detailed description of the methods involved,
- references to our recent work (Halleskog *et al*., Glia, 2011) showing increased CB_2 cannabinoid receptor expression in Alzheimer's disease,
- highlighting differential modifications to 2-AG and AEA signalling in the 'Abstract'.

For Peer Review

Q4: *'no idea of the post-mortem delay of the human brains used for this study is given in the Methods. This is an important issue since post-mortem can alter the levels of endocannabinoids.'*

- *Post-mortem* delay is one key parameter shown in Supporting Table 1 (please see 'PMD' label).
- We have referenced the work of Miklos Palkovits and colleagues showing opposing and regional *post-mortem* changes in AEA and 2-AG levels in human brain.
- We have provided regression plots for each biochemical marker (see: Fig. $6A_2$, Supporting Figs. S1, S4, S5) to exclude a relationship between protein levels and *post-mortem* delay.

For Peer Review

Associate Editors: Professors **Dimitri Kullmann** & **Patrick Chinnery**

Molecular reorganization of endocannabinoid signalling in Alzheimer's disease

(***Running title***: 2-AG signalling in Alzheimer's disease)

Jan Mulder[1,#], Misha Zilberter[2,+], Susana Pasquaré[3,4,+], Alán Alpár[1,+], Gunnar Schulte[5], Samira G. Ferreira[6], Attila Köfalvi[6], Ana M. Martín-Moreno[3], Erik Keimpema[1], Heikki Tanila[7], Masahiko Watanabe[8], Ken Mackie[9], Tibor Hortobágyi[10], Maria L. de Ceballos[3] & Tibor Harkany[1,2,*]

[1]European Neuroscience Institute at Aberdeen, University of Aberdeen, Aberdeen AB25 2ZD, United Kingdom; [2]Division of Molecular Neurobiology, Department of Medical Biochemistry and Biophysics and [5]Section for Receptor Biology & Signaling, Department of Physiology & Pharmacology, Karolinska Institutet, S-17177 Stockholm, Sweden; [3]Department of Cellular, Molecular and Developmental Neuroscience and CIBERNED, Cajal Institute, CISC, Madrid, Spain; [4]Instituto de Investigaciones Bioquímicas de Bahía Blanca, Universidad Nacional del Sur and CONICET, Bahía Blanca, Argentina; [6]Center for Neurosciences & Cell Biology, University of Coimbra, 3004-517 Coimbra, Portugal; [7]A. I. Virtanen Institute, University of Eastern Finland, F-70211 Kuopio, Finland; [8]Department of Anatomy, Hokkaido University School of Medicine, Sapporo 060-8638, Japan; [9]Gill Center for Neuroscience and Department of Psychological & Brain Sciences, Indiana University, Bloomington, IN 47405, USA and [10]Department of Clinical Neuroscience, Institute of Psychiatry, King's College London, London SE5 8AF, United Kingdom

[+]These authors contributed equally to the present study.

[#]Present address: Science for Life Laboratory, Department of Neuroscience, Karolinska Institutet, S-17177, Stockholm, Sweden

* Corresponding Author: **Dr. Tibor Harkany**, Division of Molecular Neurobiology, Department of Medical Biochemistry and Biophysics, Scheeles väg 1:A1, Karolinska Institutet, S-17177 Stockholm, Sweden; ***telephone***: +46 8 524 87835; ***fax***: +46 8 341 960; ***e-mail***: Tibor.Harkany@ki.se

Total number of words (excl. citations): **7211**

Number of figures: **8**

Supplementary material: Author contributions, supplementary text (detailed methods & figure legends), 10 supplementary figures, 2 supplementary tables.

For Peer Review

Acknowledgments:

The authors thank B. Cravatt (The Scripps Research Institute) for $MGL^{-/-}$ mouse brains, J. Jankowsky and D. Borchelt (John Hopkins University) for colony founders of the APdE9 strain, A. Avelino (University of Porto) for $TRPV_1^{-/-}$ mice, W. Härtig (University of Leipzig) for GFAP-Cy3 antibody, B. Penke and L. Fülöp (University of Szeged) for Aβ(1-42) peptide, R. Hessling and J. Lindenau (Carl Zeiss) for advice on quantitative immunofluorescence analysis, Y. Zilberter (INSERM U751) and A. Fisahn (Karolinska Institutet) for help with electrophysiology, V. Di Marzo for advice on anti-$TRPV_1$ antibodies, R.A. Ross (University of Aberdeen), A. Bacci (European Brain Research Institute, Rome) and I. Katona (Institute of Experimental Medicine, Hungarian Academy of Sciences) for constructive criticism and discussions.

This work was supported by the Scottish Universities Life Science Alliance (SULSA; THa), European Molecular Biology Organization Young Investigator Programme (THa), Swedish Medical Research Council (GS, THa), Alzheimer's Research Trust UK (THa), Alzheimer's Association (KM, THa), European Commission (HEALTH-F2-2007-201159; HT, THa), National Institutes of Health grants (DA023214 (THa), DA011322 (KM), and DA021696 (KM)), Fundação para a Ciência e a Tecnologia (PTDC/SAU-OSM/105663/2008; AK; SFRH/BD/33467/2008; SGF), the Spanish Ministry of Science and Innovation (SAF2005-02845; MLC) and Madrid Council (S-BIO/0170/2006; MLC). JM and AMM-M received fellowship support from the Alzheimer's Research Trust UK and The Spanish Ministry of Science and Innovation, respectively.

For Peer Review

ScholarOne, 375 Greenbrier Drive, Charlottesville, VA, 22901 Support (434) 964 4100

Abstract

Retrograde messengers adjust the precise timing of neurotransmitter release from the presynapse, thus modulating synaptic efficacy and neuronal activity. 2-Arachidonoyl glycerol (2-AG), an endocannabinoid, is one such messenger produced in the postsynapse that inhibits neurotransmitter release upon activating presynaptic CB_1 cannabinoid receptors (CB_1Rs). Cognitive impairment in Alzheimer's disease (AD) is due to synaptic failure in hippocampal neuronal networks. We hypothesized that errant retrograde 2-AG signalling impairs synaptic neurotransmission in AD. Comparative protein profiling and quantitative morphometry showed that overall CB_1R protein levels in the hippocampi of AD patients remain unchanged relative to age-matched controls, and CB_1R^+ presynapses engulf β-amyloid (Aβ)-containing senile plaques. Hippocampal protein concentrations for ***sn***-1-diacylglycerol lipases α and β (DAGLα/β), synthesizing 2-AG, significantly increase in definite AD (Braak stage VI), with ectopic DAGLβ expression found in microglia accumulating near senile plaques and apposing CB_1R^+ presynapses. We find that microglia expressing two 2-AG-degrading enzymes, serine hydrolase α/β-hydrolase domain-containing 6 (ABHD6) and monoacylglycerol lipase (MGL), begin to surround senile plaques in probable AD (Braak stage III). However, AD pathology differentially impacts ABHD6 and MGL in hippocampal neurons: ABHD6 expression ceases in neurofibrillary tangle-bearing pyramidal cells. In contrast, pyramidal cells containing hyperphosphorylated tau retain MGL expression, although at levels significantly lower than in neurons lacking neurofibrillary pathology. Here, MGL accumulates in CB_1R^+ presynapses. Subcellular fractionation revealed impaired MGL recruitment to biological membranes in ***post-mortem*** AD tissues, suggesting AD-related modifications to terminating 2-AG signalling. We have experimentally confirmed that altered 2-AG signalling could contribute to synapse silencing in AD by demonstrating significantly prolonged depolarization-induced suppression of inhibition when superfusing mouse hippocampi with Aβ. We propose that the temporal dynamics and cellular specificity of molecular rearrangements impairing 2-AG availability and actions may differ from those of anandamide. Thus, enhanced endocannabinoid signalling, particularly around senile plaques, can exacerbate synaptic failure in AD.

Keywords: glia / human / neurodegeneration / retrograde signalling / synapse

For Peer Review

ScholarOne, 375 Greenbrier Drive, Charlottesville, VA, 22901 Support (434) 964 4100

Introduction

Alzheimer's disease (AD) is the most common form of age-related dementia. Although two competing hypothesis exist as to the molecular sequel behind neuronal demise in AD (Small and Duff 2008), the ultimate and invariable outcome of both intracellular tau hyperphosphorylation, and overt production and extracellular release of β-amyloid (Aβ) is impaired synaptic communication, particularly in the hippocampus (Oddo ***et al.,*** 2003; Walsh and Selkoe 2004). Oligomeric Aβ can target excitatory synapses (Shemer ***et al.,*** 2006), where Aβ disrupts the molecular machinery underpinning both presynaptic neurotransmitter release and postsynaptic responsiveness, thus impairing various forms of short- and long-term synaptic plasticity (Shemer ***et al.,*** 2006; Walsh ***et al.,*** 2002). A causal relationship between Aβ-induced NMDA and AMPA receptor removal and dephosphorylation (Gu ***et al.,*** 2009; Kamenetz ***et al.,*** 2003; Hsieh ***et al.,*** 2006; Snyder ***et al.,*** 2005) and impaired intracellular Ca^{2+} signalling in the postsynapse (Kuchibhotla ***et al.,*** 2008), predominantly in dendritic spines receiving excitatory inputs, has been identified as a determinant of Aβ-induced synaptic dysfunction.

The temporal dynamics of neurotransmitter release at both excitatory and inhibitory synapses are controlled by retrograde signalling networks (Alger 2002), with retrograde messengers liberated from the subsynaptic dendrite in temporal cohesion with postsynaptic spike timing (Kano ***et al.,*** 2009). Endocannabinoid signalling is one such mechanism widely distributed in rodent (Katona ***et al.,*** 2006), primate (Harkany ***et al.,*** 2005) and human brains (Ludanyi ***et al.,*** 2010). Transgenic analyses (Gao ***et al.,*** 2010; Tanimura ***et al.,*** 2010) reveal that 2-arachidonoyl glycerol (2-AG) is a particularly efficacious endocannabinoid to tune synaptic communication in the hippocampus. The canonical pathway of 2-AG metabolism posits 2-AG synthesis by Ca^{2+}-dependent ***sn***-1-diacylglycerol lipases α and β (DAGLs) (Bisogno ***et al.,*** 2003), with DAGLs anchored at the neck of dendritic spines (Uchigashima ***et al.,*** 2007). Once released, 2-AG engages CB_1 cannabinoid receptors (CB_1Rs) at glutamatergic as well as GABAergic presynapses (Kano ***et al.,*** 2009). Monoacylglycerol lipase (MGL) (Dinh ***et al.,*** 2002) and the serine hydrolase α/β-hydrolase domain-containing 6 (ABHD6) are recruited to pre- (Hashimotodani ***et al.,*** 2007) and postsynaptic sites (Marrs ***et al.,*** 2010), respectively, to terminate 2-AG signalling.

Age-related learning and memory deficits upon CB_1R deletion (Bilkei-Gorzo ***et al.,*** 2005) or phytocannabinoid administration (Wise ***et al.,*** 2009) illustrate the physiological significance of endocannabinoid signalling in the aging brain. In AD, endocannabinoids may exert dual roles (Bisogno and Di Marzo 2008): increased endocannabinoid availability appears beneficial in reducing pro-inflammatory microglia transformation and activity through a CB_2 cannabinoid receptor (CB_2R)-dependent mechanism (Ramirez ***et al.,*** 2005; Halleskog ***et al.,*** 2011). Alternatively, CB_1R modulation can gate Aβ neurotoxicity and protect against Aβ-induced amnesia in hippocampal learning tasks (Mazzola ***et al.,*** 2003; Micale ***et al.,*** 2010). Whilst CB_1R activation during ongoing neurodegeneration clearly improves cognitive outcome by inhibiting neuronal apoptosis and gliosis,

For Peer Review

CB_1R agonist administration during advanced neurodegeneration could instead worsen Aβ-induced neuronal demise by inhibiting residual neuronal activity (van der Stelt ***et al.,*** 2006). Nevertheless, experimental evidence unequivocally identifying the impact of Aβ on endocannabinoid-mediated forms of hippocampal synaptic plasticity is as yet lacking.

Modifications to CB_1R expression and signalling efficacy in AD are ambiguous (Westlake ***et al.,*** 1994; Lee ***et al.,*** 2010). In addition, coordinated expression and subcellular distribution of CB_1Rs, DAGLs, ABHD6 and MGL, and their relationship to retrograde signalling in AD remain essentially unexplored. We hypothesized a functional relationship between errant 2-AG signalling and synaptic impairment in AD: Aβ could impact Ca^{2+}-dependent 2-AG synthesis and release, while cytoskeletal damage might alter subcellular DAGL, MGL and/or ABHD6 recruitment, thus disrupting the dynamics of 2-AG signalling. Irrespective of the primary pathogenic cascade, molecular reorganization of 2-AG signalling networks might be detrimental to maintain synaptic responsiveness and plasticity. We have tested these hypotheses by dissecting the molecular machinery of 2-AG signalling in ***post-mortem*** human brains with AD pathology, in transgenic mouse models and upon acute Aβ challenge to hippocampal neurons.

Materials & Methods

***Human tissues*.** Hippocampal tissue samples were obtained from AD patients and age-matched controls (without clinical signs of neuropsychiatric disease) at the London Neurodegenerative Diseases Brain Bank (Table S1). Neuropathological and histochemical examination, including classification of Aβ plaque burden (Fig. S1A), tau pathology (Table S1) and synaptic impairment (Fig. S1B-E), was performed as described (Supplementary Information). Tissue blocks or entire hippocampi were immersion fixed in 4% paraformaldehyde in 0.1M phosphate buffer (PB, pH7.4) for 48-72h at 4 ^{o}C followed by long-term storage in PB to which 0.1% NaN_3 had been added. Alternatively, native tissue blocks (2-3 cm^3) of ~1 cm thickness from the other hemisphere were stored at -80 ^{o}C until processing for biochemical analysis.

APdE9 mice*.** Male APPswe/PS1dE9 (APdE9) transgenic mice and littermate controls (WT) aged 7 or 14 months were used (n*** = 26 animals in total; ethical documentation of ***in vivo*** studies can be found in Supplementary Information). APdE9 mice were generated by heterozygously co-expressing mutant amyloid precursor protein (APP, KM593/594NL) and an exon 9 deletion variant of presenilin 1 (PS1), both associated with familial AD (Jankowsky ***et al.,*** 2004).

Immunohistochemistry and imaging*.** Multiple immunofluorescence histochemistry on human temporal lobe sections containing the hippocampal formation was performed by applying select combinations of primary antibodies (Fig. S2, Table S2) according to standard protocols (Halleskog ***et al., 2011; Harkany ***et al.,*** 2003; Harkany ***et al.,*** 2005; Keimpema ***et al.,*** 2010). Single ***x-y*** plane or orthogonal ***z*** image stacks were captured, after quenching tissue autofluorescence (Fig. S3), by

ScholarOne, 375 Greenbrier Drive, Charlottesville, VA, 22901 Support (434) 964 4100

For Peer Review

laser-scanning microscopy (710LSM, Zeiss) as described in Supplementary Methods. Three-dimensional reconstruction and rendering of dendrite segments to specify the spatial relationships of DAGLα/DAGLβ or MGL immunoreactivities was performed using the BioVis3D reconstruction package (Montevideo, Uruguay) according to specific imaging criteria (Supplementary Methods).

Acute brain slice preparation and electrophysiology. Patch clamp recordings, differential interference contrast imaging and stimulus protocols in hippocampal slices from postnatal 14- or 16-day-old mouse brains were performed as described (Supplementary Methods).

***Western blotting*.** Protein samples prepared from human or mouse hippocampi were analyzed under denaturing conditions. Western blot analysis was undertaken as described (Supplementary Methods) with primary antibodies listed in Table S2. Blots were scanned on a Lycor Odyssey-IR imager and quantified by using ImageJ1.32j.

WNT-3A stimulation and gene expression profiling in microglia. Primary microglia were isolated from newborn mouse brains (Halleskog ***et al.,*** 2011). Cultures typically contained >95% microglia, as validated by cytochemistry using ***Griffonia simplicifolia*** isolectin B4 (Sigma). Three independent harvests of primary microglia were seeded in six well plates and challenged 24h after plating. Serum-deprived microglia were treated with either 0.1% BSA (vehicle control) or 300 ng/ml recombinant WNT-3A for 6h. RNA was prepared and analyzed on an Affimetrix Mouse Gene 1.0 ST Array (Halleskog ***et al.,*** 2011). Real-time, quantitative PCR (qPCR) analysis was performed as reported earlier with custom-designed primers (Keimpema ***et al.,*** 2010). N13 microglia-like cells (Halleskog ***et al.,*** 2011) were exposed to fibrillar Aβ(1-42) at 100 nM final concentration for 48h.

2-AG degradation in Alzheimer's brains. Biochemical studies were conducted in an independent cohort of human cortical samples (see Supplementary Information for details). Neurohistopathological evaluation and disease classification were as above. Frontal cortices were mechanically homogenized (10%) in Tris HCl (20 mM, pH 7.2) containing 0.32 M sucrose and protease inhibitors, and centrifuged to eliminate nuclei and cellular debris (1,000***g***, 10 min, 4 ^{o}C). Supernatants were ultracentrifuged (100,000***g***, 60 min, 4ºC) to obtain membrane and soluble fractions, both presenting 2-AG-degrading activity (Blankman ***et al.,*** 2007). Protein concentrations were determined by Bradford's colorimetric method (Bradford 1976). 2-AG-degrading activity was assessed by incubating sample fractions (10 µg protein) in a solution containing Tris HCl (10 mM, pH 7.2), 1 mM EDTA, fatty acid-free BSA (1.25 mg/ml), [^{3}H]2-AG ([1,2,3-^{3}H]glycerol, 25 µM, 40 Ci/mmol specific activity; New England Nuclear) in a final volume of 200 µl for 15 min at 37ºC. Identical conditions were used to assess anandamide (AEA) degrading activity using [^{3}H]AEA ([1-^{3}H]ethanolamine, 25 µM, 40 Ci/mmol specific activity; ARC Inc). Reactions were stopped by 400 µl chloroform:methanol (2:1, v/v) and vigorous vortexing. Fractions either containing [1,2,3-^{3}H]glycerol/[1-^{3}H]ethanolamine (top) or non-hydrolyzed [^{3}H]2-AG/[^{3}H]AEA (bottom/organic) were separated by centrifugation (2,000***g***, 10 min, 4 ^{o}C), transferred into scintillation vials and radioactivity measured by liquid scintillation spectroscopy. Actual experimental conditions were

ScholarOne, 375 Greenbrier Drive, Charlottesville, VA, 22901 Support (434) 964 4100

For Peer Review

selected from pilot experiments assaying the relationship of substrate and protein concentrations to identify optimal 2-AG-degrading enzymatic activity (***data not shown***), and favoured assay conditions allowing ~50% of 2-AG converted into glycerol in membrane fractions from control brains. JZL184 (5 μM; (Long ***et al.,*** 2009)) or URB602 (1 mM; (King ***et al.,*** 2007)) served to determine the specific contribution of MGL to 2-AG degradation. URB597 (20 nM; (Mor ***et al.,*** 2004)) was used to test the changes in AEA-degrading activity in AD brains. Enzyme activity was expressed as pmol [1,2,3-^{3}H]glycerol formed/mg protein/15 min and [^{3}H]ethanolamine formed/mg protein/15 min, respectively. Human Aβ(1-40) was from PolyPeptides (France) and diluted and used as described for Aβ(1-42) (Supplementary Methods). Methods to assess $TRPV_1$ transient receptor potential cation channel binding in ***post-mortem*** hippocampal samples are provided in Supplementary Information.

Statistical analysis**.** Data were analyzed using SPSS 17.0 (SPSS Inc.). Integrated optical density of immunoreactive targets in Western blot experiments, and decay constants from electrophysiology measurements were evaluated using Student's ***t***-test (on independent samples). Linear regression analysis of CB_1R, DAGLs and MGL isoforms, synaptic markers, disease stages and/or ***post-mortem*** delay (Fig. S4) was performed by defining Pearson's correlation coefficient. Data were expressed as mean ± s.e.m. A ***p*** value of < 0.05 was considered statistically significant.

Results

Here, we focus on molecular rearrangements of 2-AG signalling networks affecting synaptic neurotransmission during AD pathology in human brain and experimental models of Aβ synaptotoxicity. Nevertheless, we present data on N-acyl-phosphatidylethanolamide-specific phospholipase D (NAPE-PLD), fatty-acid amide hydrolase (FAAH) and $TRPV_1$ significantly extending available knowledge on AD-related modifications to AEA signalling (Ramirez ***et al.,*** 2005; Benito ***et al.,*** 2003) in Fig. S5. Changes of CB_2R expression in this AD cohort have recently been reported elsewhere (Halleskog ***et al.,*** 2011).

CB_1R expression is unchanged in Alzheimer's disease

Cellular mapping studies combined with ultrastructural analysis unequivocally position CB_1Rs presynaptically in both excitatory and inhibitory nerve endings of rodent (Katona ***et al.,*** 2006), primate (Harkany ***et al.,*** 2005) and human hippocampus (Ludanyi ***et al.,*** 2010). However, the impact of aging or AD pathology on CB_1R expression and (sub-)cellular distribution in the human hippocampus remain ambiguous (Westlake ***et al.,*** 1994; Lee ***et al.,*** 2010).

We have studied clinicopathologically-verified patient material consisting of 10 subjects classified as ***controls*** (≤ Braak I stage) aged 52-96 years, 9 subjects presenting Braak stage III/IV pathology (B2-4) and aged 72-105 years, as well as 9 patients with pathological indices of Braak stage VI (B6) and aged 69-90 years (Table S1). B2-4 and B6 patients had significantly increased Aβ levels (Fig. S1A)

ScholarOne, 375 Greenbrier Drive, Charlottesville, VA, 22901 Support (434) 964 4100

For Peer Review

and synaptic modifications as suggested by decreased levels of synaptosomal-associated protein of 25 kDa (SNAP25) (Garbelli ***et al.,*** 2008) and PSD95 (Sampedro ***et al.,*** 1982), pre- and postsynaptic markers, respectively (Fig. S1C,D).

Western analysis demonstrated CB_1R expression in the aged human hippocampus (Fig. 1A). CB_1Rs were of 52 kDa molecular weight suggesting that mature, non-truncated receptors were detected in ***post-mortem*** brain homogenates (Fig. 1A,B). CB_1R levels remained unchanged in patients with B2-4 or B6 pathology (Fig. 1B). We performed correlation analysis between SNAP25 and CB_1Rs to test whether individual variations in CB_1R levels may be related to those of SNAP25 or PSD95 at excitatory synapses. However, CB_1R expression did not correlate with that of either SNAP25 (Fig. S1E) or PSD95 (***data not shown***).

Immunohistochemistry revealed a dense meshwork of CB_1R^+ axons with CB_1Rs particularly enriched in presynapses that contained synaptophysin, a pan-presynaptic marker (Schubert ***et al.,*** 1991), in the strata pyramidale and radiatum of the CA1-3 subfields (Fig. 2A,B; Fig. S6A-A_3), and the stratum moleculare of the fascia dentata (Fig. S7A) of aged human subjects. High-resolution laser-scanning microscopy confirmed that CB_1Rs localized to synaptophysin$^+$ presynapses targeting either the perisomatic segment (Fig. 2C-C_3) or distal dendrites (Fig. 2D-D_3) of pyramidal neurons. Accordingly, CB_1R^+/microtubule-associated protein 2$^+$ ($MAP2^+$) double-labelled structures were not observed (MAP2 is a ubiquitous somatodendritic marker of neurons (Peng ***et al.,*** 1986)). CB_1R distribution in B2-4/B6 cases was unaltered: CB_1R^+ axons coursed in both soma-rich laminae, including the stratum granulosum (Fig. 2E) and receptive fields (e.g., stratum moleculare; Fig. 2E). Notably, CB_1R^+ axons appeared to engulf senile plaques (Fig. 2E_1-E_3) with CB_1R^+ bouton-like varicosities commonly situated within the Aβ-dense plaque cores. Therefore, we conclude that CB_1R expression and axonal distribution remain largely unchanged in AD, as compared to age-matched controls.

DAGLβ but not DAGLα redistribution in Alzheimer's disease

The long-held view of 2-AG biosynthesis posits DAGLs as Ca^{2+}-regulated enzymes synthesizing this endocannabinoid (Bisogno ***et al.,*** 2003). DAGLs reside in the perisynaptic annulus, a proximal zone surrounding the postsynaptic density at CB_1R^+ excitatory synapses (Uchigashima ***et al.,*** 2007), also in human brain (Ludanyi ***et al.,*** 2010). Epilepsy-induced sclerotic neurodegeneration in human brain reduces DAGLα but not DAGLβ expression by ~60% suggesting that impaired 2-AG synthesis may occur under disease conditions (Ludanyi ***et al.,*** 2008).

We have tested this possibility by analyzing DAGLα and DAGLβ protein expression in B2-4, B6 and age-matched control brains (Fig. 1A and C,C_1). We find a gradual increase in the protein levels of both enzymes, paralleling AD progression (DAGLα: 145.4 ± 50.9% of control, ***n*** = 7 [B2-4], 193.9 ± 41.9% of control, ***n*** = 6, ***p*** = 0.076 ***vs***. control [B6]; DAGLβ: 155.1 ± 29.1% of control ***n*** = 7 [B2-4]; 175.9 ± 23.7% of control ***n*** = 6, ***p*** = 0.015 ***vs***. control [B6]; Fig. 1C,C_1). Next, we have explored whether DAGLα expression correlates with that of DAGLβ. Analysis of discrete subject cohorts

ScholarOne, 375 Greenbrier Drive, Charlottesville, VA, 22901 Support (434) 964 4100

For Peer Review

revealed the lack of an expressional relationship between the two enzymes in control or B2-4 brains (Fig. 1D). In contrast, we find a strong inverse relationship between DAGLα and DAGLβ protein levels in B6 brains (Fig. 1D). These findings suggest that either DAGLα is replaced by DAGLβ postsynaptically or DAGLα and DAGLβ segregate to distinct cell types with independent expressional control for DAGLs in AD.

Multiple immunofluorescence histochemistry using affinity-pure antibodies (Fig. S2), and appropriate histochemical (Fig. S3)/imaging (Fig. S6B) controls, in the CA1-CA3 of the aged human hippocampus and fascia dentata (Fig. 3A and S7B-B_2) revealed DAGLα$^+$ and DAGLβ$^+$ puncta along the dendritic trees of pyramidal neurons (Fig. 3B-B_2) and granule cells (Fig. S7B-B_2). The density of DAGLα$^+$ puncta exceeded that of DAGLβ$^+$ structures (Fig. 3B-B_2,C_1-C_3 and E_1). High-resolution microscopy along individual MAP2$^+$ dendrite segments showed frequent DAGLα/DAGLβ co-localization (Fig. 3C-C_3). Three-dimensional reconstruction of select dendrites upon capturing consecutive images in orthogonal stacks verified that both DAGLα and DAGLβ were localized within dendritic compartments and accumulated at the stem of dendritic spines (Fig. 3D,D_1). Quantitative morphometry showed that the Pearson's correlation coefficient of dual-labelled structures only marginally differs from 0, suggesting limited (if any) positive correlation (co-regulation) between signal intensities for DAGLα and DAGLβ (Fig. 3E). We quantitatively verified a higher density of DAGLα than DAGLβ along apical dendrite profiles of pyramidal cells in the CA1 stratum radiatum (Fig. 3E_1 and see 3B-B_2). Here, 24.0 ± 3.9% of DAGLα$^+$ postsynaptic (MAP2$^+$) puncta contained DAGLβ (Fig. 3E_2). In contrast, 47.7 ± 3.1% of DAGLβ$^+$ structures were dual labelled, suggesting that DAGLα can drive DAGLβ recruitment to sites of co-localization.

The distribution of DAGLα immunoreactivity remained largely unchanged in AD, including around senile plaques where DAGLα immunoreactivity has been found scattered in Aβ-laden territories (Fig. 3F). In contrast, DAGLβ immunoreactivity accumulated in small-diameter cell-like structures associated with senile plaques and apposing CB_1R^+ axons (Fig. 3F_1,F_2). By using ionized Ca^{2+}-binding adaptor molecule-1 (IBA-1) we demonstrate that activated microglia (Xu ***et al.,*** 2008) frequently surrounding senile plaques express DAGLβ in B6 brains (Fig. 3G-G_2). Together, these findings suggest that both DAGLs can co-exist in dendritic spines of hippocampal neurons in the aged human hippocampus. In addition, microglia represent a novel cellular component participating in 2-AG biosynthesis in AD. The specific accumulation of DAGLβ$^+$ microglia around senile plaques could lead to the focal enhancement of 2-AG signalling, affecting neuronal excitability (Busche ***et al.,*** 2008), unless compensated by molecular rearrangements in 2-AG degrading enzymatic capacity in AD brains.

ABHD6 expression in Alzheimer's disease

ABHD6 is a recently characterized serine hydrolase degrading 2-AG in the nervous system (Marrs ***et al.,*** 2010). While activity-based protein profiling identified ABHD6 as a candidate to hydrolyze 2-

ScholarOne, 375 Greenbrier Drive, Charlottesville, VA, 22901 Support (434) 964 4100

For Peer Review

AG in microglia-like cells, follow-up histochemical studies in rodent brain identified the somatodendritic domain of neurons as major, postsynaptic foci accumulating ABHD6 (Marrs ***et al.,*** 2010). Western blotting demonstrated that ABHD6 protein is present in the aged human hippocampus (Fig. 1A,E). Comparative analysis revealed unchanged ABHD6 levels across B2-4, B6 and age-matched control tissues (Fig. 1A,E). However, these findings do not exclude the possibility that neuronal and glial ABHD6 expression differentially contribute to total ABHD6 levels in control ***vs***. AD brains.

We show, by using affinity-pure anti-ABHD6 antibodies (Marrs ***et al.,*** 2010), ABHD6-like immunoreactivity decorating the somatic membrane and apical dendrites of pyramidal cells in the hippocampus of aged humans (Fig. 4A-A_2). We find AD progression associated with a gradual decrease of ABHD6-like immunoreactivity in hippocampal neurons (Fig. 4B,B_1). Notably, the distribution of ABHD6 and AT8, the latter identifying tau hyperphosphorylated at Ser202/Thr205 residues in degenerating neurons (Goedert ***et al.,*** 1989), is mutually exclusive in B6 brain, suggesting that AD-related cytoskeletal damage can arrest ABHD6 expression (Fig. 4C,C_1). In contrast, $ABHD6^+$ small diameter, multipolar cells lacking MAP2 accumulate in AD brains (Fig. 4B,B_1). We demonstrate that microglia can express ABHD6 (particularly in B6) by revealing an intricate network of $ABHD6^+$/$IBA1^+$ but $MAP2^-$ microglia end-feet scattered around hippocampal neurons (Fig. 4B_1,B_2). In addition, we find that Aβ-containing neuritic plaques attract $ABHD6^+$/$IBA1^+$ microglia, which accumulate both around and within senile plaques (Fig. 4D-D_3). In summary, our data uncover a postsynaptic expression site for ABHD6 in neurons of the aged human hippocampus, as well as widespread ABHD6 expression by activated microglia in AD.

MGL is recruited to presynapses and astroglia in aged human brain

Although MGL has many substrates (Nomura ***et al.,*** 2010), it is considered to be the major enzyme inactivating >80% of 2-AG in adult rodent brain (Blankman ***et al.,*** 2007). Chronic CB_1R desensitization due to increased 2-AG but not other bioactive lipid levels in $MGL^{-/-}$ mice confirms that 2-AG is primarily degraded by MGL in the nervous system (Schlosburg ***et al.,*** 2010). MGL is localized to presynapses in rodent (Dinh ***et al.,*** 2002) and human brains (Ludanyi ***et al.,*** 2010). However, MGL expression and subcellular localization during aging and AD remain elusive.

We find, by using two antibodies directed against non-overlapping MGL epitopes and validated in $MGL^{-/-}$ mice ((Keimpema ***et al.,*** 2010); Fig. S2), prominent MGL immunoreactivity at three sites in the aged human hippocampus: ***i***) the somatic region of dentate granule cells (Fig. 5A-B_1) and CA1 pyramidal neurons (Fig. 5C); ***ii***) nerve endings concentrating in the stratum moleculare of the dentate fascia (Fig. 5B_1) and the stratum radiatum of the CA subfields (Fig. 5C); ***iii***) astroglia-like cells randomly distributed across hippocampal laminae (Fig. 5B_1,H). Somatic MGL immunoreactivity in pyramidal cells is primarily present in the cytosol (Fig. 5D-D_3). Although moderate MGL immunoreactivity was occasionally seen in the proximal segment of apical dendrites, overall MGL is absent in the dendritic tree of principal neurons (Fig. 5C). MGL ubiquitously co-exists with CB_1Rs in

ScholarOne, 375 Greenbrier Drive, Charlottesville, VA, 22901 Support (434) 964 4100

For Peer Review

presynapse-like puncta apposing pyramidal cells' dendrites, suggesting that MGL retains its presynaptic localization in the aged human hippocampus (Fig. 5E-E_3). We have confirmed our histochemical findings by three-dimensional reconstruction of pyramidal cell dendrites and perisynaptic astroglia end-feet (Fig. 5F,F_1) and find a complete lack of co-localization between MGL and MAP2, a somatodendritic marker of neurons (Peng ***et al.,*** 1986), as well as glial fibrillary acidic protein (GFAP) in astroglia.

Next, we asked whether MGL and CB_1Rs co-exist throughout the hippocampal parenchyma or are only recruited to synaptic terminal-like specializations apposing $MAP2^+$ somatodendritic elements. Quantitative immunofluorescence morphometry (Fig. S6C) revealed moderate correlation between the intensities of MGL and CB_1R immunoreactivities at sites of co-localization (Fig. 5G), suggesting that recruitment of the two markers to the same sites may proceeds largely independently of one another. Next, we find that the area occupancy of MGL immunoreactivity exceeds that of the CB_1R (Fig. 5G_1) implying differences between the axonal transport, overall expression levels or subcellular recruitment of MGL and CB_1R in the aged human brain. Accordingly, we find that only 12.6 ± 1.2% of MGL^+ structures are labelled for CB_1Rs. In contrast, 25.1 ± 2.2% of CB_1R immunoreactivity co-localizes with that of MGL (Fig. 5G_2). Thus, our data suggest that MGL can accumulate in CB_1R^+ presynapses in the human hippocampus to terminate retrograde 2-AG signalling.

We used Western analysis to compare MGL protein levels in B2-4 and B6 patients as well as age-matched controls, and find significantly increased levels of both major MGL isoforms in B6 brains (Fig. 1A,F,F_1). Correlation analysis substantiated a positive relationship between expression levels of the two major MGL isoforms (Fig. 1G). Next, we have refined these results by verifying that advancing Braak stages in AD couples to gradually increased MGL levels in an isoform (Fig. 6A,A_1) and ***post-mortem*** delay (Fig. 6A_2)-independent manner. Since we performed Western analysis on total protein samples from human brain several open questions remained including: whether ***i***) increased MGL concentrations represent novel expression sites as a result of ongoing neurodegeneration as well as neuroinflammation in AD, ***ii***) defunct neurons presenting cytoskeletal abnormalities, such as hyperphosphorylated tau, lose MGL expression as seen for ABHD6, ***iii***) AD impacts the metabolic competence of MGL by impairing its recruitment to the plasmalemma.

In the Alzheimer's hippocampus, we find that MGL^+/$IBA1^+$ microglia cells accumulate around senile plaques (Fig. 6B,B_1). Although quantitative morphometry was not an objective of the present report, a clear increase in the density of MGL^+ microglia can be seen when comparing B2-4 ***vs***. B6 brains. Hippocampal principal cells – both pyramidal cells of the CA subfields and dentate granule cells – express MGL. We find that $AT8^+$ pyramidal cells retain MGL expression (Fig. 6C-C_2'), although at significantly lower levels than those without intracellular tau pathology (Fig. 6D; 121.85 ± 3.73 grey scale unit [$AT8^-$ neurons] ***vs***. 81.75 ± 8.31 grey scale unit [$AT8^+$ neurons]; $\boldsymbol{p} < 0.001$). Our data cumulatively indicate that both microglia (Fig. 6B) and astroglia (Fig. 5H) can serve as sources of MGL, and a progressive shift of MGL expression from damaged neurons to activated micro- and astroglia occurs in AD.

ScholarOne, 375 Greenbrier Drive, Charlottesville, VA, 22901 Support (434) 964 4100

For Peer Review

Gene expression profiling in mouse microglia

Activated microglia have previously been shown to express CB_2Rs in AD (Ramirez ***et al.,*** 2005; Benito ***et al.,*** 2003) or Down's syndrome (Nunez ***et al.,*** 2008), and pharmacological challenges can increase 2-AG production in this cell type (Walter ***et al.,*** 2003). However, co-existence of molecular components determining an operational 2-AG signalling network in activated microglia (that is, CB_1Rs/CB_2Rs, DAGLs, ABHD6 and MGL) capable to sustain autocrine and/or paracrine 2-AG signalling remains unknown. We performed Affymetrix gene expression profiling coupled to qPCR analysis (Fig. 7A) to test the expression of CB_1Rs, CB_2Rs, as well as 2-AG metabolic enzymes in primary mouse microglia under experimental conditions mimicking pro-inflammatory transformation in AD brains (Halleskog ***et al.,*** 2011). Under control conditions, CB_1R, CB_2R, DAGLα, DAGLβ, MGL, ABHD6 and ABHD12 expression levels exceeded the detection minimum of Affymetrix chips (***data not shown***). Microglia activation can proceed through Aβ-independent mechanisms ***in vivo*** (Halleskog ***et al.,*** 2011). Therefore, we applied WNT-3A (300 ng/ml) to induce pro-inflammatory transformation of primary mouse microglia. WNT-3A significantly increased mRNA transcript levels of interleukin 6 and tumor necrosis factor α, pro-inflammatory cytokines, relative to controls (Halleskog ***et al.,*** 2011). Simultaneously, WNT-3A reduced CB_2R, DAGLα and DAGLβ mRNA expression, whilst leaving CB_1R, MGL and ABHD6/12 expression unchanged (Fig. 7A). Quantitative PCR analysis of N18 microglia-like cells exposed to fibrillar Aβ(1-40) (100 nM ***vs***. non-treated controls), known to activate microglia (Ramirez ***et al.,*** 2005), showed significantly decreased mRNA transcript levels of CB_1Rs (-61.3 ± 3.1% of control; ***n*** = 4/condition; ***p*** = 0.017) and DAGLα (-35.2 ± 6.1% of control; ***n*** = 3-4/condition; ***p*** = 0.042) but not of other molecular components of 2-AG signalling (CB_2R: -11.6 ± 16.7%, ***p*** > 0.1, ***n*** = 4/condition; MGL: -60.3 ± 4.4%; ***p*** > 0.1, ***n*** = 3/condition; Fig. 7A). In sum, these data demonstrate that microglia can express receptor and enzyme components of 2-AG signalling networks and respond to pro-inflammatory stimuli by transcriptional regulation of rate-limiting molecular constituents of 2-AG signalling.

2-AG hydrolyzing activity in Alzheimer's disease and upon Aβ exposure

Rearrangements in 2-AG signalling networks may ultimately amplify AD-related synaptic impairment if subcellular enzyme redistribution is associated with impaired enzymatic activity. Acute Aβ infusion in the rodent hippocampus increases 2-AG concentrations, a finding that has been interpreted as an endogenous neuroprotective mechanism against Aβ-induced oxidative stress (van der Stelt ***et al.,*** 2006). Here, we have tested the alternative hypothesis that Aβ-induced increase in 2-AG levels reflects impaired 2-AG catabolism under disease conditions. We have focused on MGL as a candidate whose recruitment from the cytosol to its metabolically favoured position in the internal leaflet of the plasmalemma (Labar ***et al.,*** 2010) may be impeded by Aβ-induced oxidative damage to biological membranes in AD (Ramirez ***et al.,*** 2005; Querfurth and LaFerla 2010).

We have measured the rate of 2-AG degradation in frontal cortices of AD patients and age-matched controls by determining the amount of [1,2,3-^{3}H]glycerol after incubating membrane or cytosol

ScholarOne, 375 Greenbrier Drive, Charlottesville, VA, 22901 Support (434) 964 4100

For Peer Review

fractions with [^{3}H]2-AG. Membrane-associated 2-AG hydrolysis significantly decreased in AD, as compared with controls (28% of control, ***p*** < 0.05; Fig. 7B). In turn, 2-AG degrading capacity in the cytosol increased proportionally in AD brains relative to controls (65% of control, ***p*** < 0.05; Fig. 7B), suggesting the subcellular redistribution of 2-AG-degrading enzymes in human brain (total activity: 2468 ± 96 [control] ***vs***. 2391 ± 122 [AD] pmol 2-AG degraded/mg protein/15 min; ***p*** = 0.635, ***n*** = 9/group). Multiple enzymes, including MGL, ABHD6 and FAAH, contribute to 2-AG degradation in the adult brain (Blankman ***et al.,*** 2007). To assess MGL's specific contribution to altered 2-AG hydrolysis in AD, we have measured the rate of [^{3}H]2-AG degradation in the presence of the MGL inhibitors, JZL184 (5 μM; Fig. 7C,C_1) (Long ***et al.,*** 2009) or URB602 (1 mM; Fig. S9) (King ***et al.,*** 2007). We find that JZL184 inhibits 50.2% of 2-AG hydrolysis in membranes prepared from control brains (***p*** < 0.01; Fig. 7C). In contrast, JZL184 inhibits only 29.6% (***p*** < 0.05) of cytosolic 2-AG hydrolysis in control human cortical homogenates (Fig. 7C_1). In membrane preparations from AD brains (Fig. 7C), 11.6% of 2-AG hydrolysis activity is eliminated by JZL184, coincident with a significant reduction of MGL protein levels in the cerebral cortex of AD brains (Fig. S8A-A_2). Conversely, surplus cytosolic 2-AG hydrolysis activity in cytosol fractions of AD brains is JZL184 sensitive (32.0%; ***p*** < 0.01 ***vs***. vehicle-treated controls; Fig. 7C_1). URB602 exhibited a similar pharmacological profile (Fig. S8B,B_1). We excluded the contribution of FAAH to 2-AG degradation by showing negligible (≤10%) inhibition by URB597, a potent FAAH inhibitor (Mor ***et al.,*** 2004) (see also Fig. S8C). These data suggest that ***i***) MGL selectively undergoes subcellular redistribution, and ***ii***) the contribution of JZL184/URB602-insensitive enzymes to 2-AG degradation (e.g. ABHD6 in microglia, Fig. 4B_1) increases in AD. ***iii***) FAAH - whose activity is decreased in AD (Fig. S8C) – does not contribute to 2-AG hydrolysis in human brain ***in situ***.

Next, we hypothesized that Aβ may impact the activity of enzymes involved in 2-AG hydrolysis. Therefore, membrane and cytosolic fractions from control brains were acutely exposed to Aβ(1-40) at 1 μM final concentration. Pre-incubation with Aβ(1-40) for 10 min increased 2-AG catabolism in both membrane and cytosol fractions of human cortices (membrane: 2118 ± 73 [control; ***n*** = 9] ***vs***. 2398 ± 109 [Aβ(1-40); ***n*** = 8], ***p*** = 0.045 ; cytosol: 1038 ± 41 [control; ***n*** = 9] ***vs***. 2265 ± 112 [Aβ(1-40); ***n*** = 9], ***p*** < 0.01; pmol 2-AG degraded/mg protein/15 min; Fig. 7E) in a shallow dose-dependent fashion (Fig. 7E_1), thus mimicking changes in 2-AG hydrolyzing activity in AD brains. We find that nM Aβ(1-40) concentrations of likely pathophysiological significance (Walsh ***et al.,*** 2002) can augment 2-AG degradation (Fig. 7E_1). Thus, we conclude that Aβ contributes to the control of 2-AG catabolism in human brain, and reduces MGL's 2-AG hydrolytic capacity in membrane fractions otherwise required to inactivate 2-AG during retrograde synaptic signalling.

Aβ prolongs depolarization-induced suppression of inhibition

MGL removal from the plasma membrane could increase the duration of signalling-competent 2-AG availability following its release from postsynaptic neurons, and prolong DSI (Kano ***et al.,*** 2009). Consequently, enhanced 2-AG signalling could disrupt the balance between inhibitory and

ScholarOne, 375 Greenbrier Drive, Charlottesville, VA, 22901 Support (434) 964 4100

For Peer Review

excitatory neurotransmission. A causal relationship between high focal Aβ concentration and errant 2-AG signalling may be particularly appealing to further the mechanistic concept linking synaptic impairment to neuronal hyperexcitability (Busche ***et al.,*** 2008; Minkeviciene ***et al.,*** 2009) and excitotoxic neuronal damage (Mattson and Chan 2003).

Transgenic mouse models generating age-dependent Aβ burden in the cerebral cortex and hippocampus, e.g. APdE9 mice (Jankowsky ***et al.,*** 2004), are popular to study molecular pathomechanisms of AD. However, biochemical protein profiling suggests that APdE9 mice might be inappropriate to recapitulate molecular underpinnings of disrupted 2-AG signalling in AD (Fig. S9). Therefore, we have tested whether bath-applied Aβ(1-42) could acutely evoke AD-related subcellular rearrangements in the molecular architecture of 2-AG signalling networks. We show that non-fibrillar Aβ(1-42) – dissolved freshly in the superfusate (Minkeviciene ***et al.,*** 2009) – facilitates CB_1R removal from the cytosol (89.87 ± 2.29% of control; ***n*** = 5, ***p*** = 0.002; Fig. 8A,A_1) and enrichment in membrane fractions (123.13 ± 13.26% of control) prepared from hippocampi of juvenile wild-type mice. Subcellular DAGLα distribution appeared stochastic with a trend towards cytosolic enrichment (119.76 ± 14.59%; ***n*** = 5/condition, ***p*** > 0.1; membrane fraction: 77.48 ± 11.15%; ***n*** = 5/condition, ***p*** = 0.052; Fig. 8A,A_2). Aβ(1-42) arrested MGL in the cytosol (149.16 ± 14.59% of control; ***n*** = 6/group, ***p*** = 0.003) with unchanged membrane-associated MGL (97.95 ± 14.60% control; ***p*** > 0.8; Fig. 8A,A_3) in 1h. We hypothesized that the Aβ(1-42)-induced enhanced cell-surface availability of the CB_1R would alter 2-AG signalling. Therefore, we sought to determine whether Aβ(1-42) augments the 2-AG-mediated suppression of inhibitory neurotransmission in the hippocampus. We have studied DSI at inhibitory synapses because Aβ(1-42) accumulation in senile plaques has been shown to impair GABA neurotransmission, thus provoking focal neuronal hyperexcitability in a transgenic model of AD (Busche ***et al.,*** 2008).

Using whole-cell patch recording of CA1 hippocampal neurons in brain slices prepared from juvenile mice, we elicited a baseline DSI by briefly depolarizing (1s, from -80 to 0 mV) the pyramidal cell (Fig. 8B). DSI was detected in all control cells, had a maximal magnitude of 25.7 ± 3.1% when measured between 1-5s after postsynaptic cell depolarization and normalized to the pre-depolarization baseline (***n*** = 9). The decay time constant (τ) of DSI was 9.15 ± 1.39 (s). Bath application of Aβ(1-42) for 1h did not significantly affect maximal synaptic depression in pyramidal cells (DSI magnitude: 32.9 ± 4.4%, ***n*** = 10, ***p*** = 0.233 ***vs***. control; Fig. 8B_1,B_2). Nevertheless, the magnitude of synaptic depression upon non-fibrillar Aβ(1-42) pre-treatment was significantly different from that in control cells from 5s to 15s post-stimulus (5s: 32.5 ± 5.1% [Aβ(1-42)] ***vs***. 18.0 ± 5.1% [control], ***p*** = 0.039; 10s: 27.4 ± 4.3% [Aβ(1-42)] ***vs***. 8.8 ± 0.4% [control], ***p*** = 0.004; 15s: 19.4 ± 5.7% [Aβ(1-42)] ***vs***. 4.5 ± 4.7% [control], ***p*** = 0.047). Non-fibrillar Aβ(1-42) prolonged DSI, as indicated by a significant increase in its mean decay time constant (τ = 43.69 ± 11.99 (s), ***n*** = 10, ***p*** = 0.018 ***vs***. control). We used AM251 (1 µM) to verify that DSI was dependent on CB_1R activation (Fig. 8C, S10A,A_1). AM251 completely abolished DSI in all cases tested. Next, we sought to determine whether the Aβ(1-42)-induced enhancement of DSI is exclusively due to CB_1R activation

ScholarOne, 375 Greenbrier Drive, Charlottesville, VA, 22901 Support (434) 964 4100

For Peer Review

or if Aβ(1-42) uncovers a secondary mechanism operating at hippocampal synapses otherwise sensitive to AM251. We find that Aβ(1-42) does not induce significant DSI in the presence of AM251 (Fig. 8D,D_1). Cumulatively, our data imply that Aβ prolongs 2-AG signalling, which will impair GABAergic transmission, thus contributing to the progressive development of synaptic failure in AD.

Discussion

This report describes significant changes to ***i***) the molecular architecture, ***ii***) cellular identity and ***iii***) function of 2-AG metabolism in defined patient cohorts with clinicopathologically-verified AD, as well as in transgenic mice and acute pharmacological models of AD-like neuronal dysfunction. Although we cannot entirely rule out altered signal transduction downstream from CB_1Rs (Lee ***et al.,*** 2010), our biochemical and histochemical findings cumulatively highlight that 2-AG signalling in neurons is primarily impaired at the level of metabolic enzymatic control of 2-AG bioavailability in AD. We also propose that activated microglia, accumulating in AD brains and contributing to chronic neuroinflammation, have a fundamental role in modifying 2-AG signalling, particularly in Aβ-laden brain microdomains around senile plaques, and might impact synaptic communication.

Transsynaptic 2-AG signalling in Alzheimer's disease

Endocannabinoids and phytocannabinoids are recognized to exert profound neuroprotection in models of peripheral nerve injury (Yoles ***et al.,*** 1996), excitotoxicity (Khaspekov ***et al.,*** 2004) and neurodegeneration (Palazuelos ***et al.,*** 2009; Blazquez ***et al.,*** 2010; Ludanyi ***et al.,*** 2008) through CB_1R/CB_2R-dependent (Palazuelos ***et al.,*** 2009) or -independent mechanisms (Lastres-Becker ***et al.,*** 2005).

In microlesion models of AD, Aβ(1-42) infusion in the rat cerebral cortex significantly increases 2-AG but not AEA levels in the hippocampus (van der Stelt ***et al.,*** 2006). This Aβ(1-42)-induced elevation of 2-AG concentrations is further augmented by inhibiting endocannabinoid reuptake to reverse hippocampal neuronal damage and decrease glial activation, thus preventing the loss of memory retention (van der Stelt ***et al.,*** 2006). Our data are significant as they corroborate and notably extend the above observations by providing insights into specific AD-associated molecular rearrangements of 2-AG metabolism. We suggest that 2-AG biosynthesis may be enhanced by microglial DAGLs around Aβ-rich foci in the AD brain. In contrast, 2-AG degrading capacity in neurons could be substantially reduced if ABHD6 and MGL expressions are significantly suppressed in injured neurons with neurofibrillary pathology. Therefore, the net contribution of 2-AG signalling to suppressing presynaptic neurotransmitter release may be significantly increased. In fact, ***ex vivo*** experiments recapitulate the above scenario of Aβ-induced synaptic impairment by showing prolonged DSI at inhibitory afferents of CA1 pyramidal cells. Aβ-induced enhancement of DSI is also important to reconcile previous findings that have suggested both pre- and postsynaptic

ScholarOne, 375 Greenbrier Drive, Charlottesville, VA, 22901 Support (434) 964 4100

For Peer Review

sites of action for Aβ when disrupting spike timing-dependent plasticity at cortical synapses (Shemer ***et al.,*** 2006).

Postsynaptic NMDA and AMPA receptors are widely viewed as key molecular targets of Aβ to disrupt synaptic plasticity (Snyder ***et al.,*** 2005; Kamenetz ***et al.,*** 2003; Shemer ***et al.,*** 2006). In particular, Aβ-induced impairment of NMDA/AMPA receptor trafficking at the postsynapse can disrupt Ca^{2+} signalling in dendritic spines targeted by excitatory afferents (Snyder ***et al.,*** 2005). DAGLs accumulate at the neck of dendritic spines (Yoshida ***et al.,*** 2006) where they are anchored by homer-1 and -2 family scaffolding proteins (Jung ***et al.,*** 2007; Roloff ***et al.,*** 2010). Notably, soluble Aβ oligomers induce the disassembly of homer-containing postsynaptic clusters (Roselli ***et al.,*** 2009), thus potentially affecting the subcellular recruitment and signalling competence of DAGLs. These changes, together with increased DAGL activity upon Aβ-induced Ca^{2+} overload in neurons (provided that DAGLs are Ca^{2+}-dependent (Bisogno ***et al.,*** 2003)) and increased DAGL expression in microglia can significantly increase 2-AG availability in AD.

AD has long been viewed as a disease stemming from neuronal hypofunction. This concept has recently been challenged by demonstrating that neurons near Aβ-containing plaques are focally 'hyperactive', whilst others away from plaque-laden areas are silent (Busche ***et al.,*** 2008). Neuronal hyperactivity is suggested to be due to a relative decrease in synaptic inhibition (Busche ***et al.,*** 2008). We find that the molecular composition of 2-AG signalling networks undergoes profound modifications around Aβ-containing senile plaques in the human hippocampus in AD. These observations led us to hypothesize that if the efficacy of retrograde signalling is increased in AD then it may directly contribute to synapse silencing.

Our proof-of-concept neurophysiology experiments support this notion by showing a significant increase in DSI duration, thus suggesting that 2-AG-mediated feedback is a particular mechanism through which Aβ could disrupt inhibitory neurotransmission at GABAergic synapses. Functionally, DSI may serve to lengthen the firing duration of postsynaptic neurons by abating inhibitory inputs during periods of high excitatory activity. By prolonging DSI decay, Aβ can further extend the excitatory neurons' firing periods, thus increasing overall network excitability. Previously, we have reported (Minkeviciene ***et al.,*** 2009) that Aβ induces neuronal hyperexcitability by significantly depolarizing the resting membrane potential of excitatory neurons and lowering their response threshold. This effect is exerted without a requirement for preceding postsynaptic activation, as in the case with DSI. Thus, prolonging DSI through decay by reorganizing endocannabinoid signalling is potentially one key mechanism by which Aβ can modulate neuronal network excitability. Since inhibitory synapses are more resistant to AD than excitatory ones (Bell ***et al.,*** 2006), prolonged DSI may destabilize hippocampal networks by shifting the net balance of inhibition and excitation in favour of excitation. Thus, decreased inhibitory neurotransmission will ultimately manifest in 'hyperactivity' (Busche ***et al.,*** 2008; Minkeviciene ***et al.,*** 2009), which may explain the increased incidence of unprovoked epileptic seizures in Alzheimer's patients (Hauser ***et al.,*** 1986).

For Peer Review

ScholarOne, 375 Greenbrier Drive, Charlottesville, VA, 22901 Support (434) 964 4100

Synaptic impairment is a central feature of AD-related cognitive decline. It is widely accepted that Aβ preferentially target excitatory synapses (Lacor ***et al.,*** 2004). CB_1Rs are expressed by both inhibitory interneurons and pyramidal cells with inhibitory terminals containing exceptionally high levels of this receptor (Kawamura ***et al.,*** 2006). Our finding that CB_1R levels fail to correlate with presynaptic markers suggests that the molecular changes in 2-AG signaling networks we have identified are unlikely to reflect the overall rate of synaptic demise in moderate or severe AD. Even if Aβ induces opposing – and proportional – changes in CB_1R expression (that is, to increase CB_1R content in inhibitory but decrease CB_1R levels in excitatory terminals), the neurochemical homogeneity of perisomatic inhibitory synapses under endocannabinoid control (Kano ***et al.,*** 2009) suggest that Aβ can impose functional modifications to endocannabinoid signaling at specific synapse populations. This concept is supported by the fact that acute Aβ superfusion is unlikely to eliminate hippocampal synapses within the brief superfusion period used when studying the decay of DSI. Therefore, we propose that endocannabinoid signalling is a key neuromodulatory homeostatic system mediating adaptive responses to neurotoxic insults (Bisogno and Di Marzo 2008) and defining the dynamics of presynaptic neurotransmitter release under disease conditions.

2-AG signalling in microglia: the good, the bad or the ugly?

Microglia are central to AD pathogenesis since their activation state determines whether they are beneficial by phagocytosing cell debris or elicit neuronal injury by releasing proinflammatory cytokines. Migrating microglia express CB_2Rs whose activation suppresses proinflammatory cytokine production (Klegeris ***et al.,*** 2003). Once activated, microglia downregulate CB_2Rs, as seen upon WNT-3A challenge, to increase cytokine production. Microglia continuously monitor the functional state of synapses via the dynamic motility of their processes. Disrupting neuron-glia communication (also including astrocyes) (Rodriguez ***et al.,*** 2009) will therefore culminate in the loss of glial homeostatic control, and facilitate the onset of synaptic deficit. Thus, altered 2-AG signalling in activated microglia can have serious consequences in AD, particularly since a 2-AG 'overflow' may be viewed as a volumetric insult indiscriminately affecting synapse populations and assemblies of neurons. Overall, pathogenic modifications to 2-AG metabolism in microglia can exacerbate synaptic impairment in AD.

2-AG hydrolysis by ABHD6 and MGL in Alzheimer's disease

ABHD6 and MGL terminate surplus 2-AG to maintain temporally coordinated retrograde signalling (Marrs ***et al.,*** 2010; Dinh ***et al.,*** 2002). AD pathology will ultimately modify 2-AG signalling if it either impacts the recruitment of ABHD6 and/or MGL to signalling positions or compromises their enzymatic activity. We find that $AT8^+$ neurons cease ABHD6 expression, suggesting impaired postsynaptic 2-AG degradation when the cytoskeletal integrity of neurons becomes compromised. The loss of ABHD6 recruitment may be pathophysiologically significant since it could alter the balance of postsynaptic 2-AG synthesis and degradation such that 2-AG could continuously 'leak'

ScholarOne, 375 Greenbrier Drive, Charlottesville, VA, 22901 Support (434) 964 4100

For Peer Review

out of subsynaptic dendrites. Thus, the lack of ABHD6-mediated ligand degradation may impair the temporal precision of retrograde signalling.

MGL-dependent 2-AG degradation requires MGL's recruitment as a dimer to the internal leaflet of the plasmalemma (Labar ***et al.,*** 2010). Our findings reveal that MGL's association to the plasmalemma is particularly hindered in AD brains. Instead, MGL is sequestered in the cytosol, which we consider incompetent to degrade 2-AG targeting transmembrane receptors and participating in retrograde signalling. We propose that diminished association of MGL to the plasmalemma may be due to intracellular acidosis or membrane damage through lipid peroxidation (Querfurth and LaFerla 2010). Nevertheless, our biochemical data suggest the existence of compensatory mechanisms since the contribution of JZL184/URB602-insensitive 2-AG degrading enzymes is markedly increased in AD, compatible with our observation of increased ABDH6 expression in microglia and/or astrocytes. We also find that Aβ is central to regulating both the subcellular localization and activity of MGL. The physiological significance of this interaction may be increased intracellular 2-AG degradation preventing receptor-independent antioxidant actions of 2-AG (Bisogno and Di Marzo 2008), thus predisposing neurons to Aβ-induced oxidative damage.

Previous studies demonstrate that cannabinoids may rescue neurons under AD-like conditions by suppressing pro-inflammatory microglia activity (Ramirez ***et al***., 2005). Our present results uncover novel mechanistic insights in neuronal (synaptic) 2-AG signalling, as well as 2-AG-mediated neuron-glia interactions. We suggest that reduced pre- as well as postsynaptic 2-AG degradation coincident with increased and ectopic 2-AG synthesis can disrupt the temporal and spatial control of retrograde signalling, and - consequently - aggravate synapse impairment in AD. Therefore, endocannabinoid signalling networks may represent novel targets to reinstate the precision of synaptic communication under neurodegenerative conditions associated with cognitive deficit.

For Peer Review

ScholarOne, 375 Greenbrier Drive, Charlottesville, VA, 22901 Support (434) 964 4100

Legends to Figures

Figure 1 **Changes in DAGL and MGL protein expression in human hippocampus coincide with Alzheimer's progression.** (A) Representative images of molecular targets resolved by Western blotting. Data (in kDa) indicate the calculated molecular weights of the molecules of interest. Solid and open arrowheads identify MGL's 33 kDa and 30 kDa, respectively. Calculated molecular weights corresponded with those measured in particular experiments in all cases. We did not observe modifications to the molecular weights of any of the targets analyzed (otherwise represented as vertical size shifts) when comparing data from control, moderate or severe Alzheimer's (B2-4 and B6, respectively) cohorts. Normalized expression (average of controls = 1.0) of CB_1Rs (B), DAGLα (C; $^{+}$***p*** < 0.1), DAGLβ (C_1), ABHD6 (E), 30 kDa (F) and 33 kDa (F_1) isoforms of MGL. Individual data points and their colour coding correspond to ***post-mortem*** cases listed in Table S1. β-actin was used as loading control to normalize our data (Fig. S1B,B_1). Horizontal lines represent the mean value of particular patient cohorts. (D) DAGLα and DAGLβ levels correlated positively in controls (***not marked***), lost correlation in B2-4, while exhibited a strong negative expressional relationship in B6. (red dashed line; G) MGL isoform expression positively correlates during AD progression. ****p*** < 0.05 (Student's ***t***-test).

Figure 2 **CB_1R distribution in aged human hippocampus and in Alzheimer's.** (A) Schema of the human hippocampal formation. Open rectangles identify the general location of images in (B) and (E). (B) CB_1R immunoreactivity overlaps with synaptophysin^{+} nerve terminals targeting the perisomatic region (C) as well as apical dendrites (D) of CA1 pyramidal neurons. High-resolution microscopy reveals CB_1R^{+}/synaptophysin^{+} terminals (***arrowheads***) around pyramidal cell perikarya (C-C_3) and dendrites (D-D_3). Note the mutually exclusive localization of CB_1Rs and MAP2^{+} dendrites. Dashed lines encircle neuronal somata (C) and dendrite (D). Asterisks in (C) are overlain on neuronal nuclei. (E) CB_1R^{+} afferents engulf cells in the granular layer abundantly immunoreactive for Aβ(17-24), likely localizing intracellular APP, as well as Aβ(17-24)$^{+}$ senile plaque (***open rectangle***). (E_1-E_3) The density of CB_1R^{+} axons and synapses appear unchanged in the proximity of senile plaques. Instead, CB_1R^{+} processes appear to accumulate locally around, and even penetrate senile plaques (***arrows***). ***Abbreviations***: CA, Ammon's horn; DF, dentate fascia; sub., subiculum. ***Scale bars*** = 20 μm (B,E,E_3), 12 μm (C_3,), 4 μm (D_3).

For Peer Review

ScholarOne, 375 Greenbrier Drive, Charlottesville, VA, 22901 Support (434) 964 4100

Figure 3 **Differential DAGLα and DAGLβ expression and localization in aged human hippocampus and in Alzheimer's.** (A) Schematic overview of hippocampal subfields with open rectangles identifying the localization of dendritic fields shown in (B,F). (B) MAP2$^+$ dendritic shafts (***arrows***) are embedded in a fine meshwork of DAGLα$^+$ and/or DAGLβ$^+$ puncta, with the density of DAGLα immunoreactivity surpassing that of DAGLβ in the aged human hippocampus (control). (C) High-resolution imaging reveals co-existence of DAGLα and DAGLβ (***arrowheads***) in MAP2$^+$ compartments. (D) Three-dimensional reconstruction of a MAP2$^+$ pyramidal dendrite verifies the postsynaptic recruitment of DAGLs, and high-power rendering positions both DAGLα and DAGLβ in the dendritic spine neck (D_1). (E) Pearson's correlation coefficient suggests moderate positive correlation between the fluorescence maxima of DAGLα and DAGLβ. (E_1,E_2) Area occupancy and co-localization coefficients for DAGLα and DAGLβ immunoreactivities verify the greater abundance of DAGLα, and reveal differences in their probability of co-localization, respectively. Data were expressed as means ± s.e.m. (F) The distribution of DAGLα does not change around Aβ(17-24)$^+$ senile plaques in AD. However, DAGLβ immunoreactivity focally concentrates in periplaque regions (F_1) in small-diameter cell-like structures (***arrowheads***, F_1) but not CB_1R^+ processes (***open arrows***). Such DAGLβ$^+$ cells closely appose (***arrowheads***, F_2) CB_1R^+ axon terminals (***arrows***, F_2), and, based on their IBA-1 expression, were identified as activated microglia in Alzheimer's brains (***arrows***; G-G_2). Asterisks in G-G_2 pinpoint the soma of the microglial cell. ***Abbreviations***: DF, dentate fascia; sub., subiculum. ***Scale bars*** = 40 μm (B_2), 10 μm (F,F_1), 4 μm (C_3,F_2,G_3).

Figure 4 **Pathological alterations in the cellular distribution of serine hydrolase ABHD6 in Alzheimer's hippocampus.** (A-A_2) ABHD6 is distributed along the somatodendritic axis of hippocampal pyramidal cells in aged (control) human hippocampus. (B) We find ABHD6 expression in small, multipolar MAP2$^-$ cells, presumed microglia, coincident with a decrease in dendrite labelling in neurons (***asterisk***) in Braak 2-4 disease. (B_1,B_2) This AD-related ABHD6 distribution pattern is exacerbated in Braak 6 with ABHD6 immunoreactivity localized to small calibre, IBA1$^+$ microglia processes. (C,C_1) ABHD6 is excluded from AT8$^+$ neurons (***asterisk***), though retained in proximal dendrites of cells without appreciable neurofibrillary pathology. (D-D_3) ABHD6$^+$/IBA1$^+$ microglia populate plaque-laden regions in severe AD. Open and solid arrowheads point throughout to ABHD6$^+$ dendrites and microglia-like cells, respectively. ***Scale bars*** = 12 μm.

Figure 5 **MGL in the aged human hippocampus**. (A) Schematic overview of the human hippocampal formation with open rectangles identifying the surface areas presented in panels (B), (C) and (H). (B,B_1) MGL immunoreactivity (***open arrowheads***) is confined not only to the somata of granule cells but also to ramifying astroglia-like cells in the

ScholarOne, 375 Greenbrier Drive, Charlottesville, VA, 22901 Support (434) 964 4100

For Peer Review

dentate gyrus (***open arrowheads***). (C) CB_1R^+ afferents target MGL^+ CA1 pyramidal cells. Open rectangles point out the location of insets in (D,E). (D-D_3) MGL decorates the cytoplasm of pyramidal cells. (E-E_3) MGL accumulates in presynapses as revealed by the presence of MGL^+/CB_1Rs^+ terminals on pyramidal cell dendrites (***arrows***). Dashed lines encircle neuronal somata (D) and dendrite (E). (F,F_1) Three-dimensional reconstruction of a dendrite segment confirms that MGL (***open arrowheads***) is excluded from dendrites/dendritic spines, as well as astroglial end-feet. (G) Pearson's correlation coefficient of MGL and CB_1R fluorescence intensities. (G_1) Relative area coverage of MGL^+ and CB_1R^+ structures over pyramidal cell dendrites in the stratum radiatum. (G_2) Co-localization coefficients for MGL and CB_1R immunoreactivities reveal differential probabilities for these molecular targets to coexist. (H) MGL accumulates on the membrane surface of a subset of astroglia in aged human brain. ***Scale bars*** = 80 μm (B_1), 20 μm (C,H), 6 μm (D_3,E_3).

Figure 6 **MGL localization in Alzheimer hippocampus.** (A,A_1) MGL isoform expression exhibits positive correlation with AD progression. (A_2) This relationship is not biased by the ***post-mortem*** delay (h). (B,B_1) IBA-1^+ microglia cells (***arrowheads***) recruited to senile amyloid plaques express MGL in AD. (C-C_2) MGL expression is retained at reduced levels in neurons with moderate (C, **) and severe (C_1,C_2, *) neurofibrillary pathology. (D) Quantitative immunofluorescence analysis of MGL levels in neurons with ($AT8^+$) or without ($AT8^+$) hyperphosphorylated tau. Symbols in brackets denote group means. ***Abbreviation***: g.s.u., grey-scale unit. ****p*** < 0.001 (Student's ***t***-test). ***Scale bars*** = 12 μm (C'-C_2''), 8 μm (B,B_1).

Figure 7 **2-AG degradation in Alzheimer's and its Aβ(1-40)-induced activation.** (A) Pro-inflammatory transformation by WNT-3A (300 ng/ml, 6h) (Halleskog ***et al.,*** 2011) down-regulates MGL expression in primary mouse microglia. Interleukin-6 and tumor necrosis factor (TNF) were used as positive (internal) controls. (B) 2-AG is differentially metabolized in AD frontal cortex: membrane-associated 2-AG-degrading enzymatic activity is decreased, while cytosolic 2-AG-degrading activity is significantly increased, relative to controls. (C) Membrane-associated MGL activity accounts for ~60% of total 2-AG hydrolysis activity as revealed by JZL184 application (see also Fig. S8B,B_1) in membrane samples prepared from control human specimens. Note that JZL184-sensitive 2-AG degrading activities are selectively lost in AD. (C_1) 2-AG hydrolysis activity significantly increases in cytosol fractions from AD brains, as compared to controls. JZL184 partially reduces 2-AG degradation in cytosolic fractions prepared from control brains and eliminates disease-associated enhancement of 2-AG catabolism in AD brains. (D) FAAH does not contribute to 2-AG degradation at either subcellular fraction as tested by URB597. (E) Pre-incubation of cortical tissue homogenates from control subjects with Aβ1-40 significantly increases both

ScholarOne, 375 Greenbrier Drive, Charlottesville, VA, 22901 Support (434) 964 4100

For Peer Review

membrane-bound and cytosolic 2-AG metabolism. (E_1) Aβ1-40 induces 2-AG degrading enzymatic activity in a dose-dependent manner. **p* < 0.05, ***p* < 0.01 ***vs***. controls; $^{\#}$*p* < 0.05, $^{\#\#}$ *p* < 0.01 ***vs***. non-treated samples. ***Abbreviations***: n/a, not analyzed; n.s., not significant; N.T., non-treated.

Figure 8 **Aβ(1-42) triggers subcellular redistribution of 2-AG signalling networks and prolongs DSI.** (A-A_3) Representative images of molecular targets resolved by Western blotting. Cytosol and membrane fractions are from the same sample to establish the impact of Aβ(1-42) on subcellular receptor and enzyme recruitment, as compared to controls in artificial cerebrospinal fluid (aCSF). Aβ(1-42) exposure significantly alters intracellular ***vs***. cell-surface concentrations of CB_1Rs (A_1), DAGLα (A_2) and MGL (A_3). Data on MGL shows cumulative changes in this enzyme's 33 and 30 kDa isoforms. (B) Representative experiment showing DSI induced by a step depolarization of a CA1 pyramidal neuron. (B_1) Postsynaptic depolarization-induced reduction of spontaneous IPSCs (downward deflection from baseline) is prolonged by bath-applied Aβ(1-42) (1 μM). (B_2) Summary of DSI magnitude and kinetics measured in control (open circles; ***n*** = 10 cells) or in the presence of Aβ(1-42) (solid circles; ***n*** = 11). AM251 (1 μM) abolishes DSI in control (C), as well as Aβ(1-42)-superfused CA1 pyramidal neurons (D,D_1). ***p* < 0.01 (Student's ***t***-test). Data were expressed as means ± s.e.m.

For Peer Review

ScholarOne, 375 Greenbrier Drive, Charlottesville, VA, 22901 Support (434) 964 4100

References

Alger BE. Retrograde signaling in the regulation of synaptic transmission: focus on endocannabinoids. Prog Neurobiol 2002; 68: 247-286.

Bell KF, Ducatenzeiler A, Ribeiro-da-Silva A, Duff K, Bennett DA, Cuello AC. The amyloid pathology progresses in a neurotransmitter-specific manner. Neurobiol Aging 2006; 27: 1644-1657.

Benito C, Nunez E, Tolon RM, Carrier EJ, Rabano A, Hillard CJ ***et al***. Cannabinoid CB2 receptors and fatty acid amide hydrolase are selectively overexpressed in neuritic plaque-associated glia in Alzheimer's disease brains. J Neurosci 2003; 23: 11136-11141.

Bilkei-Gorzo A, Racz I, Valverde O, Otto M, Michel K, Sastre M ***et al***. Early age-related cognitive impairment in mice lacking cannabinoid CB1 receptors. Proc Natl Acad Sci U S A 2005; 102: 15670-15675.

Bisogno T, Di Marzo V. The role of the endocannabinoid system in Alzheimer's disease: facts and hypotheses. Curr Pharm Des 2008; 14: 2299-3305.

Bisogno T, Howell F, Williams G, Minassi A, Cascio MG, Ligresti A ***et al***. Cloning of the first sn1-DAG lipases points to the spatial and temporal regulation of endocannabinoid signaling in the brain. J Cell Biol 2003; 163: 463-468.

Blankman JL, Simon GM, Cravatt BF. A comprehensive profile of brain enzymes that hydrolyze the endocannabinoid 2-arachidonoylglycerol. Chem Biol 2007; 14: 1347-1356.

Blazquez C, Chiarlone A, Sagredo O, Aguado T, Pazos MR, Resel E ***et al***. Loss of striatal type 1 cannabinoid receptors is a key pathogenic factor in Huntington's disease. Brain 2010.

Bradford MM. A rapid and sensitive method for the quantitation of microgram quantities of protein utilizing the principle of protein-dye binding. Anal Biochem 1976; 72: 248-254.

Busche MA, Eichhoff G, Adelsberger H, Abramowski D, Wiederhold KH, Haass C ***et al***. Clusters of hyperactive neurons near amyloid plaques in a mouse model of Alzheimer's disease. Science 2008; 321: 1686-1689.

Dinh TP, Carpenter D, Leslie FM, Freund TF, Katona I, Sensi SL ***et al***. Brain monoglyceride lipase participating in endocannabinoid inactivation. Proc Natl Acad Sci U S A 2002; 99: 10819-10824.

Gao Y, Vasilyev DV, Goncalves MB, Howell FV, Hobbs C, Reisenberg M ***et al***. Loss of retrograde endocannabinoid signaling and reduced adult neurogenesis in diacylglycerol lipase knock-out mice. J Neurosci 2010; 30: 2017-2024.

Garbelli R, Inverardi F, Medici V, Amadeo A, Verderio C, Matteoli M ***et al***. Heterogeneous expression of SNAP-25 in rat and human brain. J Comp Neurol 2008; 506: 373-386.

Goedert M, Spillantini MG, Jakes R, Rutherford D, Crowther RA. Multiple isoforms of human microtubule-associated protein tau: sequences and localization in neurofibrillary tangles of Alzheimer's disease. Neuron 1989; 3: 519-526.

Gu Z, Liu W, Yan Z. {beta}-Amyloid impairs AMPA receptor trafficking and function by reducing Ca2+/calmodulin-dependent protein kinase II synaptic distribution. J Biol Chem 2009; 284: 10639-10649.

Halleskog C, Mulder J, Dahlstrom J, Mackie K, Hortobagyi T, Tanila H ***et al***. WNT signaling in activated microglia is proinflammatory. Glia 2011; 59: 119-131.

Harkany T, Dobszay MB, Cayetanot F, Hartig W, Siegemund T, Aujard F ***et al***. Redistribution of CB1 cannabinoid receptors during evolution of cholinergic basal forebrain territories and their cortical projection areas: a comparison between the gray mouse lemur (Microcebus murinus, primates) and rat. Neuroscience 2005; 135: 595-609.

Harkany T, Hartig W, Berghuis P, Dobszay MB, Zilberter Y, Edwards RH ***et al***. Complementary distribution of type 1 cannabinoid receptors and vesicular glutamate transporter 3 in basal

ScholarOne, 375 Greenbrier Drive, Charlottesville, VA, 22901 Support (434) 964 4100

forebrain suggests input-specific retrograde signalling by cholinergic neurons. Eur J Neurosci 2003; 18: 1979-1992.

Hashimotodani Y, Ohno-Shosaku T, Kano M. Presynaptic monoacylglycerol lipase activity determines basal endocannabinoid tone and terminates retrograde endocannabinoid signaling in the hippocampus. J Neurosci 2007; 27: 1211-1219.

Hauser WA, Morris ML, Heston LL, Anderson VE. Seizures and myoclonus in patients with Alzheimer's disease. Neurology 1986; 36: 1226-1230.

Hsieh H, Boehm J, Sato C, Iwatsubo T, Tomita T, Sisodia S ***et al***. AMPAR removal underlies Abeta-induced synaptic depression and dendritic spine loss. Neuron 2006; 52: 831-843.

Jankowsky JL, Fadale DJ, Anderson J, Xu GM, Gonzales V, Jenkins NA ***et al***. Mutant presenilins specifically elevate the levels of the 42 residue beta-amyloid peptide in vivo: evidence for augmentation of a 42-specific gamma secretase. Hum Mol Genet 2004; 13: 159-170.

Jung KM, Astarita G, Zhu C, Wallace M, Mackie K, Piomelli D. A key role for diacylglycerol lipase-alpha in metabotropic glutamate receptor-dependent endocannabinoid mobilization. Mol Pharmacol 2007; 72: 612-621.

Kamenetz F, Tomita T, Hsieh H, Seabrook G, Borchelt D, Iwatsubo T ***et al***. APP processing and synaptic function. Neuron 2003; 37: 925-937.

Kano M, Ohno-Shosaku T, Hashimotodani Y, Uchigashima M, Watanabe M. Endocannabinoid-mediated control of synaptic transmission. Physiol Rev 2009; 89: 309-380.

Katona I, Urban GM, Wallace M, Ledent C, Jung KM, Piomelli D ***et al***. Molecular composition of the endocannabinoid system at glutamatergic synapses. J Neurosci 2006; 26: 5628-5637.

Kawamura Y, Fukaya M, Maejima T, Yoshida T, Miura E, Watanabe M ***et al***. The CB1 cannabinoid receptor is the major cannabinoid receptor at excitatory presynaptic sites in the hippocampus and cerebellum. J Neurosci 2006; 26: 2991-3001.

Keimpema E, Barabas K, Morozov YM, Tortoriello G, Torii M, Cameron G ***et al***. Differential subcellular recruitment of monoacylglycerol lipase generates spatial specificity of 2-arachidonoyl glycerol signaling during axonal pathfinding. J Neurosci 2010; 30: 13992-14007.

Khaspekov LG, Brenz Verca MS, Frumkina LE, Hermann H, Marsicano G, Lutz B. Involvement of brain-derived neurotrophic factor in cannabinoid receptor-dependent protection against excitotoxicity. Eur J Neurosci 2004; 19: 1691-1698.

King AR, Duranti A, Tontini A, Rivara S, Rosengarth A, Clapper JR ***et al***. URB602 inhibits monoacylglycerol lipase and selectively blocks 2-arachidonoylglycerol degradation in intact brain slices. Chem Biol 2007; 14: 1357-1365.

Klegeris A, Bissonnette CJ, McGeer PL. Reduction of human monocytic cell neurotoxicity and cytokine secretion by ligands of the cannabinoid-type CB2 receptor. Br J Pharmacol 2003; 139: 775-786.

Kuchibhotla KV, Goldman ST, Lattarulo CR, Wu HY, Hyman BT, Bacskai BJ. Abeta plaques lead to aberrant regulation of calcium homeostasis in vivo resulting in structural and functional disruption of neuronal networks. Neuron 2008; 59: 214-225.

Labar G, Bauvois C, Borel F, Ferrer JL, Wouters J, Lambert DM. Crystal structure of the human monoacylglycerol lipase, a key actor in endocannabinoid signaling. Chembiochem 2010; 11: 218-227.

Lacor PN, Buniel MC, Chang L, Fernandez SJ, Gong Y, Viola KL ***et al***. Synaptic targeting by Alzheimer's-related amyloid beta oligomers. J Neurosci 2004; 24: 10191-10200.

Lastres-Becker I, Molina-Holgado F, Ramos JA, Mechoulam R, Fernandez-Ruiz J. Cannabinoids provide neuroprotection against 6-hydroxydopamine toxicity in vivo and in vitro: relevance to Parkinson's disease. Neurobiol Dis 2005; 19: 96-107.

Lee JH, Agacinski G, Williams JH, Wilcock GK, Esiri MM, Francis PT ***et al***. Intact cannabinoid CB1 receptors in the Alzheimer's disease cortex. Neurochem Int 2010.

For Peer Review

Long JZ, Li W, Booker L, Burston JJ, Kinsey SG, Schlosburg JE ***et al***. Selective blockade of 2-arachidonoylglycerol hydrolysis produces cannabinoid behavioral effects. Nat Chem Biol 2009; 5: 37-44.

Ludanyi A, Eross L, Czirjak S, Vajda J, Halasz P, Watanabe M ***et al***. Downregulation of the CB1 cannabinoid receptor and related molecular elements of the endocannabinoid system in epileptic human hippocampus. J Neurosci 2008; 28: 2976-2990.

Ludanyi A, Hu SS, Yamazaki M, Tanimura A, Piomelli D, Watanabe M ***et al***. Complementary synaptic distribution of enzymes responsible for synthesis and inactivation of the endocannabinoid 2-arachidonoylglycerol in the human hippocampus. Neuroscience 2010.

Marrs WR, Blankman JL, Horne EA, Thomazeau A, Lin YH, Coy J ***et al***. The serine hydrolase ABHD6 controls the accumulation and efficacy of 2-AG at cannabinoid receptors. Nat Neurosci 2010; 13: 951-957.

Mattson MP, Chan SL. Neuronal and glial calcium signaling in Alzheimer's disease. Cell Calcium 2003; 34: 385-397.

Mazzola C, Micale V, Drago F. Amnesia induced by beta-amyloid fragments is counteracted by cannabinoid CB1 receptor blockade. Eur J Pharmacol 2003; 477: 219-225.

Micale V, Cristino L, Tamburella A, Petrosino S, Leggio GM, Di Marzo V ***et al***. Enhanced cognitive performance of dopamine D3 receptor "knock-out" mice in the step-through passive-avoidance test: assessing the role of the endocannabinoid/endovanilloid systems. Pharmacol Res 2010; 61: 531-536.

Minkeviciene R, Rheims S, Dobszay MB, Zilberter M, Hartikainen J, Fulop L ***et al***. Amyloid beta-induced neuronal hyperexcitability triggers progressive epilepsy. J Neurosci 2009; 29: 3453-3462.

Mor M, Rivara S, Lodola A, Plazzi PV, Tarzia G, Duranti A ***et al***. Cyclohexylcarbamic acid 3'- or 4'-substituted biphenyl-3-yl esters as fatty acid amide hydrolase inhibitors: synthesis, quantitative structure-activity relationships, and molecular modeling studies. J Med Chem 2004; 47: 4998-5008.

Nomura DK, Long JZ, Niessen S, Hoover HS, Ng SW, Cravatt BF. Monoacylglycerol lipase regulates a fatty acid network that promotes cancer pathogenesis. Cell 2010; 140: 49-61.

Nunez E, Benito C, Tolon RM, Hillard CJ, Griffin WS, Romero J. Glial expression of cannabinoid CB(2) receptors and fatty acid amide hydrolase are beta amyloid-linked events in Down's syndrome. Neuroscience 2008; 151: 104-110.

Oddo S, Caccamo A, Shepherd JD, Murphy MP, Golde TE, Kayed R ***et al***. Triple-transgenic model of Alzheimer's disease with plaques and tangles: intracellular Abeta and synaptic dysfunction. Neuron 2003; 39: 409-421.

Palazuelos J, Aguado T, Pazos MR, Julien B, Carrasco C, Resel E ***et al***. Microglial CB2 cannabinoid receptors are neuroprotective in Huntington's disease excitotoxicity. Brain 2009; 132: 3152-3164.

Peng I, Binder LI, Black MM. Biochemical and immunological analyses of cytoskeletal domains of neurons. J Cell Biol 1986; 102: 252-262.

Querfurth HW, LaFerla FM. Alzheimer's disease. N Engl J Med 2010; 362: 329-344.

Ramirez BG, Blazquez C, del Pulgar TG, Guzman N, de Ceballos MAL. Prevention of Alzheimer's disease pathology by cannabinoids: Neuroprotection mediated by blockade of microglial activation. Journal of Neuroscience 2005; 25: 1904-1913.

Rodriguez JJ, Olabarria M, Chvatal A, Verkhratsky A. Astroglia in dementia and Alzheimer's disease. Cell Death Differ 2009; 16: 378-385.

Roloff AM, Anderson GR, Martemyanov KA, Thayer SA. Homer 1a gates the induction mechanism for endocannabinoid-mediated synaptic plasticity. J Neurosci 2010; 30: 3072-3081.

For Peer Review

Roselli F, Hutzler P, Wegerich Y, Livrea P, Almeida OF. Disassembly of shank and homer synaptic clusters is driven by soluble beta-amyloid(1-40) through divergent NMDAR-dependent signalling pathways. PLoS One 2009; 4: e6011.

Sampedro MN, Bussineau CM, Cotman CW. Turnover of brain postsynaptic densities after selective deafferentation: detection by means of an antibody to antigen PSD-95. Brain Res 1982; 251: 211-220.

Schlosburg JE, Blankman JL, Long JZ, Nomura DK, Pan B, Kinsey SG ***et al***. Chronic monoacylglycerol lipase blockade causes functional antagonism of the endocannabinoid system. Nat Neurosci 2010; 13: 1113-1119.

Schubert W, Prior R, Weidemann A, Dircksen H, Multhaup G, Masters CL ***et al***. Localization of Alzheimer beta A4 amyloid precursor protein at central and peripheral synaptic sites. Brain Res 1991; 563: 184-194.

Shemer I, Holmgren C, Min R, Fulop L, Zilberter M, Sousa KM ***et al***. Non-fibrillar beta-amyloid abates spike-timing-dependent synaptic potentiation at excitatory synapses in layer 2/3 of the neocortex by targeting postsynaptic AMPA receptors. Eur J Neurosci 2006; 23: 2035-2047.

Small SA, Duff K. Linking Abeta and tau in late-onset Alzheimer's disease: a dual pathway hypothesis. Neuron 2008; 60: 534-542.

Snyder EM, Nong Y, Almeida CG, Paul S, Moran T, Choi EY ***et al***. Regulation of NMDA receptor trafficking by amyloid-beta. Nat Neurosci 2005; 8: 1051-1058.

Tanimura A, Yamazaki M, Hashimotodani Y, Uchigashima M, Kawata S, Abe M ***et al***. The endocannabinoid 2-arachidonoylglycerol produced by diacylglycerol lipase alpha mediates retrograde suppression of synaptic transmission. Neuron 2010; 65: 320-327.

Uchigashima M, Narushima M, Fukaya M, Katona I, Kano M, Watanabe M. Subcellular arrangement of molecules for 2-arachidonoyl-glycerol-mediated retrograde signaling and its physiological contribution to synaptic modulation in the striatum. J Neurosci 2007; 27: 3663-3676.

van der Stelt M, Mazzola C, Esposito G, Matias I, Petrosino S, De Filippis D ***et al***. Endocannabinoids and beta-amyloid-induced neurotoxicity in vivo: effect of pharmacological elevation of endocannabinoid levels. Cell Mol Life Sci 2006; 63: 1410-1424.

Walsh DM, Klyubin I, Fadeeva JV, Cullen WK, Anwyl R, Wolfe MS ***et al***. Naturally secreted oligomers of amyloid beta protein potently inhibit hippocampal long-term potentiation in vivo. Nature 2002; 416: 535-539.

Walsh DM, Selkoe DJ. Deciphering the molecular basis of memory failure in Alzheimer's disease. Neuron 2004; 44: 181-193.

Walter L, Franklin A, Witting A, Wade C, Xie Y, Kunos G ***et al***. Nonpsychotropic cannabinoid receptors regulate microglial cell migration. J Neurosci 2003; 23: 1398-1405.

Westlake TM, Howlett AC, Bonner TI, Matsuda LA, Herkenham M. Cannabinoid receptor binding and messenger RNA expression in human brain: an in vitro receptor autoradiography and in situ hybridization histochemistry study of normal aged and Alzheimer's brains. Neuroscience 1994; 63: 637-652.

Wise LE, Thorpe AJ, Lichtman AH. Hippocampal CB(1) receptors mediate the memory impairing effects of Delta(9)-tetrahydrocannabinol. Neuropsychopharmacology 2009; 34: 2072-2080.

Xu H, Chen M, Manivannan A, Lois N, Forrester JV. Age-dependent accumulation of lipofuscin in perivascular and subretinal microglia in experimental mice. Aging Cell 2008; 7: 58-68.

Yoles E, Belkin M, Schwartz M. HU-211, a nonpsychotropic cannabinoid, produces short- and long-term neuroprotection after optic nerve axotomy. J Neurotrauma 1996; 13: 49-57.

Yoshida T, Fukaya M, Uchigashima M, Miura E, Kamiya H, Kano M ***et al***. Localization of diacylglycerol lipase-alpha around postsynaptic spine suggests close proximity between

ScholarOne, 375 Greenbrier Drive, Charlottesville, VA, 22901 Support (434) 964 4100

For Peer Review

production site of an endocannabinoid, 2-arachidonoyl-glycerol, and presynaptic cannabinoid CB1 receptor. J Neurosci 2006; 26: 4740-4751.

For Peer Review

ScholarOne, 375 Greenbrier Drive, Charlottesville, VA, 22901 Support (434) 964 4100

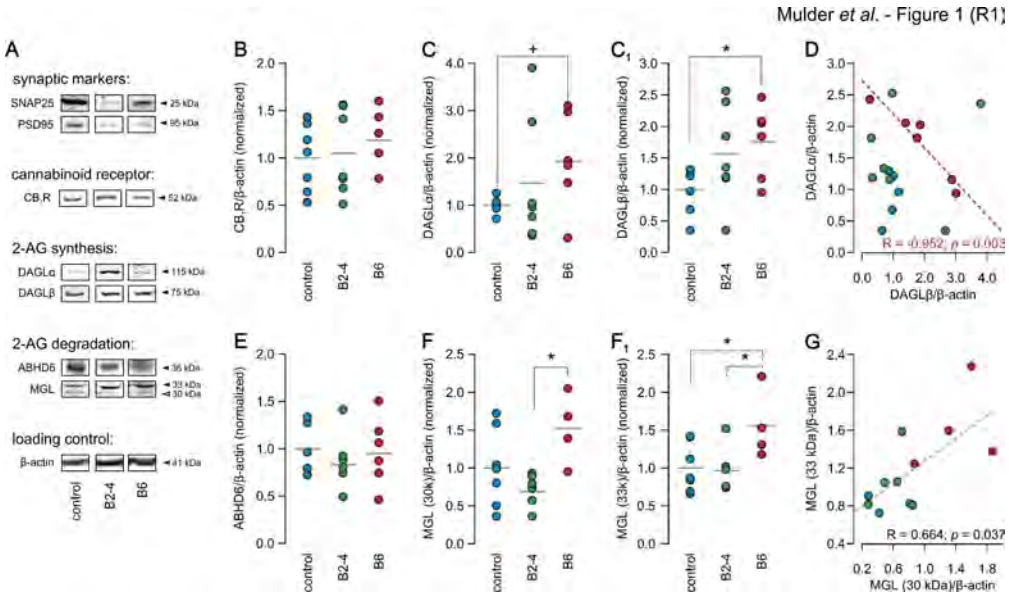

Figure 1
189x110mm (600 x 600 DPI)

er Review

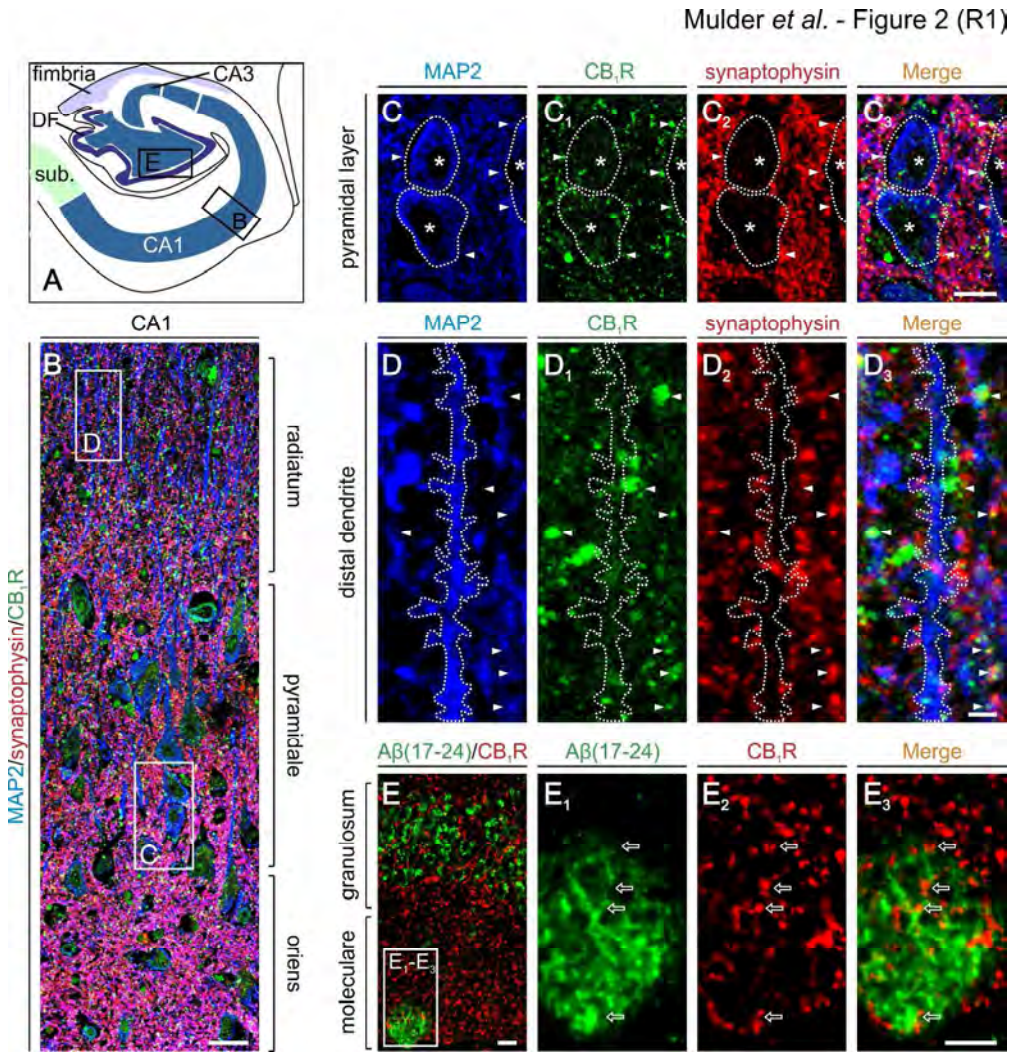

Figure 2
133x139mm (600 x 600 DPI)

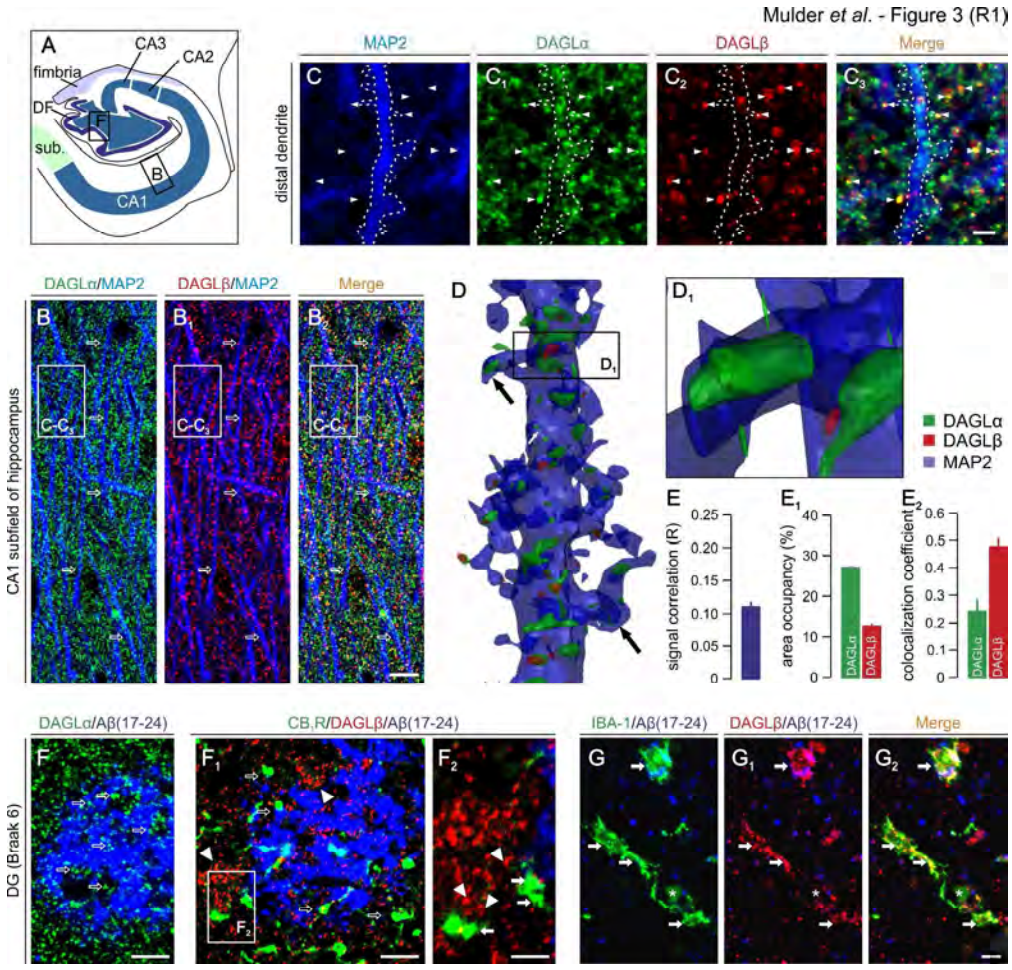

Figure 3
177x169mm (600 x 600 DPI)

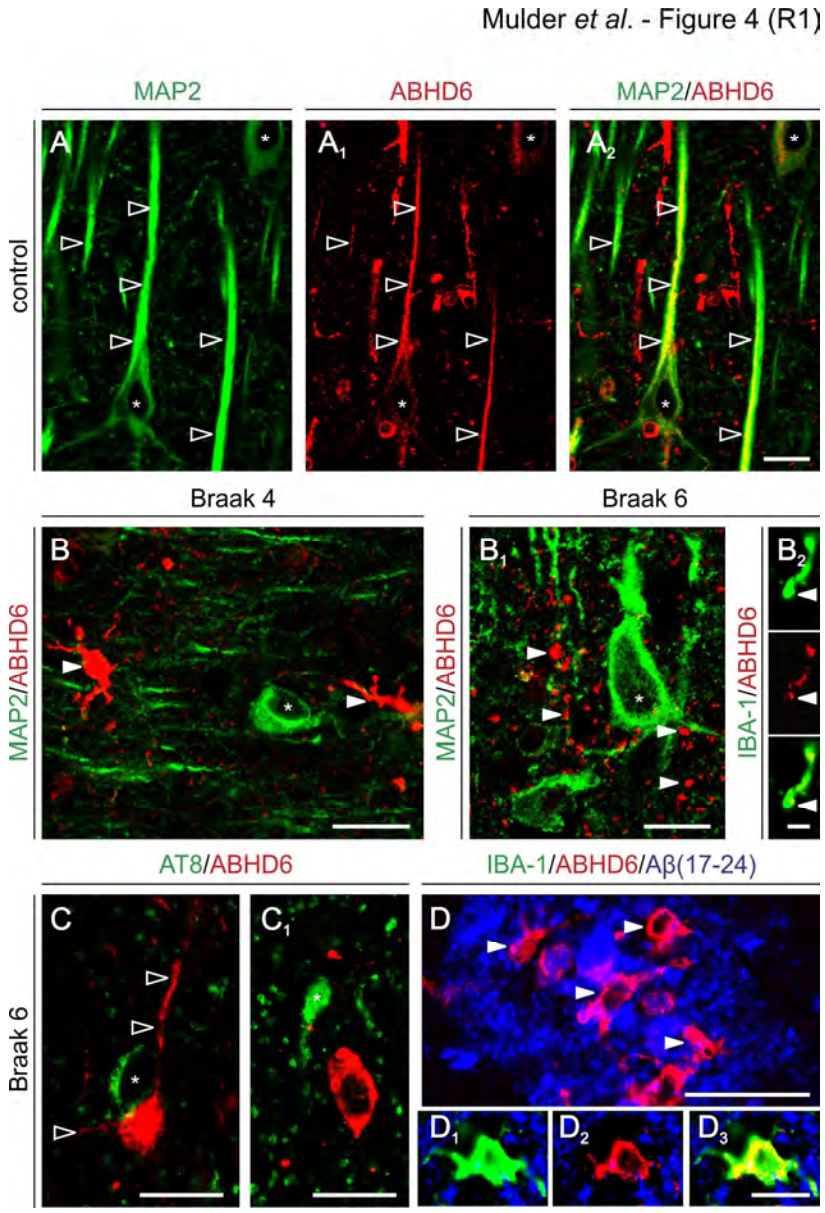

Figure 4
103x153mm (600 x 600 DPI)

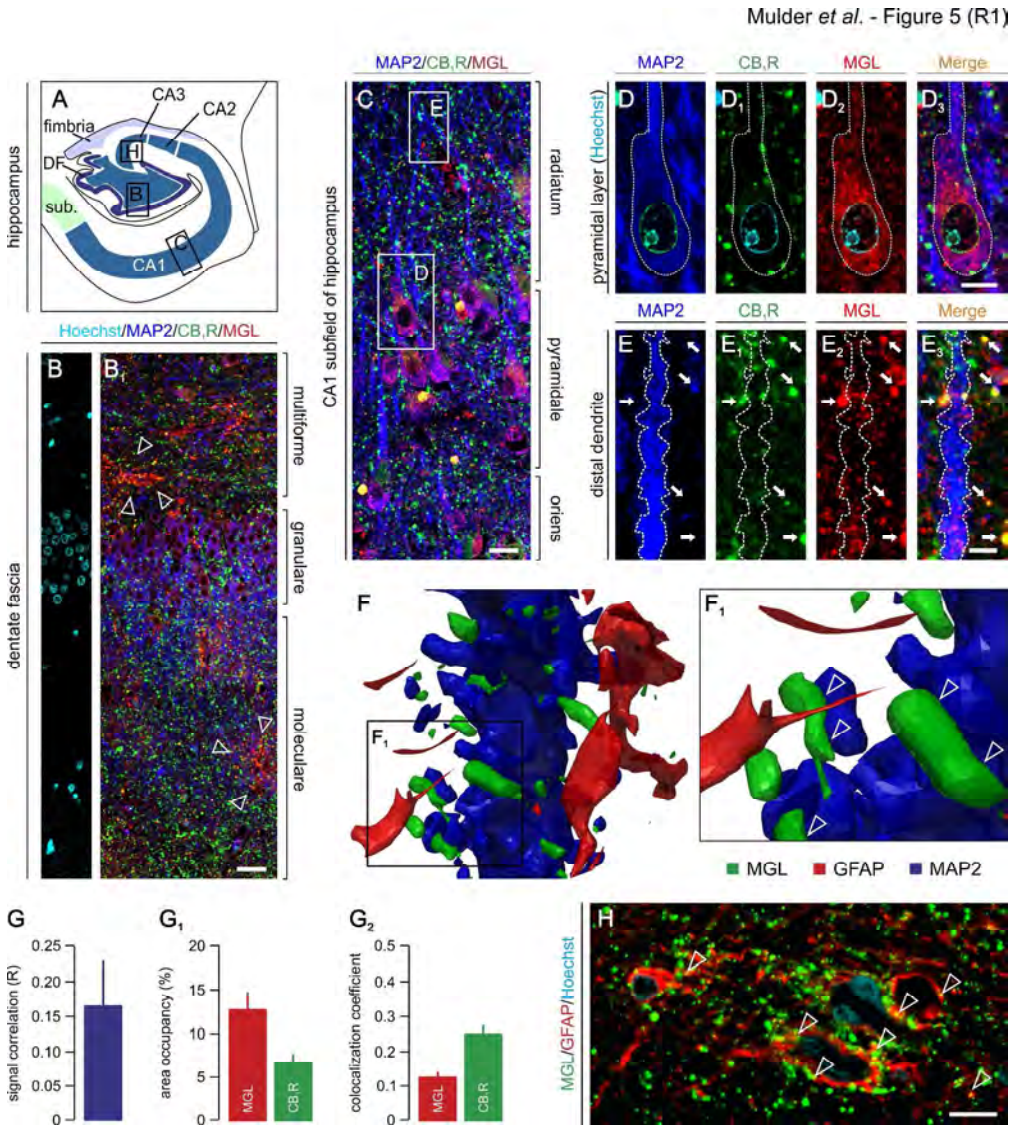

Figure 5
166x185mm (600 x 600 DPI)

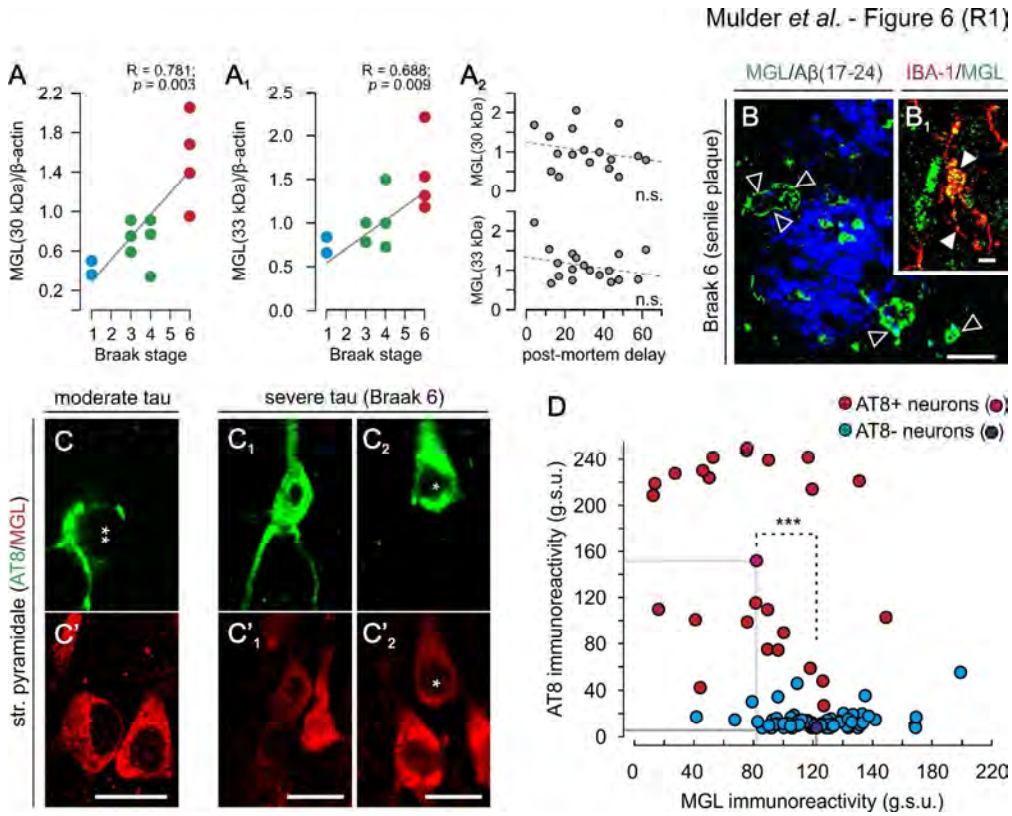

Figure 6
142x114mm (600 x 600 DPI)

For Review

Mulder *et al.* - Figure 7 (R1)

A

Affymetrix probe set	Δ (change)	*p* value	Gene name	qPCR validation (*vs.* 100 nM Aβ)
10520452	+243.69	0.030	Interleukin 6 (Il6)	n/a
10450501	+4.60	0.001	TNF (tnf)	n/a
10503902	+1.04	0.147	CB_1 receptor (Cnr1)	-61.3% (p = 0.017)
10509122	-3.94	0.148	CB_2 receptor (Cnr2)	n.s. (p = 0.445)
10465943	-2.28	0.002	DAGLα (dagla)	-35.2% (p = 0.042)
10527213	-1.88	0.137	DAGLβ (daglb)	n/a
10539894	-1.03	0.962	MGL (mgll)	n.s. (p = 0.069)
10412607	+1.10	0.418	α/β hydrolase domain containing 6 (Abhd6)	n/a
10488507	-1.22	0.331	α/β hydrolase domain containing 12 (Abhd12)	n/a

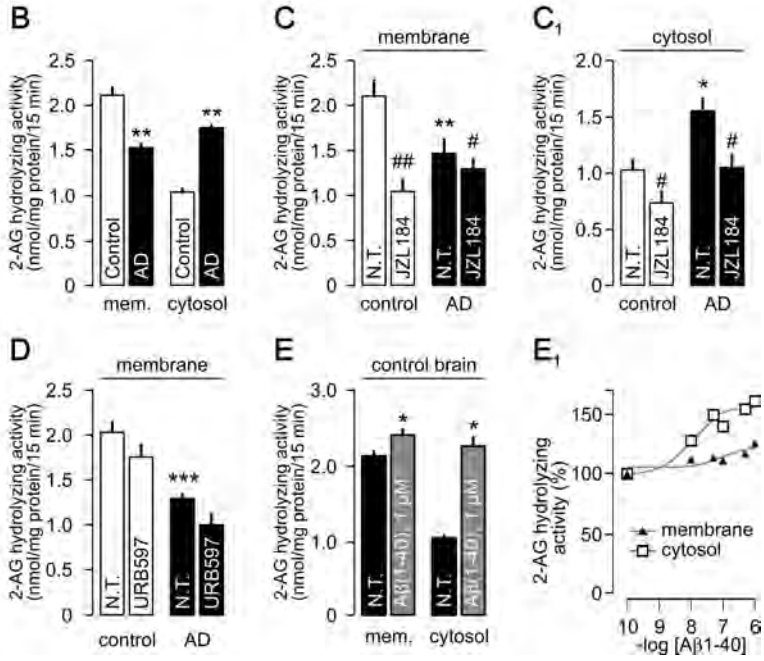

Figure 7
98x155mm (600 x 600 DPI)

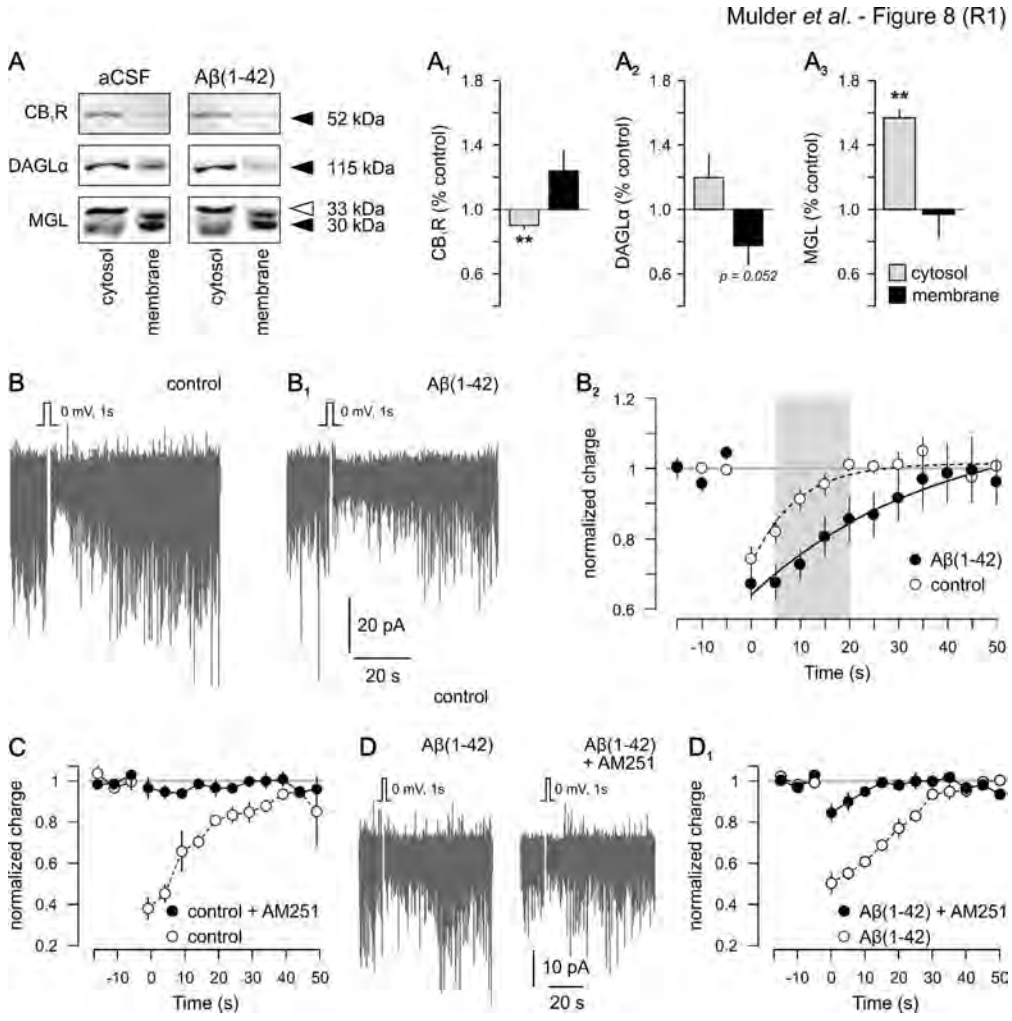

Figure 8
155x156mm (600 x 600 DPI)

Supplementary information to the manuscript:

Molecular reorganization of endocannabinoid signalling in Alzheimer's disease

(*Running title*: 2-AG signalling in Alzheimer's disease)

Jan Mulder[1,#], Misha Zilberter[2,+], Susana Pasquaré[3,4,+], Alán Alpár[1,+], Gunnar Schulte[5], Samira G. Ferreira[6], Attila Köfalvi[6], Ana M. Martín-Moreno[3], Erik Keimpema[1], Heikki Tanila[7], Masahiko Watanabe[8], Ken Mackie[9], Tibor Hortobágyi[10], Maria L. de Ceballos[3] & Tibor Harkany[1,2,*]

[1]European Neuroscience Institute at Aberdeen, University of Aberdeen, Aberdeen AB25 2ZD, United Kingdom; [2]Division of Molecular Neurobiology, Department of Medical Biochemistry and Biophysics and [5]Section for Receptor Biology & Signaling, Department of Physiology & Pharmacology, Karolinska Institutet, S-17177 Stockholm, Sweden; [3]Department of Cellular, Molecular and Developmental Neuroscience and CIBERNED, Cajal Institute, CISC, Madrid, Spain; [4]Instituto de Investigaciones Bioquímicas de Bahía Blanca, Universidad Nacional del Sur and CONICET, Bahía Blanca, Argentina; [6]Center for Neurosciences & Cell Biology, University of Coimbra, 3004-517 Coimbra, Portugal; [7]A. I. Virtanen Institute, University of Eastern Finland, F-70211 Kuopio, Finland; [8]Department of Anatomy, Hokkaido University School of Medicine, Sapporo 060-8638, Japan; [9]Gill Center for Neuroscience and Department of Psychological & Brain Sciences, Indiana University, Bloomington, IN 47405, USA and [10]Department of Clinical Neuroscience, Institute of Psychiatry, King's College London, London SE5 8AF, United Kingdom

[+]These authors contributed equally to the present study.

[#]Present address: Science for Life Laboratory, Department of Neuroscience, Karolinska Institutet, S-17177, Stockholm, Sweden

* Corresponding Author: **Dr. Tibor Harkany**, Division of Molecular Neurobiology, Department of Medical Biochemistry and Biophysics, Scheeles väg 1:A1, Karolinska Institutet, S-17177 Stockholm, Sweden; *telephone*: +46 8 524 87835; *fax*: +46 8 341 960; *e-mail*: Tibor.Harkany@ki.se

This file contains:

Author contributions
Supplementary text: Materials & methods
Legends to supplementary figures
Supplementary references
Supplementary figures
Supplementary tables

For Peer Review

Author contributions

T.Ha. and M.L.C. designed experiments. J.M., A.A. and E.K. performed histochemistry and Western blotting. M.Z. contributed electrophysiology data. S.P., A.M.M.-M. and M.L.C. measured MGL and FAAH activity in human brain. S.G.F. and A.K. measured $TRPV_1$ receptor binding. G.S. performed WNT-3A induction studies and Affymetrix analysis. H.T. and T.Ho. provided APdE9 mice and histochemically-characterized *post-mortem* human tissues, respectively. M.W. and K.M. provided immunoreagents. T.Ha. wrote the manuscript. All authors have reviewed and commented on the manuscript.

Supplementary text: **Materials & methods**

Human tissues and ethical approval of the studies. Hippocampal tissues were obtained from Alzheimer's (AD) patients and age-matched controls (without clinical signs of neuropsychiatric disease) at the London Neurodegenerative Diseases Brain Bank. Local ethical committee approval (#231/2001) and informed consent from the next of kin have been obtained to harvest *post-mortem* tissues (Table S1). All patient material was coded to ensure anonymity throughout tissue processing. Classification of Aβ plaque burden (Fig. S1A) and tau pathology (Table S1) was performed as specified by the CERAD (Mirra *et al.,* 1991) in patients with 'sparse', 'moderate' and 'frequent/severe' Aβ plaque burden, qualifying for 'low', 'intermediate', and 'high' likelihood of AD/dementia according to the NIA-Reagan Institute diagnostic criteria (Hyman and Trojanowski, 1997). Twenty-eight cases were assigned to this study (Table S1) and grouped as: *controls* (*n* = 7, mean age of death: 74.42 ± 6.11 years) also including likely Braak stage I cases (*n* = 3, mean age of death: 80.33 ± 1.20 years); *moderate AD* from patients with Braak stage III (*n* = 4, mean age of death: 91.75 ± 5.7 years) and IV (*n* = 5, mean age of death: 84.00 ± 3.33 years); and *severe AD* with patients exhibiting pathological signs of Braak stage VI disease (*n* = 9, mean age of death: 82.00 ± 2.69 years).

An independent cohort of AD and age-matched control cases was made available by the London Neurodegenerative Diseases Brain Bank for use in MGL and FAAH enzyme activity measurements: *controls* (*n* = 18, mean age of death: 71.8 ± 2.6 years, mean post-mortem delay (h): 38.7 ± 4.7h), *AD patient pool* (*n* = 18; mean age of death: 77.4 ± 2.2 years; mean post-mortem delay (h): 33.3 ± 5.3), matched for sex (13 females/5 males).

Ethical approval of studies in rodents. Experimental procedures on mice were approved by the Home Office of the United Kingdom and conformed to the European Communities Council Directive #86/609/EEC. Particular care was taken to minimize the number of animals and their suffering throughout the experiments.

Aβ measurements. Soluble and detergent-resistant/insoluble Aβ fractions were separated by centrifugation (14,000*g* for 30 min) as described (Walsh *et al.,* 2002). Insoluble Aβ was extracted from

For Peer Review

the pellet using 5M guanidine followed by sandwich ELISA detection of Aβ(1-42) (Invitrogen). Aβ(1-42) concentrations were expressed as pg/μg protein (Fig. S1A).

***Immunohistochemistry*.** Multiple immunofluorescence histochemistry was performed on 7 μm-thick human temporal lobe sections containing the hippocampal formation cut from paraffin-embedded blocks on a sliding microtome, and mounted onto glass slides coated with 3-aminopropyltriethoxysilane (Sigma). Sections were de-waxed in xylene, rinsed in ethanol, and endogenous peroxidase activity was blocked by 1% H_2O_2 in 100% methanol (30 min). Antigen retrieval was routinely carried out by incubating sections in 5% urea in 0.1M Tris-HCl (pH 9.5) and microwaving (800W, 8 min) followed by incubation in ice-cold $NaHBO_4$ (0.5%, in PB for 5-10 min). Non-specific immunoreactivity was suppressed by incubating our specimens in a cocktail of 10% normal donkey serum (NDS; Jackson), 5% BSA (Sigma) and 0.3% Triton X-100 (Sigma) in PB. Sections were exposed to combinations of primary antibodies (Table S2) in PB also containing 1% NDS and 0.2% Triton X-100 for 16-72 h at 4 ^{o}C. After extensive rinsing in PB, immunoreactivities were revealed by carbocyanine (Cy2) 2, 3 or 5-tagged secondary antibodies raised in donkey (1:200 [Jackson], 2 h at 22-24 ^{o}C). Tissues were routinely counterstained by Hoechst 35,528 nuclear dye (Sigma). Lipofuscin autofluorescence was blocked by applying Sudan Black-B (1%, dissolved in 70% ethanol; Fig. S3) (Schnell *et al.,* 1999). Sections were coverslipped by Aquamount (DAKO).

Laser-scanning microscopy. Sections were inspected and images were acquired on a 710LSM confocal laser-scanning microscope (Zeiss). Emission spectra for each dye were limited as follows: Hoechst (420-485 nm), Cy2 (505-530 nm), Cy3 (560-610 nm), and Cy5 (640-720 nm). Image surveys were generated using the tile scan function with optical zoom ranging from 0.6x to 1.5x at 10x primary magnification (objective: EC Plan-Neofluar 10x/0.30). Co-localization was defined as immunosignals being present without physical signal separation in ≤ 1.0-μm optical slices at 40x (Plan-Neofluar 40x/1.30) or 63x (Plan-Apochromat 63x/1.40) primary magnification (Mulder *et al.,* 2009; Keimpema *et al.,* 2010). The co-localization utility of the ZEN2009 software package was used (Keimpema *et al.,* 2010) to determine *i*) the relative area occupancy for each fluorochrome, defined as the density of fluorescence pixels normalized to a 1 μm^2 surface area, *ii*) the co-localization coefficient of CB_1R, DAGLα, DAGLβ and MGL immunoreactivities along apical dendrites of hippocampal pyramidal neurons, expressed as the relative number of co-localizing pixels in one channel as compared to the total number of pixels above threshold in another channel, and *iii*) Pearson's correlation coefficient defining the intensity distribution within co-localizing regions (ranging from -1 to +1 with 0 indicating no correlation). Images were processed using the ZEN2009 software (Zeiss). Multi-panel figures were assembled in CorelDraw X5 (Corel Corp.).

Autofluorescence background artifacts and *post-mortem* delay-related staining variations may introduce bias in quantitative immunohistochemical analysis. Therefore, we have routinely quenched tissue autofluorescence (lipofuscin, myelin) by applying Sudan Black-B. By means of spectral unmixing (Halleskog *et al.,* 2011) we have verified that Sudan Black-B quenched ≥ 90% of non-specific background fluorescence in individual emission spectra used for quantitative analysis (Fig.

For Peer Review

S3A,B and C_1-C_3). Thus, we sampled specific immunosignals restricted to Cy2-Cy5 emitting fluorophores (Fig. S3C) during quantitative analyses.

Quantitative subcellular immunohistochemistry was performed on specimens stained simultaneously. Differences in *post-mortem* delay are unlikely to affect the histochemical outcome (considering that *post-mortem* delay (h) does not significantly alter protein concentrations of our molecular targets; Fig. S4A-E). Nevertheless, we controlled the sampling errors in our quantification protocols by minimizing the population spread in the fluorescence intensity spectra of the tissue samples analyzed (Fig. S6A_3-C) (Halleskog *et al.,* 2011). Fluorescence intensities at relevant excitation/emission wavelengths were simultaneously adjusted such that random over- or under-sampling of fluorescently-labelled structures was eliminated (Fig. S6A_3-C). A relationship between MGL and AT8 immunofluorescence intensities was established after manually delineating individual hippocampal principal cells and calculating integrated fluorescence intensity values by an experimenter blind to the case conditions. This approach effectively minimized data spread and sampling error.

Three-dimensional reconstruction. Serial orthogonal images (*z*-stacks) of select dendrite segments in CA1 stratum radiatum were captured at 40x primary objective magnification (EC Plan-Neofluar 40x/1.3 oil, 2x optical zoom, pinhole: 20 µm, 1024 x 1024 pixel resolution) resulting in image stacks containing 32 - 36 *z* levels scaled as x = 0.104 µm, y = 0.104 µm and z = 0.324 µm. Single channels in individual images were exported as grey-scaled graphic images (*.tiff), and imported into BioVis3D reconstruction package (Montevideo, Uruguay) using original scale settings to retain the correct size and position of each pixel in a given *z*-stack. First, the contour of a select dendrite was established by using serial $MAP2^+$ images. Dendrites oriented in an acute angle were preferred since their shaft could precisely be followed through the entire series of images, and all spine-like structures could be defined. The outline of a dendrite cumulated from the entire image stack was then used to render the three-dimensional model of a single dendrite fragment. Spines that were outlined but not connected to the selected dendritic shaft were discarded. Next, images in separate LSM channels representing DAGLα, DAGLβ, MGL or GFAP were loaded into the reconstruction package to define the immunoreactivity for each protein in the close proximity of the selected dendrite through each *z* level. Individual outlines were overlaid and rendered simultaneously to produce a detailed three-dimensional structural model. Subsequently, protein distribution inside a dendrite segment and dendritic spines was visualized by using a transparency utility of BioVis3D.

***Western blotting*.** Blocks of human hippocampi were homogenized in TNE buffer containing 0.5% Triton X-100 (Sigma), 1% octyl-β-D-glucopyranoside (Calbiochem), 5 mM NaF, 100 µM Na_3VO_4 and a cocktail of protease inhibitors (Complete™, Roche) by using an Ultra Turrax® tube drive (IKA). Whole mouse hippocampi were homogenized in TNE buffer containing 1% Triton X-100 (Sigma), 5 mM NaF, 100 µM Na_3VO_4 and a cocktail of protease inhibitors (Complete™).

Tissues from acute hippocampal slices were processed by ultrasonication in TNE lysis buffer also containing 0.32 M sucrose, 1% octyl-β-D-glucopyranoside, 5 mM NaF, 100 µM Na_3VO_4, and protease inhibitors (Paratcha *et al.,* 2003). Cell debris and nuclei were removed by centrifugation (800*g*, 10 min

For Peer Review

at 4 °C). Membrane and cytosol fractions were separated using the same buffer by centrifugation at 14,000*g* for 30 min at 4 °C. Membrane fractions were washed in TNE buffer containing 5mM NaF, 100μM Na_3VO_4 and protease inhibitors, and lysed in TNE buffer supplemented with 0.5% Triton X-100, 1% octyl-β-D-glucopyranoside, 5 mM NaF, 100 μM Na_3VO_4, and protease inhibitors (Complete™) for 90 min. Protein concentrations were determined by Bradford's colorimetric method (Bradford 1976).

Samples were diluted to a final protein concentration of 2 μg/μl, denatured in 5x Laemmli buffer, and analyzed by SDS-PAGE on 8% or 10% resolving gels (Berghuis *et al.,* 2004). After transferring onto Immobilon-FL polyvinylidene difluoride membranes (Millipore), protein samples on membranes were blocked in Odyssey blocking buffer (LiCor Biosciences; 1h) and exposed to primary antibodies (Table S2; Fig. S2) overnight at 4 °C. Appropriate combinations of IRDye-800CW and IRDye-680-conjugated secondary antibodies were used for signal detection (LiCor Biosciences; from goat or rabbit hosts; 1:10,000, 2h). Image acquisition and analysis were performed on a LiCor Odyssey IR imager. β-III-tubulin (1:4,000; Promega) and β-actin (1:10,000; Sigma) served as loading controls.

Dot blot. A Bio-dot microfiltration blotting device (Bio-Rad) was used. Samples (25 μg protein/well) were blotted onto Hybond-P PVDF protein membranes (GE Healthcare), air dried, washed in 50 mM Tris HCl buffer (pH 7.4) containing 0.1% Tween-20 (TT solution), blocked in 5% BSA in TT solution, and exposed to primary antibodies overnight at 4 °C. Specificity of the polyclonal anti-$TRPV_1$ antibody was verified in $TRPV_1^{-/-}$ mice (V. Di Marzo, *personal communication*) (Cristino *et al.,* 2008). Tissues from adult mouse cerebellum were used as positive control (*data not shown*) (Cristino *et al.,* 2008). The enhanced chemiluminescence method was used for signal amplification and detection (Bio-Rad Chemidoc XRS^+). β-Actin was used as loading control.

Membrane preparation for [^{3}H]resiniferatoxin binding. Membrane preparation was carried out according to previously published protocols (Hartshorne and Catterall 1984) with slight modifications. Wild-type (WT, *n* = 4, 3 months of age) and age-matched $TRPV_1^{-/-}$ mice (*n* = 4; kindly provided by A. Avelino) (Caterina *et al.,* 2000), as well as Wistar rats (Charles River, Barcelona, Spain; *n* = 4 at 3 months of age) were decapitated under halothane anaesthesia. Whole brains were rapidly removed, striata were dissected out, and homogenized in ice-cold sucrose solution [0.32 M sucrose, 10 mM HEPES, 1 mM EDTA, protease inhibitor cocktail (Sigma), pH = 7.4]. Whole brain and striatal homogenates were centrifuged at 700*g*/10 min and 3,000*g*/5 min, respectively. Pellets were discarded. Supernatants were centrifuged at 28,000*g* for 40 min and the resultant pellets were re-suspended in 20 ml of ice-cold washing solution [Trish/HCl (50 mM), $MgCl_2$ (3 mM), $CaCl_2$ (2.5 μM), and protease inhibitor cocktail, pH 8.2]. After another washing/centrifugation (28,000*g*/40 min) step, the final pellet was stored at -20 ºC until analysis.

Optimization of [^{3}H]resiniferatoxin binding. First, we determined [^{3}H]resiniferatoxin ([^{3}H]RTX) binding by establishing saturation curves in WT and $TRPV_1^{-/-}$ membranes (Fig. S5G,G_1), in the presence of (*E*)-capsaicin (1 μM, Tocris; dissolved in DMSO whose final concentration was 0.1% in all

For Peer Review

experiments), a potent and selective $TRPV_1$ agonist or its inactive enantiomer, (*Z*)-capsaicin (1 μM; Tocris). Binding assays were performed in triplicate in conical 96-well plates. The reaction mixture consisted of 100 μg protein sample (50 μl of 2mg/ml homogenate), capsaicin solution or vehicle (100 μl), [^{3}H]RTX (PerkinElmer, specific activity: 40.5 μCi/mmol) as 100 μl solution at concentrations ranging from 20 pM to 1.5 nM. Protein samples were substituted by assay solution in separate control experiments to measure radioactivity retention by absorption filters in the presence or absence of cold ligands. The assay solution contained: Trish/HCl (50 mM), $MgCl_2$ (1 mM), $MgSO_4$ (2 mM), $CaCl_2$ (2.5 μM), and protease inhibitor cocktail (pH 7.4). We omitted BSA from the assay solution since, in pilot experiments, we failed to find [^{3}H]RTX binding displaced by (*E*)-capsaicin when BSA (1.6 mg/ml) was present (*data not shown*). Samples were incubated at 37 ºC for 1h. After incubation, samples were vacuum-filtered and washed on GF/B filters (Whatman) with ice-cold Trish/HCl solution (50 mM). Filters were harvested into 20 ml scintillation tubes containing 3 ml scintillation liquid (Aquasafe, Zinsser), and assayed for radioactivity three times in three consecutive days. Radioactivity was converted to fmol [^{3}H]RTX/mg protein binding values after subtracting non-specific retention values from filters without protein samples.

Optimal [^{3}H]RTX saturation was obtained by subtracting the average total binding values from $TRPV_1^{-/-}$ from corresponding values in WTs (illustrated in red, Fig. $S5G_1$). (*E*)-Capsaicin failed to completely displace [^{3}H]RTX binding in WTs membranes (in blue, Fig. $S5G_1$) as explained by the phenomenon that lipophilic unlabeled ('cold') ligands can increase non-specific binding. That is, both (*E*)-capsaicin and (*Z*)-capsaicin in KO membranes as well as (*Z*)-capsaicin in WT membranes augmented total (non-specific) binding. This increase was 19.1 ± 4.4% by (*E*)-capsaicin in WT membranes at a [^{3}H]RTX concentration of 1.5 nM. This phenomenon is at least partly responsible for the inability of (*E*)-capsaicin to produce an 'ideal' [^{3}H]RTX saturation curve in WTs. Therefore, we used a normalizing factor of 0.84.

[^{3}H]resiniferatoxin binding in human hippocampus. Specific [^{3}H]RTX binding was determined in *post-mortem* hippocampi (100 μg protein/sample) from moderate AD (B2-4; *n* = 7), severe AD (B6; *n* = 5) and age-matched controls (*n* = 5) using a [^{3}H]RTX concentration of 1.5 nM. Rat striatal synaptosomes (100 μg protein/well, 4 preparations in triplicate), in which postsynaptic $TRPV_1$s have been identified earlier (Maccarrone *et al.,* 2008), were used as positive control (Fig. $S5G_2$). Data were expressed as specific [^{3}H]RTX binding (fmol [^{3}H]RTX/mg protein).

Acute brain slice preparation and electrophysiology. Sagittal brain slices (300 μm) were prepared from 14- or 16-day-old C57Bl/6N mice. Animals were killed by decapitation. Whole brains were removed, placed in ice-cold cutting solution containing (mM):140 K-gluconate, 15 Na-gluconate, 0.2 EGTA, 4 NaCl, 10 HEPES, and sectioned on a Leica VT1000S vibratome. Brains slices were acutely equilibrated for 1h in extracellular solution containing (mM): 126 NaCl, 3.5 KCl, 2 $CaCl_2$, 1.3 $MgCl_2$, 26 $NaHCO_3$, 1.2 NaH_2PO_4 and 10 glucose, at room temperature. In biochemical experiments, hippocampal slices were transferred to a submerged chamber containing oxygenated (95% O_2/5% CO_2) extracellular solution with/without Aβ(1-42) (provided by Drs. B. Penke and L. Fülöp, University

For Peer Review

of Szeged, Hungary). Aβ(1-42), containing a mixture of oligomers and protofibrils (Minkeviciene *et al.,* 2009), was directly dissolved in extracellular solution at a final concentration of 1 μM. Slices were snap-frozen in liquid N_2 after 1h Aβ(1-42) exposure and stored at -80 ^{o}C until processing.

CA1 pyramidal cells were visualized by infrared differential interference contrast microscopy (Olympus BX51) and whole-cell recordings were performed at 22-24 ^{o}C. Patch electrodes had 4-8 MΩ resistance when filled with intracellular solution consisting of (mM): 125 K-gluconate, 20 KCl, 4 ATP-Mg, 10 Na-phosphocreatine, 0.3 GTP and 10 HEPES (pH 7.3). Spontaneous IPSCs (sIPSCs) were recorded on a Multiclamp 700A amplifier (Axon Instruments), sampled at 20 μs intervals, filtered at 2 kHz and stored for off-line analysis using Igor Pro 6.0 software (Wavemetrix). Recordings were performed in the presence of CNQX (20 μM, Tocris), D-AP5 (50 μM, Tocris) to eliminate ionotropic glutamatergic neurotransmission, as well as carbamoylcholine chloride (5 μM [carbachol], Tocris). Access resistance was not compensated but frequently monitored and cells showing large deviations (>25%) were excluded from analysis.

Aβ(1-42) effects on depolarization-induced suppression of inhibition (DSI) were determined by pre-incubating sister (consecutive) slices for 1h in a bath solution also containing 1 μM Aβ(1-42), and by alternating recordings between control *vs.* Aβ(1-42)-exposed slices to eliminate methodological artifacts (Minkeviciene *et al.,* 2009). We refrained from using ionic (buffer) conditions (e.g. $CsCl_2$) or inhibitor(s) that may affect voltage-gated channel conductances to minimize unwanted interference with Aβ(1-42) actions and, consequently, physiological outcome.

sIPSCs were measured in voltage clamp mode, at a holding potential of -80 mV. DSI was elicited by step depolarization to 0 mV for 1s. A 15s period prior to the depolarization step served as control. DSI was calculated over a 50s period starting 1s after the depolarizing pulse's end (the 1s period eliminated the latency period of DSI (Wilson and Nicoll 2001) from our analysis). Mean sIPSC transfer charge was calculated over 5s time bins (Makara *et al.,* 2007). AM251 (Tocris) was applied at a final concentration of 1μM. DSI was calculated based on data from *n* = 1-4 DSI/condition/cell. The recovery time course of DSI (Straiker *et al.,* 2009) was fitted with a single-exponential decay curve (GraFit 5.0; Erithacus Software).

For Peer Review

Legends to Supplementary Tables & Figures

Table S1 **Characteristics of the control and Alzheimer's subjects**. *Abbreviations*: BW, brain weight; h, hour; IH, sample processed for immunohistochemistry; PMD, *post-mortem* delay; WB, sample analyzed by Western blotting; y, year.

Table S2 **List of markers used for immunofluorescence labelling.** Panels of antibodies applied to study the molecular composition (A) and cell-type-specificity (A_1) of 2-AG signalling in human and mouse brain. Staining methods (Riedel *et al.,* 2002; Harkany *et al.,* 2003) and antibody specificities were described in detail elsewhere unless otherwise stated. Table

(A) and (A_1) list antibodies against molecular constituents of 2-AG and AEA signalling networks (Katona *et al.,* 1999; Katona *et al.,* 2001; Harkany *et al.,* 2003; Okamoto *et al.,* 2004; Van Sickle *et al.,* 2005; Yoshida *et al.,* 2006; Berghuis *et al.,* 2007; Rimmerman *et al.,* 2008; Cristino *et al.,* 2008; Straiker *et al.,* 2009; Marrs *et al.,* 2010) and neuronal identity markers (Binder *et al.,* 1986; Braak *et al.,* 1994; Thal *et al.,* 1999; Von Kriegstein *et al.,* 1999; Hartig *et al.,* 2003; Nagy *et al.,* 2004; Studer *et al.,* 2006; Bouchard *et al.,* 2007; Persson *et al.,* 2010), respectively. *Abbreviations:* ABHD6, serine hydrolase α/β-hydrolase domain 6; CB_1R/CB_2R, CB_1 or CB_2 cannabinoid receptor; DB, dot blot; DAGLα/β, *sn*-1-diacylglycerol lipase α/β; GFAP, glial fibrillary acidic protein; IBA-1, ionized Ca^{2+}-binding adaptor molecule 1; IH, immunohistochemistry; MAP2, microtubule-associated protein 2; MGL, monoacylglycerol lipase; PHF, paired helical filament; PSD95, postsynaptic density protein 95; SNAP25, synaptosomal-associated protein of 25 kDa; VGLUT1, vesicular glutamate transporter 1; WB, Western blotting.

Fig. S1 **Aβ load, and biochemical indices of pre- and postsynaptic deficit in Alzheimer's tissues**. (A) Detergent-insoluble Aβ concentrations in hippocampal tissues as determined by ELISA. Data were expressed as pg of full-length Aβ(1-42) per µg protein. (B) β-Actin was used as loading control throughout. (B_1) Although β-actin concentrations exhibited individual variations, these did not correlate with *post-mortem* delay. (C) AD is characterized by a progressive decrease in synaptosomal-associated protein of 25 kDa (SNAP25), a presynaptic marker of glutamatergic terminals in human brain (Garbelli *et al.,* 2008). (D) Coincident reduction in postsynaptic density protein 95 (PSD95) (Von Kriegstein *et al.,* 1999) levels indicates a loss of glutamatergic postsynapses in AD. SNAP25 and CB_1R loads did not correlate across either the entire cohort (E) or particular disease states (*data not shown*). **p* < 0.05 (Student's *t*-test). The colours of individual data points identify subject subsets and correspond to those in Table S1. *Abbreviations:* B2-4, Braak stage II-IV cohort; B6, Braak stage VI group.

Fig. S2 **Quality control of novel antibodies**. The specificity of our antibodies raised against the full N-terminus of the CB_1R (in rabbit, A_1), the AA205-287 fragment of DAGLβ (in rabbit, A_2), AA790-908 of DAGLα (in guinea pig, A_2), AA104-141 sequence of ABHD6 (in rabbit, A_3), NAPE-PLD (41 AAs in its N terminus, in rabbit; A_4) and AA171-206 of MGL (in rabbit, A_5) have been tested by Western blotting. (A_6) The specificity of our antibody raised against an internal epitope of MGL has been further validated in fetal $MGL^{-/-}$ mice (MGL KO, embryonic day 16) by the lack of specific immunoreactivity in axons (*arrows*) populating the intermediate zone (IZ) of the cerebral cortex (Wu *et al.,* 2010). β-III-tubulin was used as histochemical control, as well as a neuromorphological marker to delineate specific brain regions. *Abbreviation*: CP, cortical plate. *Scale bars* = 40 µm.

For Peer Review

Fig. S3 **Comparative analysis of the emission spectra of carbocyanine fluorophores after histochemical manipulations to human brain tissues**. (A) Tissue autofluorescence in aged human hippocampus upon excitation by 488 (Cy2), 543 (Cy3) and 633 nm (Cy5) lasers. The glass-mounted section was not exposed to either primary or secondary antibodies. Emission spectra were presented as '*Background*' in panels (C_1) – (C_3). Note that tissue autofluorescence primarily interferes with Cy2 signals. (B) Consecutive section exposed to Sudan Black-B but not to primary or secondary antibodies. Note that Sudan Black-B effectively reduces tissue autofluorescence at all three excitation wavelengths used. Emission spectra are shown as '*Sudan Black'* in panels (C_1) – (C_3). Simultaneous immunofluorescence detection of Cy2 (DAGLα), Cy3 (DAGLβ) and Cy5 (MAP2) signals on Sudan Black-B-treated tissue background. Sharp emission peaks at expected wavelengths ('*Cy2/Cy3/Cy5*') with robust gain in signal intensity relative to Sudan Black-B-stained tissues demonstrate the specificity of our histochemical techniques.

Fig. S4 ***Post-mortem* delay does not affect the levels of synaptic and 2-AG signalling-related proteins.** AEA and 2-AG levels rapidly change after death: *post-mortem* delay longer than 1h increases AEA concentrations. In contrast, 2-AG concentrations rapidly decline (within the first hour) after death (Palkovits *et al.,* 2008). We therefore sought to determine whether *post-mortem* delay affects enzyme and receptor components of 2-AG signalling. Correlation analysis failed to establish a significant effect of *post-mortem* delay on protein levels from total brain homogenates (n.s.; non-significant) in our overall subject cohort as well as sample subsets (*data for the latter not shown*) when analyzing synaptosomal-associated protein of 25 kDa (SNAP25; A), postsynaptic density protein 95 (PSD95; B), CB_1 cannabinoid receptor (CB_1R, C), *sn*-1-diacylglycerol lipase α (DAGL α ; D) and β (DAGLβ; D_1), and serine hydrolase α/β-hydrolase domain 6 (ABHD6) concentrations.

Fig. S5 **Alzheimer's disease affects the expression of neither the metabolic enzymes implicated in regulating anandamide (AEA) availability nor transient receptor potential V1 ($TRPV_1$) channels.** (A) Representative Western samples of fatty-acid amide hydrolase (FAAH) and N-acyl phosphatidylethanolamine-specific phospholipase D (NAPE-PLD) from control, moderate AD (B2-4) and severe AD (B6) cases. Neither AD progression (B) nor *post-mortem* delay impacts FAAH protein levels. Note the relative increase in severe AD (B6) that corroborates previous data on FAAH overexpression by plaque-associated microglia (Benito *et al.,* 2003). (C,C_1) Similarly, NAPE-PLD levels remain stable in AD. (D-D_2) Cortical as well as hippocampal pyramidal cells (*arrows*) exhibit $TRPV_1$-like immunoreactivity in human brain. Open rectangle identifies the position of (E-E_2). TRPV1-like immunoreactivity decorates a subset of pyramidal cell dendrites in human brain, and appears as intermittent clusters of immunoreactive puncta (*arrows*). Open arrowheads point to a $TRPV1^-$ dendrite. (F) Representative image of $TRVP_1$ dot-

For Peer Review

blot signal. β-Actin was used as loading control. (F_1) $TRPV_1$ levels undergo an incremental – albeit non-significant – increase in B2-4 and B6 disease. (F_2) *Post-mortem* delay does not affect $TRPV_1$ concentrations. (G) [^{3}H]resiniferatoxin ([^{3}H]RTX) binding in total brain membranes of $TRPV_1^{-/-}$ and wild-type C57Bl/6 mice. (G_1) The saturation curve in red represents 'optimal' saturation depicting the difference in specific binding (B_{max}: 130.2 ± 33.0 fmol/mg protein; K_d: 559 ± 94 pM) between WT and $TRPV_1^{-/-}$ mice in (G). (*E*)-capsaicin, a selective $TRPV_1$ agonist (1 μM) failed to produce a displacement of similar amplitude (in blue; B_{max}: 122.5 ± 10.6 fmol/mg protein; K_d: 1.26 ± 0.55 nM). This is partly due to (*E*)-capsaicin and its $TRPV_1$-inactive enantiomer (*Z*)-capsaicin (1 μM) ligating the radioligand to the membranes in a non-specific manner. Accordingly, (*E*)-capsaicin causes 'negative' displacement in the $TRPV_1^{-/-}$ (KO) mice and (*Z*)-capsaicin mimics this in WTs. This we took into account when calculating specific binding in the human and rat samples shown in (G_2). (G_2) $TRPV_1$ binding in *post-mortem* control and AD brains using a 1.5 nM final concentration of [^{3}H]RTX. Rat striatal synaptosomes were used as positive control. We find a transient (non-significant) increase in $TRPV_1$ binding in B2-4 brains. Overall, AD does not affect $TRPV_1$ binding capacity of the human hippocampus.

Fig. S6 **Analysis settings to minimize bias in data sampling for quantitative immunofluorescence.** (A) Relative area coverage of CB_1R^+ and synaptophysin$^+$ structures over pyramidal cell dendrites in the stratum radiatum. (A_1) Co-localization coefficients for CB_1R and synaptophysin immunoreactivities. (A_2) Pearson's correlation coefficient of CB_1R and synaptophysin fluorescence intensities is approximately 0, suggesting a lack of regulatory interplay in the two proteins. (A_3-C) Fluorescence intensity profiles of markers analyzed by quantitative sampling procedures. Continuous lines represent population means, whereas dashed lines indicate population minima and maxima. Note that imaging settings were rigorously adjusted to eliminate bias through variable sampling. These data cumulatively support that quantitative data in this report represent the result of balanced sampling of aged control and/or AD tissues.

Fig. S7 **Image surveys of human hippocampi stained for CB_1R or DAGLα/DAGLβ.** (A-A_2) Control hippocampus triple-stained for MAP2, a dendritic marker (A), CB_1Rs (A_1), and synaptophysin, a presynaptic marker (A_2). (B-B_2) Similar histochemical arrangements made to coincidently localize MAP2 (B), DAGLα (B_1), and DAGLβ (B_2). Dashed lines encircle anatomically distinct hippocampal subfields. *Abbreviations*: CA1-CA4, Ammon's horn first-fourth subfields; GL, stratum granulare; mol, stratum moleculare; or, stratum oriens; pyr, stratum pyramidale; rad, stratum radiatum. *Scale bars* = 500 μm.

Fig. S8 **MGL protein content, URB602 and URB597 effects in Alzheimer's *vs.* control frontal cortices used in biochemical assays.** Note the significant decrease in both

For Peer Review

soluble (A) and membrane-associated MGL (A_1) in AD. Numbers correspond to independent samples per each subject group. (A_2) Means ± s.e.m. (n = 9) of integrated, grey-scaled optical densities from experiments in (A,A_1). (B) Membrane-associated MGL activity accounts for ~60% of total 2-AG hydrolysis activity as confirmed by URB602 (King *et al.,* 2007) application in membrane samples prepared from control human specimens. Note that URB602-sensitive 2-AG degrading activities are selectively lost in AD. (B_1) 2-AG hydrolysis activity significantly increases in cytosol fractions from AD brains, as compared to controls. URB602 partially reduces 2-AG degradation in cytosolic fractions prepared from control brains and eliminates disease-associated enhancement of 2-AG catabolism in AD brains. (C) We also assessed the rate of AEA degradation in the same control and AD samples. Unlike MGL, FAAH protein levels did not change in the sample cohort (*data not shown*). Membrane-associated AEA hydrolysis significantly decreased, as compared to controls. Cytosolic FAAH activity was negligible (*data not shown*). URB597 eliminated ~ 63% of AEA hydrolysis activity in controls. Similarly, URB597 decreased AEA degradation by 51% in AD, confirming the contribution of FAAH. These data show that FAAH enzymatic activity is decreased in AD. ***p < 0.001, **p < 0.01 *vs*. controls; $^{\#}p$ < 0.05, $^{\#\#}$ p < 0.01 *vs*. non-treated samples. *Abbreviations*: N.T., non-treated.

Fig. S9 **Molecular components of 2-AG signalling in APdE9 mice**. We have explored whether APdE9 mice present phenotypic changes in 2-AG signalling, paralleling the neurochemical changes found in *post-mortem* human brains. (A) Comparison of protein expression profiles in wild-type mice (n = 2/group are shown) at 7 months (7 m) and 14 months (14 m) of age. Expression profiling of excitatory synapse markers (SNAP25, vesicular glutamate transporter 1 (VGLUT1), and postsynaptic density protein 95 (PSD95)) and 2-AG signalling network components at 7 months (A_1) or 14 months of age (A_2) reveals significant aging effects, but limited transgene contribution. (B-G) Quantitative analysis of SNAP25 (B; p < 0.05 *vs*. wild-type), VGLUT1 (C; p < 0.05; 7 *vs*. 14 months for both genotypes), PSD95 (D; p < 0.05 *vs*. wild-type), CB_1R (E; p < 0.05 *vs*. wild-type), DAGLα (F; p < 0.05; 7 *vs*. 14 months for wild-type control) and MGL (G) reveals age-independent SNAP25 upregulation, age- but not genotype-related loss of VGLUT1 (C), DAGLα (F) and MGL (G) expressions, and stochastic PSD95 (D) and CB_1R (E) increases in APdE9 mice, as compared to wild-type littermates. Total MGL levels remained unchanged throughout the age-range analyzed. (H_1-H_3) Linear regression analysis of select neurochemical targets identifies a close, genotype-specific relationship between SNAP25 levels, possibly representing ectopic glutamatergic axonal sprouting around Aβ plaques (Bell *et al.,* 2003; Hu *et al.,* 2003), and CB_1R (H_1), DAGLα (H_2) or MGL (H_3) contents in APdE9 mice. Linear regression plots overall (all animals), in APdE9 and wild-type subgroups are represented by dotted, dashed/dotted and dashed lines, respectively. Data were normalized to β-III-tubulin loading controls. These data, and

For Peer Review

unchanged 2-AG concentrations in the cerebral cortex of APdE9 transgenic mice at 12 months of age (H. Tanila, *unpublished information*), cumulatively suggest that APdE9 transgenics might be inappropriate to recapitulate molecular underpinnings of disrupted 2-AG signalling in AD. Data were expressed as mean ± s.e.m.

Fig. S10 **Depolarization-induced suppression of inhibition (DSI) under control recording conditions**. (A) A brief (1s) depolarization step to 0 mV in CA1 pyramidal cells invariably induces significant DSI. (A_1) AM251 occluded DSI in all neurons tested. (A) and (A_1) are representative example traces. Cumulative data are referred to in Fig. 8C.

For Peer Review

References

Bell KF, de Kort GJ, Steggerda S, Shigemoto R, Ribeiro-da-Silva A, Cuello AC. Structural involvement of the glutamatergic presynaptic boutons in a transgenic mouse model expressing early onset amyloid pathology. Neurosci Lett 2003; 353: 143-147.

Benito C, Nunez E, Tolon RM, Carrier EJ, Rabano A, Hillard CJ *et al*. Cannabinoid CB2 receptors and fatty acid amide hydrolase are selectively overexpressed in neuritic plaque-associated glia in Alzheimer's disease brains. J Neurosci 2003; 23: 11136-11141.

Berghuis P, Dobszay MB, Sousa KM, Schulte G, Mager PP, Hartig W *et al*. Brain-derived neurotrophic factor controls functional differentiation and microcircuit formation of selectively isolated fast-spiking GABAergic interneurons. Eur J Neurosci 2004; 20: 1290-1306.

Berghuis P, Rajnicek AM, Morozov YM, Ross RA, Mulder J, Urban GM *et al*. Hardwiring the brain: endocannabinoids shape neuronal connectivity. Science 2007; 316: 1212-1216.

Binder LI, Frankfurter A, Rebhun LI. Differential localization of MAP-2 and tau in mammalian neurons in situ. Ann N Y Acad Sci 1986; 466: 145-166.

Bouchard C, Lee S, Paulus-Hock V, Loddenkemper C, Eilers M, Schmitt CA. FoxO transcription factors suppress Myc-driven lymphomagenesis via direct activation of Arf. Genes Dev 2007; 21: 2775-2787.

Braak E, Braak H, Mandelkow EM. A sequence of cytoskeleton changes related to the formation of neurofibrillary tangles and neuropil threads. Acta Neuropathol 1994; 87: 554-567.

Bradford MM. A rapid and sensitive method for the quantitation of microgram quantities of protein utilizing the principle of protein-dye binding. Anal Biochem 1976; 72: 248-254.

Caterina MJ, Leffler A, Malmberg AB, Martin WJ, Trafton J, Petersen-Zeitz KR *et al*. Impaired nociception and pain sensation in mice lacking the capsaicin receptor. Science 2000; 288: 306-313.

Cristino L, Starowicz K, De Petrocellis L, Morishita J, Ueda N, Guglielmotti V *et al*. Immunohistochemical localization of anabolic and catabolic enzymes for anandamide and other putative endovanilloids in the hippocampus and cerebellar cortex of the mouse brain. Neuroscience 2008; 151: 955-968.

Garbelli R, Inverardi F, Medici V, Amadeo A, Verderio C, Matteoli M *et al*. Heterogeneous expression of SNAP-25 in rat and human brain. J Comp Neurol 2008; 506: 373-386.

Halleskog C, Mulder J, Dahlstrom J, Mackie K, Hortobagyi T, Tanila H *et al*. WNT signaling in activated microglia is proinflammatory. Glia 2011; 59: 119-131.

Harkany T, Hartig W, Berghuis P, Dobszay MB, Zilberter Y, Edwards RH *et al*. Complementary distribution of type 1 cannabinoid receptors and vesicular glutamate transporter 3 in basal forebrain suggests input-specific retrograde signalling by cholinergic neurons. Eur J Neurosci 2003; 18: 1979-1992.

Hartig W, Riedel A, Grosche J, Edwards RH, Fremeau RT, Jr., Harkany T *et al*. Complementary distribution of vesicular glutamate transporters 1 and 2 in the nucleus accumbens of rat: Relationship to calretinin-containing extrinsic innervation and calbindin-immunoreactive neurons. J Comp Neurol 2003; 465: 1-10.

Hartshorne RP, Catterall WA. The sodium channel from rat brain. Purification and subunit composition. J Biol Chem 1984; 259: 1667-1675.

Hu L, Wong TP, Cote SL, Bell KF, Cuello AC. The impact of Abeta-plaques on cortical cholinergic and non-cholinergic presynaptic boutons in alzheimer's disease-like transgenic mice. Neuroscience 2003; 121: 421-432.

Hyman BT, Trojanowski JQ. Consensus recommendations for the postmortem diagnosis of Alzheimer disease from the National Institute on Aging and the Reagan Institute Working Group on

For Peer Review

diagnostic criteria for the neuropathological assessment of Alzheimer disease. J Neuropathol Exp Neurol 1997; 56: 1095-1097.

Katona I, Rancz EA, Acsady L, Ledent C, Mackie K, Hajos N *et al*. Distribution of CB1 cannabinoid receptors in the amygdala and their role in the control of GABAergic transmission. J Neurosci 2001; 21: 9506-9518.

Katona I, Sperlagh B, Sik A, Kafalvi A, Vizi ES, Mackie K *et al*. Presynaptically located CB1 cannabinoid receptors regulate GABA release from axon terminals of specific hippocampal interneurons. J Neurosci 1999; 19: 4544-4558.

Keimpema E, Barabas K, Morozov YM, Tortoriello G, Torii M, Cameron G *et al*. Differential subcellular recruitment of monoacylglycerol lipase generates spatial specificity of 2-arachidonoyl glycerol signaling during axonal pathfinding. J Neurosci 2010; 30: 13992-14007.

King AR, Duranti A, Tontini A, Rivara S, Rosengarth A, Clapper JR *et al*. URB602 inhibits monoacylglycerol lipase and selectively blocks 2-arachidonoylglycerol degradation in intact brain slices. Chem Biol 2007; 14: 1357-1365.

Maccarrone M, Rossi S, Bari M, De C, V, Fezza F, Musella A *et al*. Anandamide inhibits metabolism and physiological actions of 2-arachidonoylglycerol in the striatum. Nat Neurosci 2008; 11: 152-159.

Makara JK, Katona I, Nyiri G, Nemeth B, Ledent C, Watanabe M *et al*. Involvement of nitric oxide in depolarization-induced suppression of inhibition in hippocampal pyramidal cells during activation of cholinergic receptors. J Neurosci 2007; 27: 10211-10222.

Marrs WR, Blankman JL, Horne EA, Thomazeau A, Lin YH, Coy J *et al*. The serine hydrolase ABHD6 controls the accumulation and efficacy of 2-AG at cannabinoid receptors. Nat Neurosci 2010; 13: 951-957.

Minkeviciene R, Rheims S, Dobszay MB, Zilberter M, Hartikainen J, Fulop L *et al*. Amyloid beta-induced neuronal hyperexcitability triggers progressive epilepsy. J Neurosci 2009; 29: 3453-3462.

Mirra SS, Heyman A, McKeel D, Sumi SM, Crain BJ, Brownlee LM *et al*. The Consortium to Establish a Registry for Alzheimer's Disease (CERAD). Part II. Standardization of the neuropathologic assessment of Alzheimer's disease. Neurology 1991; 41: 479-486.

Mulder J, Zilberter M, Spence L, Tortoriello G, Uhlen M, Yanagawa Y *et al*. Secretagogin is a Ca2+-binding protein specifying subpopulations of telencephalic neurons. Proc Natl Acad Sci U S A 2009; 106: 22492-22497.

Nagy G, Reim K, Matti U, Brose N, Binz T, Rettig J *et al*. Regulation of releasable vesicle pool sizes by protein kinase A-dependent phosphorylation of SNAP-25. Neuron 2004; 41: 417-429.

Okamoto Y, Morishita J, Tsuboi K, Tonai T, Ueda N. Molecular characterization of a phospholipase D generating anandamide and its congeners. J Biol Chem 2004; 279: 5298-5305.

Palkovits M, Harvey-White J, Liu J, Kovacs ZS, Bobest M, Lovas G *et al*. Regional distribution and effects of postmortal delay on endocannabinoid content of the human brain. Neuroscience 2008; 152: 1032-1039.

Paratcha G, Ledda F, Ibanez CF. The neural cell adhesion molecule NCAM is an alternative signaling receptor for GDNF family ligands. Cell 2003; 113: 867-879.

Persson A, Lindwall C, Curtis MA, Kuhn HG. Expression of ezrin radixin moesin proteins in the adult subventricular zone and the rostral migratory stream. Neuroscience 2010; 167: 312-322.

Riedel A, Hartig W, Seeger G, Gartner U, Brauer K, Arendt T. Principles of rat subcortical forebrain organization: a study using histological techniques and multiple fluorescence labeling. J Chem Neuroanat 2002; 23: 75-104.

Rimmerman N, Hughes HV, Bradshaw HB, Pazos MX, Mackie K, Prieto AL *et al*. Compartmentalization of endocannabinoids into lipid rafts in a dorsal root ganglion cell line. Br J Pharmacol 2008; 153: 380-389.

Schnell SA, Staines WA, Wessendorf MW. Reduction of lipofuscin-like autofluorescence in fluorescently labeled tissue. J Histochem Cytochem 1999; 47: 719-730.

For Peer Review

Straiker A, Hu SS, Long J, Arnold A, Wager-Miller J, Cravatt BF *et al*. Monoacyl glycerol lipase (MGL) limits the duration of endocannabinoid-mediated depolarization-induced suppression of excitation (DSE) in autaptic hippocampal neurons. Mol Pharmacol 2009.

Studer FE, Fedele DE, Marowsky A, Schwerdel C, Wernli K, Vogt K *et al*. Shift of adenosine kinase expression from neurons to astrocytes during postnatal development suggests dual functionality of the enzyme. Neuroscience 2006; 142: 125-137.

Thal DR, Hartig W, Schober R. Diffuse plaques in the molecular layer show intracellular A beta(8-17)-immunoreactive deposits in subpial astrocytes. Clin Neuropathol 1999; 18: 226-231.

Van Sickle MD, Duncan M, Kingsley PJ, Mouihate A, Urbani P, Mackie K *et al*. Identification and functional characterization of brainstem cannabinoid CB2 receptors. Science 2005; 310: 329-332.

Von Kriegstein K, Schmitz F, Link E, Sudhof TC. Distribution of synaptic vesicle proteins in the mammalian retina identifies obligatory and facultative components of ribbon synapses. Eur J Neurosci 1999; 11: 1335-1348.

Walsh DM, Klyubin I, Fadeeva JV, Cullen WK, Anwyl R, Wolfe MS *et al*. Naturally secreted oligomers of amyloid beta protein potently inhibit hippocampal long-term potentiation in vivo. Nature 2002; 416: 535-539.

Wilson RI, Nicoll RA. Endogenous cannabinoids mediate retrograde signalling at hippocampal synapses. Nature 2001; 410: 588-592.

Wu CS, Zhu J, Wager-Miller J, Wang S, O'Leary D, Monory K *et al*. Requirement of cannabinoid CB(1) receptors in cortical pyramidal neurons for appropriate development of corticothalamic and thalamocortical projections. Eur J Neurosci 2010.

Yoshida T, Fukaya M, Uchigashima M, Miura E, Kamiya H, Kano M *et al*. Localization of diacylglycerol lipase-alpha around postsynaptic spine suggests close proximity between production site of an endocannabinoid, 2-arachidonoyl-glycerol, and presynaptic cannabinoid CB1 receptor. J Neurosci 2006; 26: 4740-4751.

For Peer Review

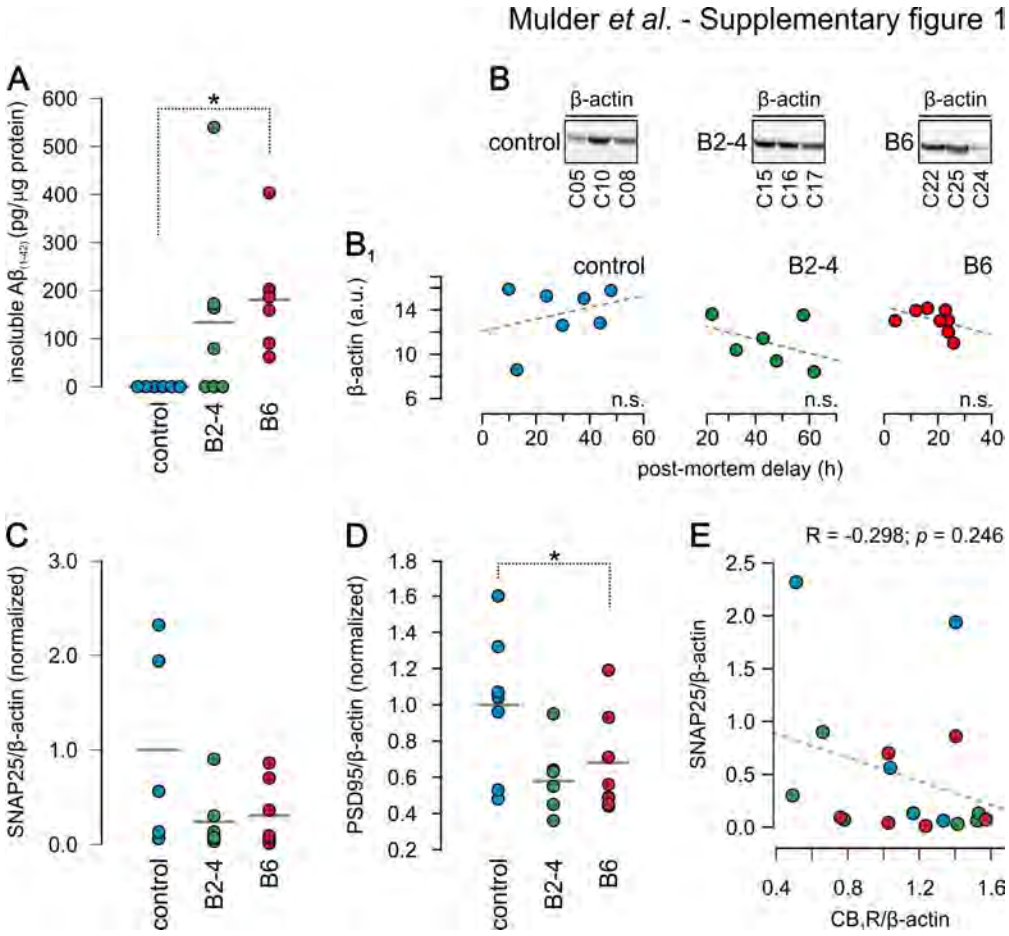

Figure S1
117x108mm (600 x 600 DPI)

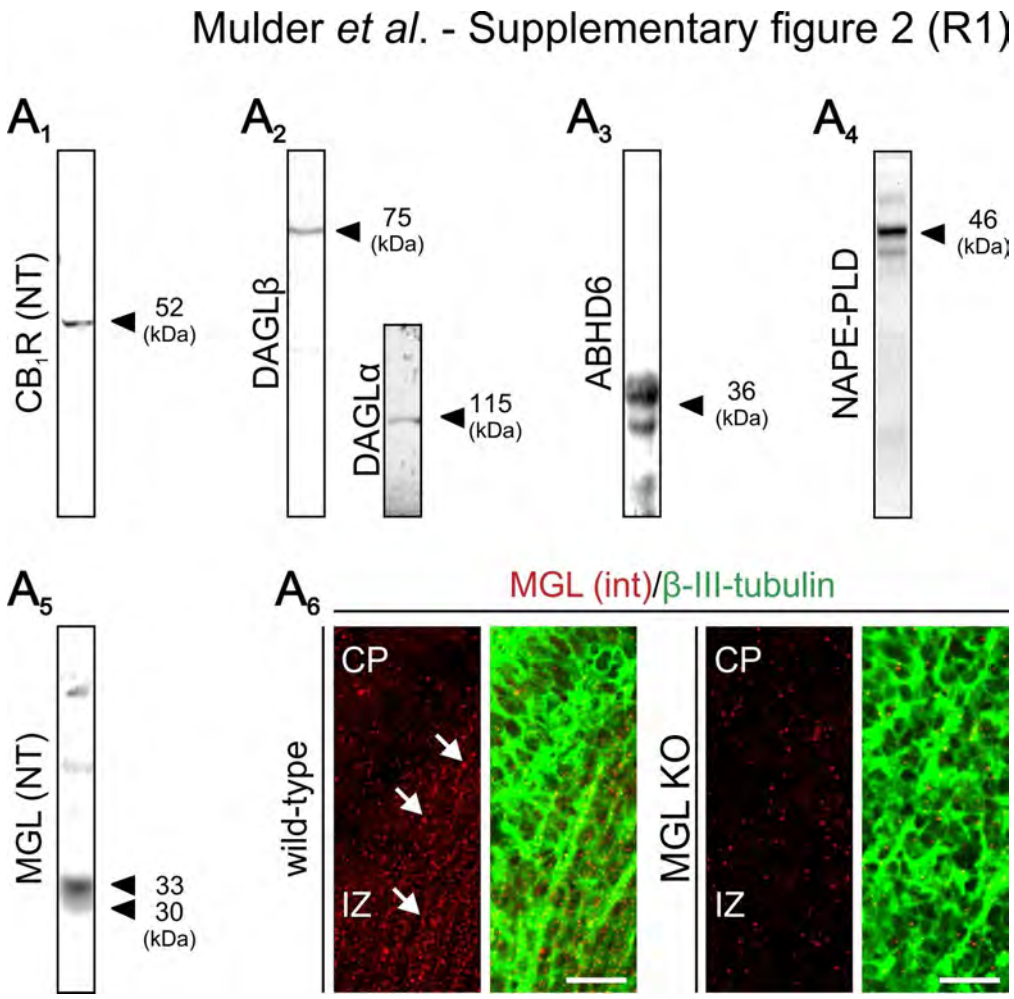

Figure S2
81x80mm (600 x 600 DPI)

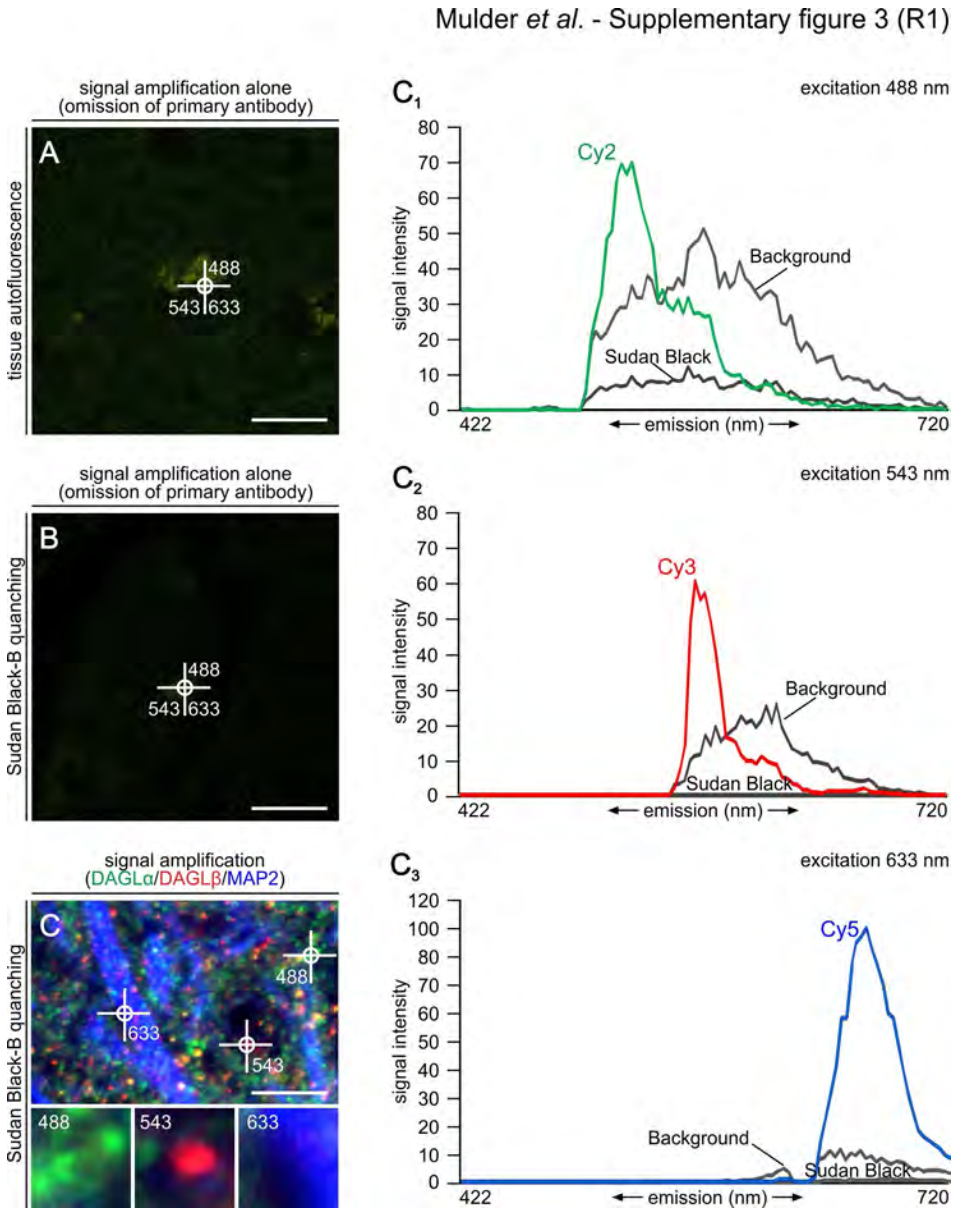

Figure S3
122x156mm (600 x 600 DPI)

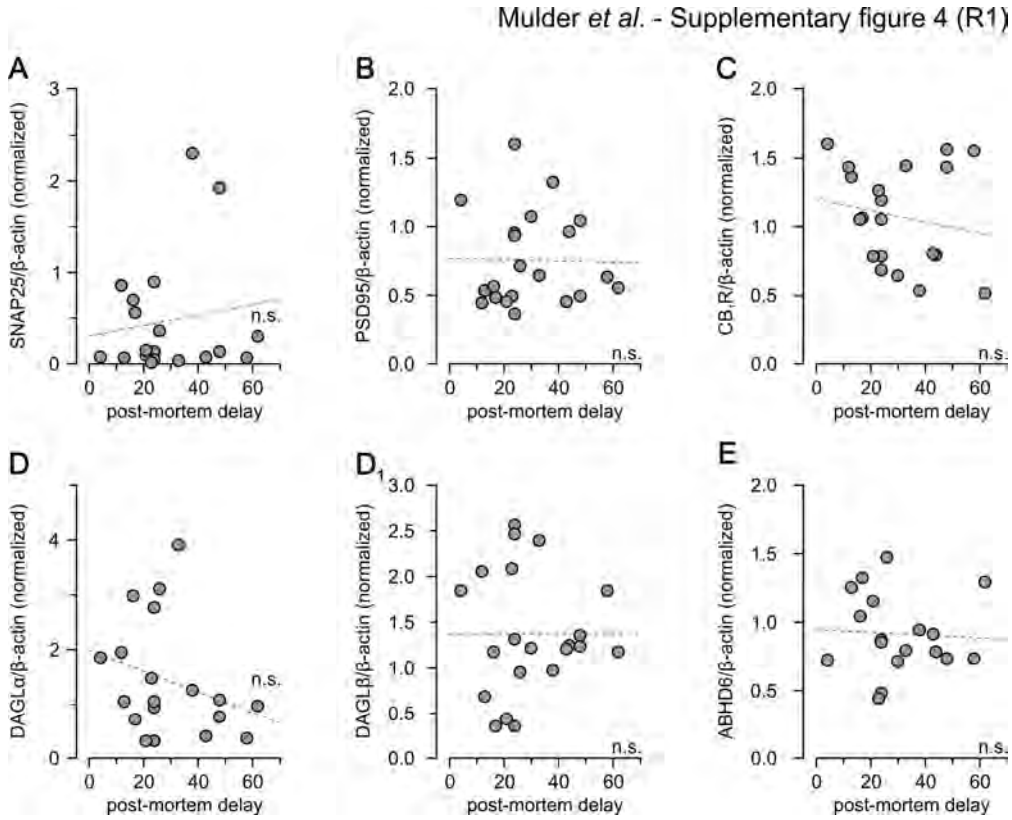

Figure S4
130x105mm (600 x 600 DPI)

For Review

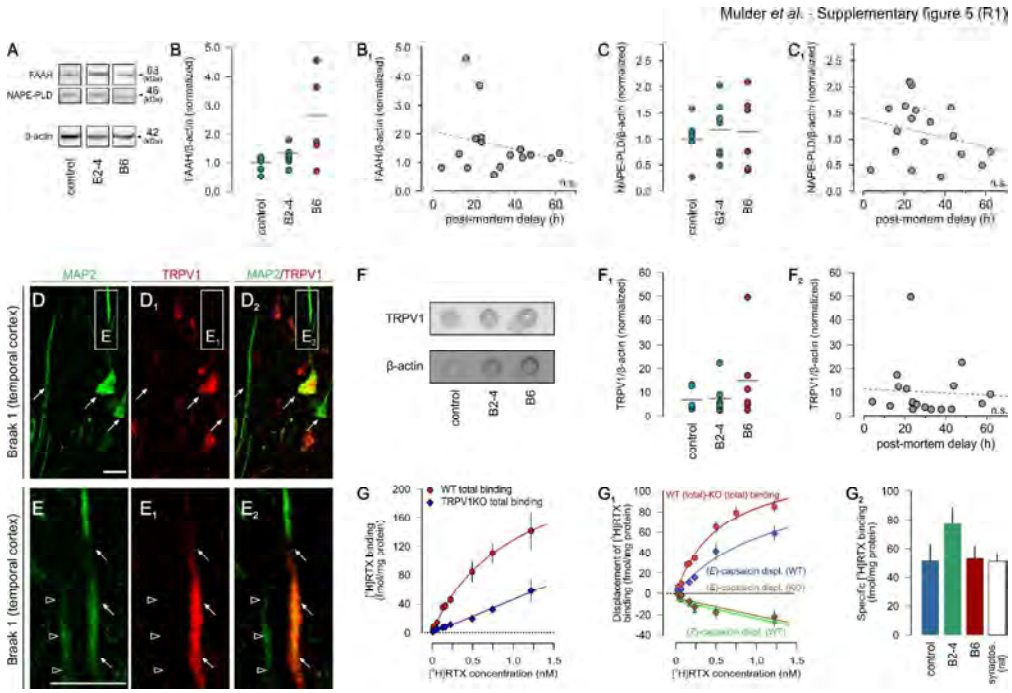

Figure S5
233x159mm (600 x 600 DPI)

Review

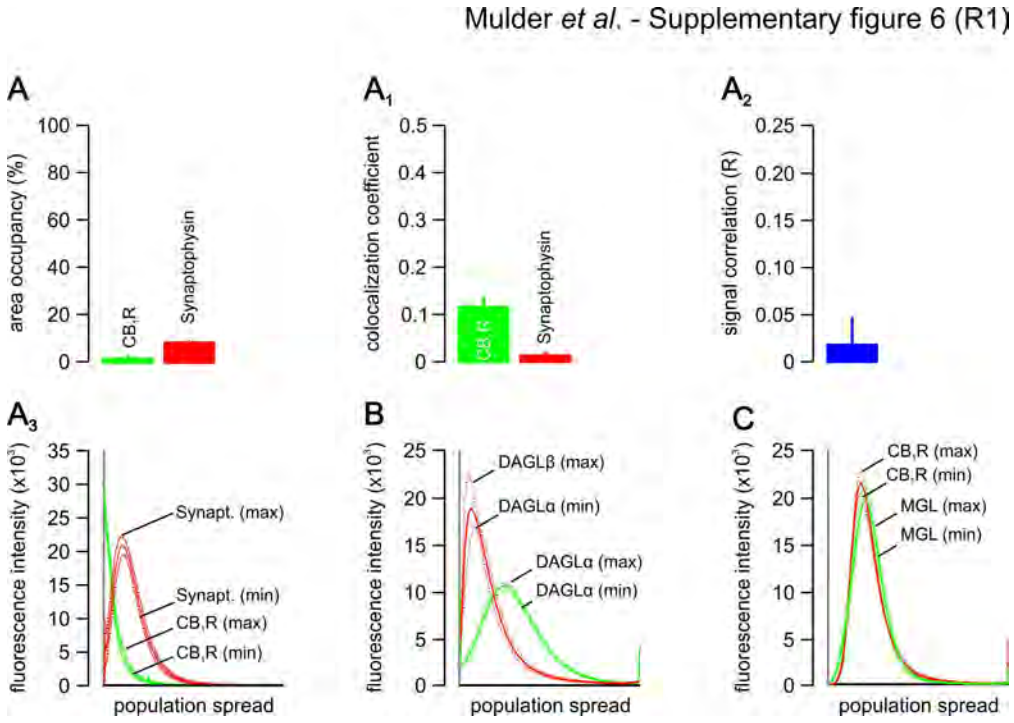

Figure S6
122x87mm (600 x 600 DPI)

Review

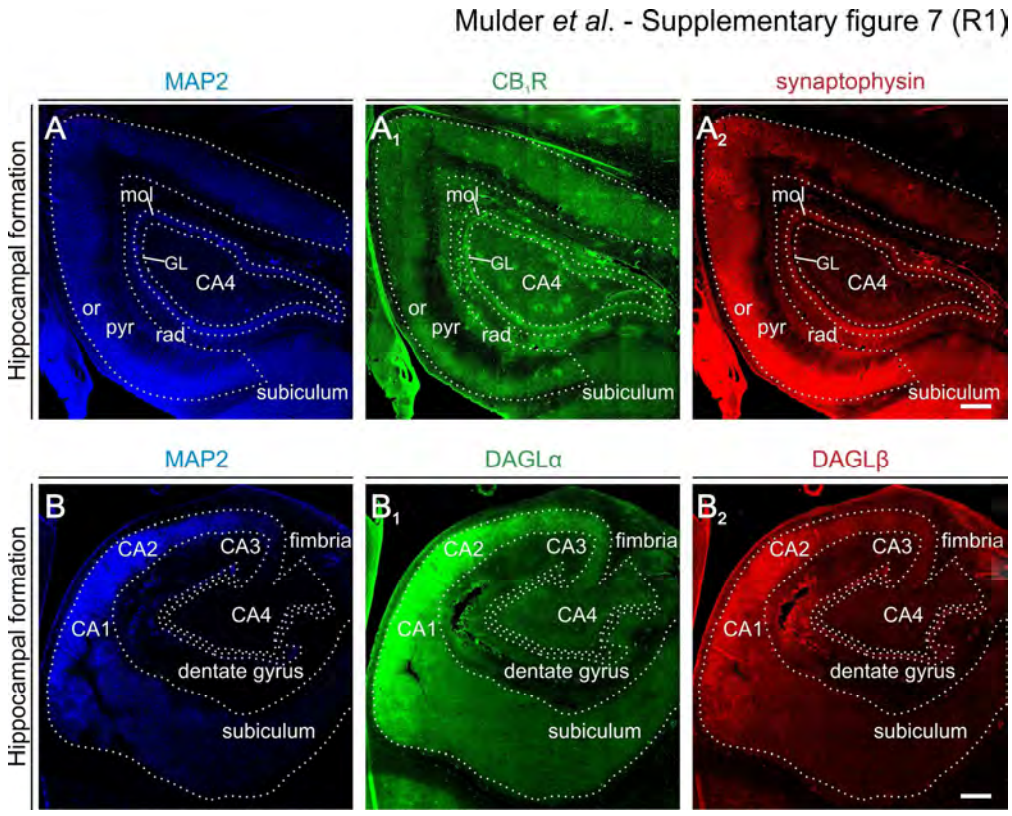

Figure S7
120x96mm (600 x 600 DPI)

For Review

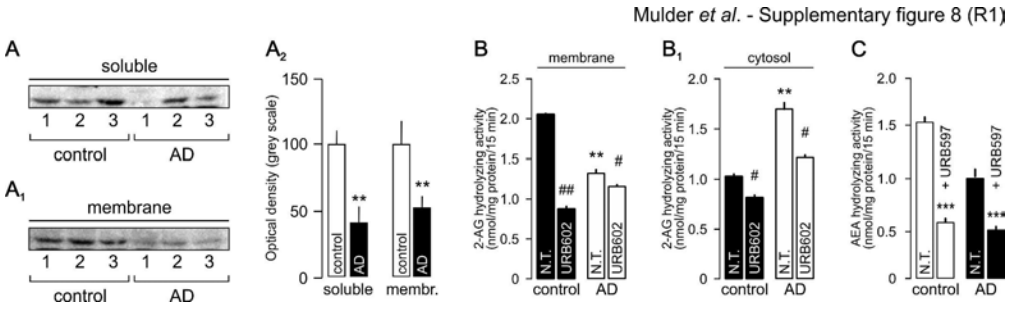

Figure S8
179x53mm (600 x 600 DPI)

For Peer Review

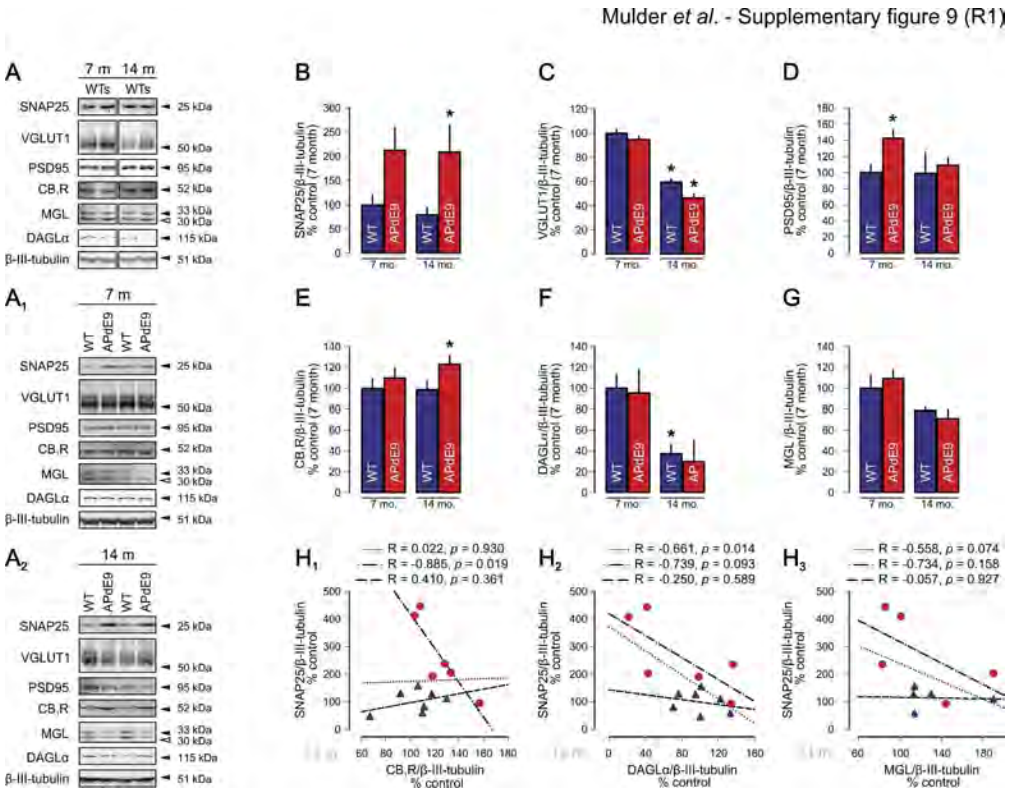

Figure S9
165x129mm (600 x 600 DPI)

For Review

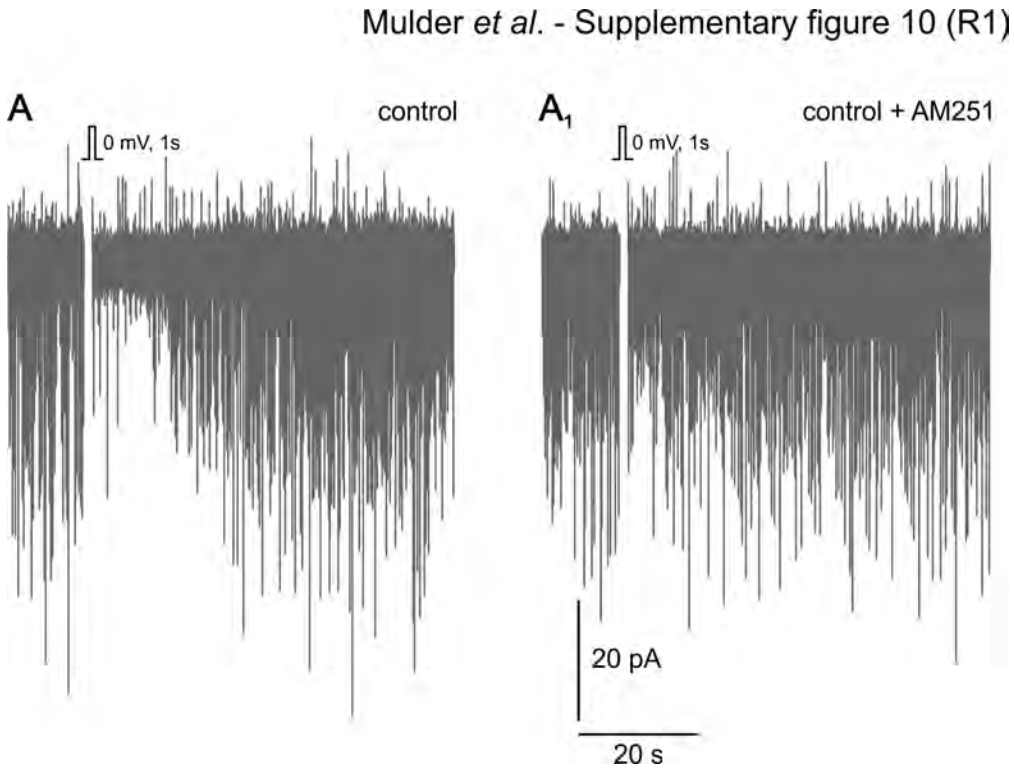

Figure S10
106x80mm (600 x 600 DPI)

For Review

Mulder *et al.* - Supplementary Table 1 (R1)

Group	Case ID	Braak stage	CERAD	Age (y)	Gender	PMD (h)	pH	BW (g)	Analysis
Control	C01	Control	Normal	79	Female	38	6.70	1190	WB
	C02	Control	Normal	55	Female	24	6.73	1290	WB
	C03	Control	Normal	52	Female	44	6.37	1296	WB
	C04	Control	Normal	82	Female	48	6.63	1113	WB
	C05	Control	Normal	71	Female	30	6.30	1169	WB
	C06	Control	Normal	96	Female	16	6.55	1115	IH
	C07	Control	Normal	86	Male	6	6.60	1158	IH
	C08	Braak I	Possible	81	Female	17	6.10	1132	WB & IH
	C09	Braak I	Possible	78	Male	9	n.a.	940	IH
	C10	Braak I	Possible	82	Female	13	6.48	1218	WB & IH
moderate AD	C11	Braak III	Possible	93	Male	33	6.57	1324	WB
	C12	Braak III	Possible	105	Female	58	6.90	1369	WB
	C13	Braak III	Possible	92	Male	11	n.a.	1236	IH
	C14	Braak III/IV	Probable	77	Female	43	6.63	1168	WB & IH
	C15	Braak IV	Probable	82	Male	<24	6.78	1116	WB
	C16	Braak IV	Probable	87	Female	48	6.28	1156	WB
	C17	Braak IV	Probable	91	Male	62	6.31	1115	WB
	C18	Braak IV	Probable	72	Female	29	n.a.	985	IH
	C19	Braak IV	Probable	88	Female	24	6.49	990	WB
severe AD	C20	Braak VI	Definite	69	Female	16.3	7.43	940	WB
	C21	Braak VI	Definite	82	Female	12	6.40	910	WB
	C22	Braak VI	Definite	79	Female	24	6.31	912	WB
	C23	Braak VI	Definite	80	Female	4.3	6.52	950	WB
	C24	Braak VI	Definite	91	Female	23	6.36	954	WB
	C25	Braak VI	Definite	71	Female	21	6.46	1270	WB
	C26	Braak VI	Definite	90	Female	6.5	n.a.	1190	IH
	C27	Braak VI	Definite	85	Female	29	n.a.	910	IH
	C28	Braak VI	Definite	89	Female	26	6.50	1038	WB

Table S1
208x134mm (600 x 600 DPI)

For Review

Mulder *et al.* - Supplementary table 2 (R1)

A

Marker	Host	IH dilution	DB/WB dilution	Source	Reference
ABHD6	rabbit	1:500	1:1,000	Dr. Mackie	Marrs *et al* (2010)
CB_1R (L15)	rabbit	1:500-1:1,000	1:1,000	Dr. Mackie	Katona *et al* (2001)
CB_1R (N-terminal)	rabbit	1:500	n.a.	Dr. Mackie	Katona *et al* (1999)
CB_2R	rabbit	1:500	1:500	Dr. Mackie	Van Sickle *et al* (2005)
DAGLα	guinea pig	n.a.	1:500	Dr. Watanabe	Yoshida *et al* (2006)
DAGLα	goat	1:500	1:500	Dr. Watanabe	present report
DAGLβ	rabbit	1:500	1:500	Dr. Mackie	Berghuis *et al* (2007)
FAAH	rabbit	n.a.	1:1,000	Dr. Mackie	Harkany *et al.* (2003)
MGL (internal)	rabbit	n.a.	1:1,000	Dr. Mackie	Straiker *et al* (2009)
MGL (N-terminal)	rabbit	1:500	1:500	Dr. Mackie	present report
NAPE-PLD	rabbit	n.a.	1:400	Dr. Mackie	Rimmerman *et al.* (2008)
TRPV1	rabbit	n.a.	1:100	Santa Cruz	Cristino *et al.* (2008)

A_1

Marker	Host	IH dilution	WB dilution	Source	Reference
β-Amyloid	mouse (4G8)	1:200	n.a.	Millipore	Thal *et al* (1999)
β-Actin	mouse (AC15)	n.a.	1:10,000	Sigma	Bouchard *et al* (2007)
GFAP-Cy3	rabbit	1:2,000	n.a.	Dr. Härtig	Studer *et al* (2006)
IBA-1	goat	1:200	n.a.	Abcam	Persson *et al* (2007)
MAP2	mouse (AP20)	1:200	n.a.	Sigma	Binder *et al* (1986)
PHF tau	mouse (AT8)	1:1,000	n.a.	Pierce	Braak *et al* (1994)
PSD95	rabbit	n.a.	1:1,000	Synaptic Systems	Von Kriegstein *et al* (2007)
SNAP25	rabbit	n.a.	1:1,000	Synaptic Systems	Nagy *et al* (2004)
Synaptophysin	rabbit	1:1,000	n.a.	Synaptic Systems	Von Kriegstein *et al* (1999)
VGLUT1	rabbit	n.a.	1:1,000	Synaptic Systems	Härtig *et al* (2003)

Table S2
182x133mm (600 x 600 DPI)

Review